
QUAECUMQUE VERA

THE UNIVERSITY OF ALBERTA

RELEASE FORM

NAME OF AUTHOR SHELLEY ANNE LORIMER

TITLE OF THESIS ACOUSTIC FINITE ELEMENT ANALYSIS OF AXISYMMETRIC COMBUSTION CHAMBERS

DEGREE FOR WHICH THESIS WAS PRESENTED MASTER OF SCIENCE

YEAR THIS DEGREE GRANTED FALL 1983

Permission is hereby granted to THE UNIVERSITY OF ALBERTA LIBRARY to reproduce single copies of this thesis and to lend or sell such copies for private, scholarly or scientific research purposes only.

The author reserves other publication rights, and neither the thesis nor extensive extracts from it may be printed or otherwise reproduced without the author's written permission.

THE UNIVERSITY OF ALBERTA

ACOUSTIC FINITE ELEMENT ANALYSIS OF AXISYMMETRIC COMBUSTION CHAMBERS

by

© SHELLEY ANNE LORIMER

A THESIS
SUBMITTED TO THE FACULTY OF GRADUATE STUDIES AND RESEARCH
IN PARTIAL FULFILMENT OF THE REQUIREMENTS FOR THE DEGREE
OF MASTER OF SCIENCE

DEPARTMENT OF MECHANICAL ENGINEERING

EDMONTON, ALBERTA
FALL 1983

THE UNIVERSITY OF ALBERTA

FACULTY OF GRADUATE STUDIES AND RESEARCH

The undersigned certify that they have read, and recommend to the Faculty of Graduate Studies and Research, for acceptance, a thesis entitled ACOUSTIC FINITE ELEMENT ANALYSIS OF AXISYMMETRIC COMBUSTION CHAMBERS submitted by SHELLEY ANNE LORIMER in partial fulfilment of the requirements for the degree of MASTER OF SCIENCE in MECHANICAL ENGINEERING.

Dedication

To my parents

Pete and Norma Balascak

Abstract

A three-dimensional prism acoustic finite element was developed to model cavity resonances of three axisymmetric combustion chamber-cylinder configurations. The lowest cavity resonances were examined in detail as a function of cylinder depth.

Experimental models were constructed to compare experimental results to the finite element results for both cavity resonances and mode shapes for each configuration. In addition, analytical theory for a cylindrical enclosure was examined in some detail. Agreement between experimental, finite element and analytical results was good for the lowest mode.

Acknowledgements

The most important contributions to a project such as this are the unseen contributions of other individuals that one receives throughout. Without the guidance and support of my supervisor, fellow students and family, this thesis would have never been completed.

I would like to take this opportunity to express my utmost gratitude to Dr. A. Craggs for his patience, guidance and understanding throughout this entire project. Thanks also goes to Mr. M. Kamal and Mr. R. Hickling of General Motors Research Laboratories for their assistance throughout. I would also like to thank the Mechanical Engineering Department for providing financial support, Mr. L. Henderson of Student Awards where I obtained some financial assistance through a Province of Alberta Scholarship and as well to money provided by Dr. Craggs through an NSERC grant.

There are numerous computing services staff members, graduate students and technicians who provided assistance throughout this project. I will take this opportunity to thank each of them, although they are not specifically mentioned herein. Special thanks to T. Nord and A. Muir for their assistance with the experimental portion of the work.

I am extremely grateful to my mother who looked after my daughter. Without her assistance I would not have been able to successfully complete this undertaking. Last, but not least, I would like to thank my husband, Jerry, for his

encouragement to complete that which I set out to do.

Table of Contents

Chapter Page

List of Figures

Figure Page

List of Plates

Nomenclature

a	radius of cylinder
C	continuity specification
c	velocity of sound
f	natural frequency in Hertz
$\lfloor F \rfloor$	interpolation polynomial
$[G]$	natural co-ordinate matrix
$I(p)$	functional
J_m	Bessel function
$[J]$	Jacobian matrix
k	ratio of specific heats
L_x, L_y, L_z	reference lengths
m	number of nodes of an element
Mode (mnz)	mode specification
$\lfloor N \rfloor$	interpolation or shape function
p	acoustic pressure
$\{p\}$	acoustic pressure column vector
$[P]$	potential energy matrix
R	gas constant
(r, θ, z)	cylindrical co-ordinate system
$[S]$	kinetic energy matrix
t	time
T	temperature
W_i, W_k	weighting factors
(x, y, z)	global co-ordinate system or cartesian co-ordinate system
α_{mn}	frequency coefficients

∇^2	Laplacian operator
(ξ,η,ζ)	natural co-ordinate system
ω	natural circular frequency
$(\omega/c)^2$	non-dimensional eigenvector
$\lfloor \; \rfloor$	row vector
$\{ \; \}$	column vector
$[\;]$	matrix
$[\;]^T$	transpose matrix
$[\;]^{-1}$	inverse matrix
$[^{-1}]^T$	transpose of inverse matrix
$\det[\;]$	determinant of a matrix

1. INTRODUCTION

1.1 Engine Knock Related to Acoustics

Knock in the internal combustion engine is a phenomenon which has received considerable attention in the past. Engine knock is described as gas vibrations caused by a rapid pressure rise in the combustion chamber of the engine (1,2,3). An audible noise or "ping" emanates from the engine as a result of the vibrations of the gas-cylinder system at frequencies of the order of 5,000 Hz. A detailed discussion of engine knock is given by Obert (2). He describes several of the undesirable characteristics of engine knock, such as engine component vibration, scrubbing action on the chamber walls and localized overheating, which suggest that knock should be avoided in the combustion engine. Knock prevention has generated a need to determine some of the theoretical characteristics of the knock phenomenon.

C.S. Draper (1) proposed a theory that engine knock was related to the lowest acoustical cavity resonance of the combustion chamber. Draper considered an engine which consisted of a circular cylinder with flat ends at right angles to the cylinder axis. His results indicated that the knocking frequency of the engine was the fundamental cavity resonance of the combustion chamber. This was an important conclusion as it provided a means to predict the frequency of engine knock by calculating the acoustical cavity

resonances of the combustion chamber-cylinder configuration. This information is required for design of suitable knock detection systems (4).

The results presented by Draper (1) were based on the analytical solution of the wave equation for a cylindrical enclosure as given by Morse (5). Many combustion chambers are not simple cylindrical enclosures. The Internal Combustion Engine (6), shows a selection of various combustion chambers. Often, the diameter of the combustion chamber differs from that of the engine cylinder. As knock occurs near top dead center (2), see Figure 1.1, and continues for a portion of the stroke, the combined geometry of the combustion chamber and cylinder at various piston positions (i.e. cylinder depths) must be studied to completely describe the engine knock phenomenon. A study on knock in spark ignition engines (3), mentions the dependence of the knocking frequency on piston position shown by earlier investigators (7).

The study of combustion chamber-cylinder configurations, such as those shown in reference (6) is extremely difficult using the method developed by Draper. The difficulty stems from the irregular boundary of the combustion chamber-cylinder configuration. The solution provided by Draper was for an axisymmetric cylinder solved analytically using the wave equation in cylindrical co-ordinates with the given boundary conditions. There are inherent difficulties in describing a combustion chamber

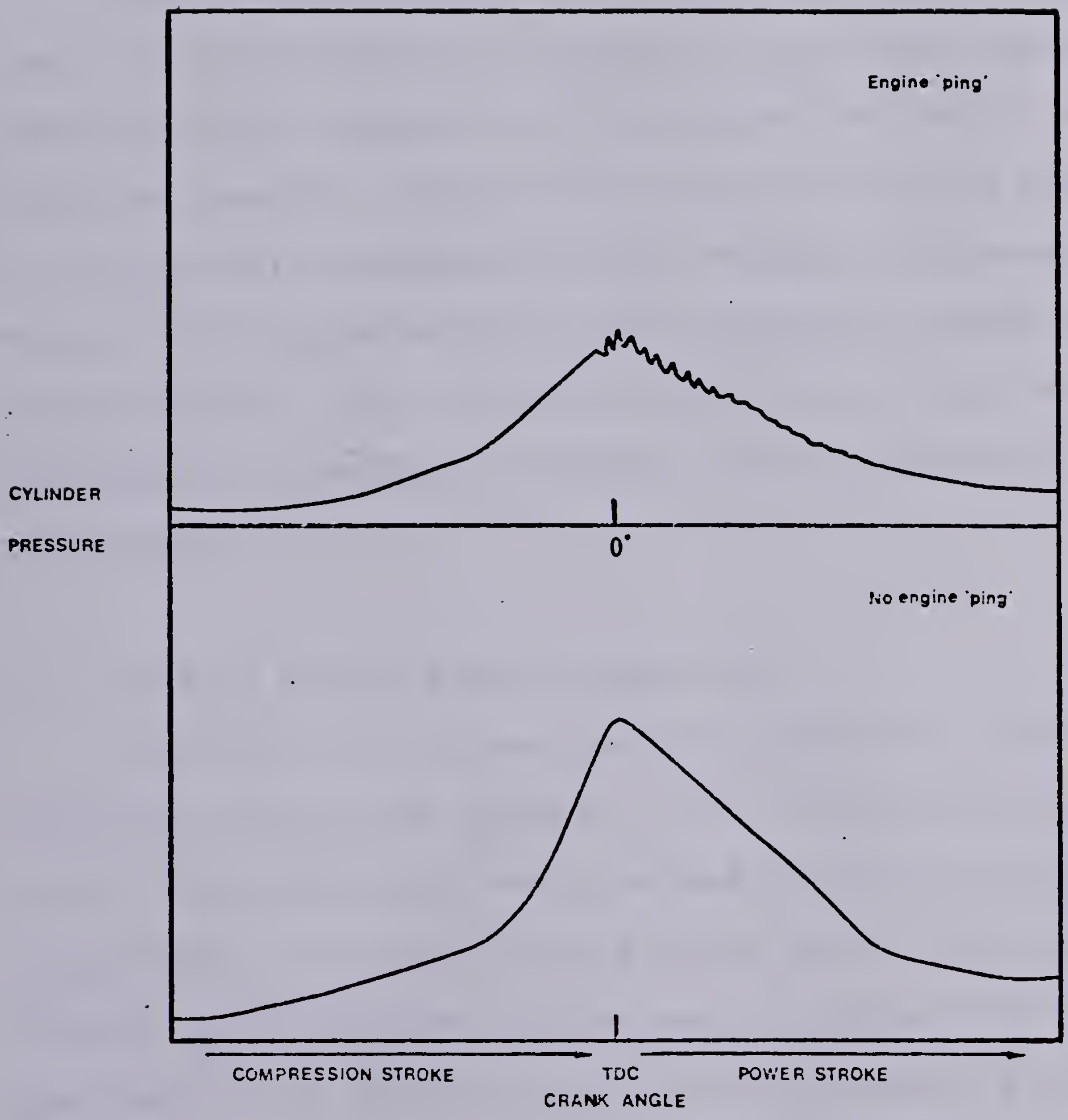

Figure 1.1 Engine Knock as a Function of Cylinder Depth

-cylinder configuration if the diameter of the combustion chamber differs from that of the cylinder. A technique which lends itself to solving these types of problems is the use of acoustic finite elements, as described by A. Craggs (8) to obtain an approximate numerical solution.

From the standpoint of cavity resonances, diesel and spark ignition engines are treated in the same manner, by considering the geometry of the combustion chamber and cylinder together. Because the cavity resonances are related to the geometry considered, this analysis is concerned mainly with the geometry of the combustion chamber-cylinder configurations rather than the engine operating conditions. Consequently, the study considers air in enclosures at room temperature.

1.2 Acoustic Finite Element Modelling

Acoustic finite elements were presented in their simplest form by G.M. Gladwell (9). A one-dimensional column of air with rigid ends was examined to evaluate the natural frequencies using the finite element method. The finite element approximations of the natural frequencies for the one-dimensional problem were in good agreement with the acoustic theory. This spurred further examination into the usage of acoustic finite element modelling.

The acoustic finite element method was extended to three-dimensional problems by A. Craggs (8). Different acoustic finite elements were used to determine the natural

frequencies and mode shapes of complex shaped enclosures. Good agreement was shown between the finite element predictions and experimental results.

Because of the relationship of engine knock to acoustical cavity resonances (1), acoustic finite elements were used to model combustion chamber configurations (4,10,11). These studies showed good agreement between acoustic finite element model predictions and experimental results for various shapes of combustion chambers.

Hickling et al (4) proposed that additional investigation should be done on the nodal patterns of the cavity resonances within the cylinder during a cycle, or, in other words, as a function of cylinder depth. Craggs et al (11) investigated the cavity resonances and mode shapes for a Chevette engine combustion chamber as a function of cylinder depth. This provided the impetus for this research.

1.3 Purpose of the Research

The purpose of this research is to examine the cavity resonances of three axisymmetric combustion chamber-cylinder configurations, see Figure 1.2, as a function of cylinder depth using acoustic finite elements. The combustion chambers have the same volume [1] and the cylinders have the same diameter. One combustion chamber, Figure 1.2a , has a larger diameter than the cylinder. In Figure 1.2b the combustion chamber has the same diameter as the cylinder and

---

[1] The volumes of the combustion chambers were selected to depict a compression ratio = 9.

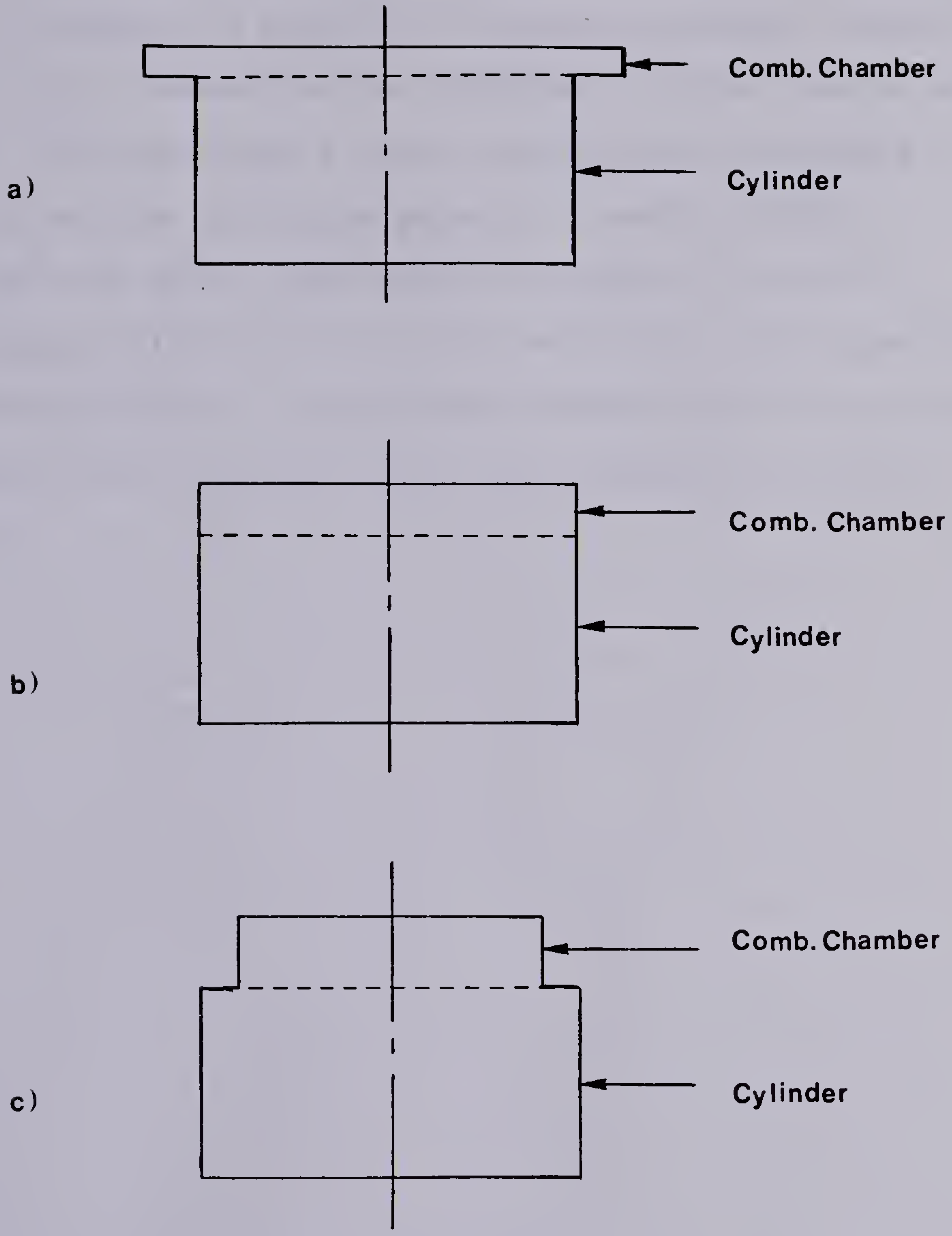

Figure 1.2 Combustion Chamber-Cylinder Configurations

in Figure 1.2c the combustion chamber has a smaller diameter than the cylinder. In each of the cases considered, several of the natural frequencies for different cylinder depths are examined. The mode shape for the lowest mode is examined in detail for each of the three cases at a small cylinder depth. The form of the mode shape is needed in order to obtain the best location for knock detectors. This research is concentrated on the lowest mode because engine knock has been shown to be related to the lowest acoustical cavity resonance.

2. ACOUSTIC THEORY

2.1 Basic Acoustic Theory

Some of the fundamental concepts which are discussed throughout this report are those associated with standing waves of sound in three-dimensional enclosures. An excellent description of sound in enclosures is given by Morse (5). A brief summary of some of the acoustical terminology follows.

Acoustic pressure is defined as the pressure in excess of the ambient, see Figure 2.1. Zero acoustic pressure indicates that there is no excess pressure. In acoustic terms, a "nodal surface" is a three-dimensional surface where the acoustic pressure is zero.

Sound is defined as fluctuations in the acoustic pressure due to some vibrating source. The vibrating source creates compressions and rarefactions in the medium, in this case air, which are defined as wave motion. The speed of propagation of sound waves, in a given medium, is defined as the velocity of sound. It is a function of the density, pressure and temperature of the medium. This study concentrates on sound waves in air. The velocity of sound in air is given the symbol c:

$$c = \sqrt{kRT}$$

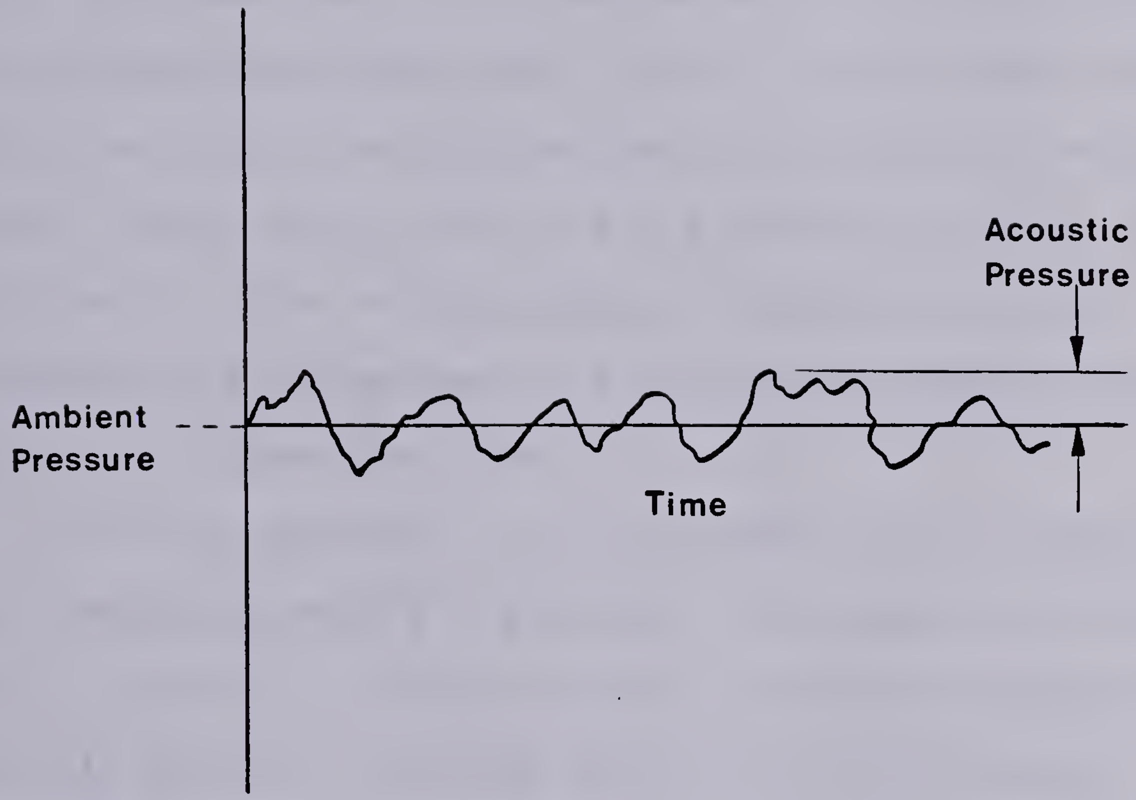

Figure 2.1 Acoustic Pressure

where

k = the ratio of specific heats of air = 1.4

R = the gas constant for air = 287 J/kg-°K

T = the absolute temperature = °C + 273 = °K

For this analysis, the results are given at T = 25 °C. Therefore, c is given the value 346 m/sec.

Three-dimensional enclosures containing air have normal modes of vibration. If a sound source is placed within a three-dimensional enclosure, it will excite these modes of vibration similar to the excitation of standing waves on a string. These sound waves are a function of space (x,y,z) and time (t). The normal modes of vibration of air in an enclosure are variations in the acoustic pressure as a function of space and time.

For this analysis, it is assumed that the enclosures have perfectly smooth rigid walls. The boundary condition for a rigid wall is such that air velocity perpendicular to the wall is zero. The wave equation in rectangular co-ordinates (5) is given as:

$$\frac{\partial^2 p}{\partial x^2} + \frac{\partial^2 p}{\partial y^2} + \frac{\partial^2 p}{\partial z^2} = \frac{1}{c^2}\frac{\partial^2 p}{\partial t^2} \tag{2.1.1}$$

This is the partial differential equation of the acoustic pressure p(x,y,z,t). The rigid wall boundary condition is given as:

$$\frac{\partial p}{\partial n} = 0 \tag{2.1.2}$$

For the analysis of the combustion chamber-cylinder configurations, the variation in the acoustic pressure as a function of space only is used. The resulting equation is called the Helmholtz equation. The Helmholtz equation can be obtained from equation (2.1.1) using a separation of variables technique. Therefore, the differential equation used in this analysis is given in terms of the Laplacian operator as:

$$\nabla^2 p + \left(\frac{\omega}{c}\right)^2 p = 0 \tag{2.1.3}$$

with the same boundary condition as given by equation (2.1.2), or:

$$\overline{n} \cdot \nabla p = 0 \tag{2.1.4}$$

Using the above differential equation (2.1.3) and the given boundary condition (2.1.4), the Helmholtz equation can be solved analytically for certain enclosures. The acoustic pressure p can be found in closed form solution as a function of the spatial co-ordinates. Morse (5) deals specifically with the solution for rectangular and cylindrical enclosures.

For a rectangular enclosure, the Helmholtz equation in Cartesian co-ordinates is given as:

$$\frac{\partial^2 p}{\partial x^2} + \frac{\partial^2 p}{\partial y^2} + \frac{\partial^2 p}{\partial z^2} + \left(\frac{\omega}{c}\right)^2 p = 0 \qquad (2.1.5)$$

The solution as given by Morse (5) with a harmonic time variation exp($i\omega t$) is:

$$p = \begin{matrix}\cos\\ \sin\end{matrix}\left(\frac{\omega_x x}{c}\right) \begin{matrix}\cos\\ \sin\end{matrix}\left(\frac{\omega_y y}{c}\right) \begin{matrix}\cos\\ \sin\end{matrix}\left(\frac{\omega_z z}{c}\right) \qquad (2.1.6)$$

where the origin of the (x,y,z) co-ordinates is located at the centre of the enclosure. Equation (2.1.6) describes the acoustic pressure variation as a function of the spatial co-ordinates (x,y,z). The values ω_x,ω_y,and ω_z represent the natural circular frequencies of the waves in each of the three directions.

For a cylindrical enclosure, the Helmholtz equation in cylindrical co-ordinates is given as:

$$\frac{\partial^2 p}{\partial r^2} + \frac{1}{r}\frac{\partial p}{\partial r} + \frac{1}{r}\frac{\partial^2 p}{\partial \theta^2} + \frac{\partial^2 p}{\partial z^2} + \left(\frac{\omega}{c}\right)^2 p = 0 \qquad (2.1.7)$$

The solution as given by Morse (5) with a harmonic time variation exp($i\omega t$) is:

$$p = \begin{matrix}\cos\\ \sin\end{matrix}(m\theta) \cos\left(\frac{\omega_z z}{c}\right) J_m \left(\frac{\omega_r r}{c}\right) \qquad (2.1.8)$$

where the origin is located in the centre of one of the circular ends of the cylinder. Equation (2.1.8) describes the acoustic pressure variation as a function of the spatial co-ordinates (r,θ,z). The values ω_z and ω_r represent the

natural circular frequencies for waves in each of the three directions (ω_r encompassing both the r and θ directions). The quantity J_m represents the Bessel function which is described in detail by Morse (5). Since the Bessel function is not used explicitly in this analysis, the reader is referred to Morse (5) for further explanation if so required.

Equations (2.1.6) and (2.1.8) give the acoustic pressure variations for two different enclosures. These acoustic pressure variations have natural frequencies and mode shapes associated with them. For this analysis, the combustion chamber-cylinder configurations are examined as rigid enclosures and the natural frequencies are referred to as "cavity resonances". The mode shapes are important in establishing the location of zero acoustic pressure or "nodal surfaces". For the exact solutions the mode shapes are given by the sin/cos function for the rectangular solution (2.1.6) and by a cos/sin and Bessel function for the cylindrical enclosure (2.1.8).

At this point, the problem of determining cavity resonances for simple rigid enclosures has been described by a differential equation and boundary condition in terms of acoustic pressure. The solution yields natural circular frequencies and mode shapes obtained in closed form for rectangular and cylindrical enclosures.

Another important quantity in acoustic terms is the energy associated with the acoustic pressure waves. The

energy of the sound wave can be broken down into potential energy and kinetic energy (5). Using the derivation of energy intensity for a plane wave, the average potential and kinetic energies for a three-dimensional wave are as follows:

$$\text{Potential Energy} = \frac{1}{2\rho c^2} \int_{\text{volume}} p^2 dv \tag{2.1.9}$$

$$\text{Kinetic Energy} = \frac{1}{2\rho \omega^2} \int_{\text{volume}} (\nabla p)^2 \, dv \tag{2.1.10}$$

These equations represent the average energy of a simple harmonic acoustic pressure wave of frequency $f = \omega/2\pi$. These energies together represent the total average energy of sound waves in enclosures with rigid walls as there are no dissipative agencies associated with the pressure waves in rigid enclosures. The kinetic and potential energies take on a significant meaning in the finite element analysis.

2.2 Acoustic Theory as an Approximation to Complex Geometries

Acoustic theory is extremely important in understanding the concept of cavity resonances of enclosures. It is particularly important to be able to compare the results of numerical models to some exact solution, to establish bounds

for the numerical results. The object of this analysis is to model complex shaped combustion chamber-cylinder configurations of which there is no known closed form solution, to obtain cavity resonances and mode shapes. The exact solution for rectangular and cylindrical enclosures can be used to determine the convergence of the numerical method by modelling these enclosures and comparing the results to the exact solution. This procedure gives an indication as to the accuracy of the acoustic finite element models used.

It is for this reason that the solution of the Helmholtz equation for a cylindrical enclosure is used repeatedly throughout this analysis, even for the combustion chambers whose radii differ from that of the cylinder. The exact solution is used to establish upper and lower bounds for the numerical results. In the three cases considered, the combustion chamber and cylinder are axisymmetric cylindrical enclosures joined together to form a more complicated geometry (see Figure 1.2). At top dead centre, when the cylinder depth is negligible, the solution should be governed by the radius of the combustion chamber. This establishes a bound for the numerical results based on the analytical solution for a cylindrical enclosure with a radius equal to that of the combustion chamber. As the cylinder depth increases, such that the cylinder volume dominates, the solution should be governed by the radius of the cylinder. This establishes the second bound for the

numerical results. In the first case, the mode shapes for the combustion chamber should be similar to those for a cylindrical enclosure. In the second case, because the combustion chamber is present the mode shapes for a cylindrical enclosure cannot be used as an approximation. The effect of the combustion chamber on mode shapes of the combined geometry is unknown.

Rectangular and cylindrical enclosures will be dealt with in some detail in the next two sections.

2.3 On Rectangular Enclosures

Using equation (2.1.5) with the rigid wall boundary condition, the solution for the acoustic pressure variation in a rectangular enclosure as given by Morse (5) is given by equation (2.1.6). This leads to the following characteristic values of the natural frequencies in Hertz which represent the cavity resonances:

$$f_x = n_x c/2L_x$$
$$f_y = n_y c/2L_y \qquad (2.3.1)$$
$$f_z = n_z c/2L_z$$ [2]

This solution gives the characteristic values of a rectangular enclosure with spatial orientation and dimensions as shown in Figure 2.2. The lengths L_x, L_y, and L_z used to calculate the natural frequencies are as indicated.

---

[2] Note: n_x, n_y, and n_z = 0, 1, 2 . . . When n is even, the cosine function for the acoustic pressure variation is used. When n is odd, the sine function is used (5).

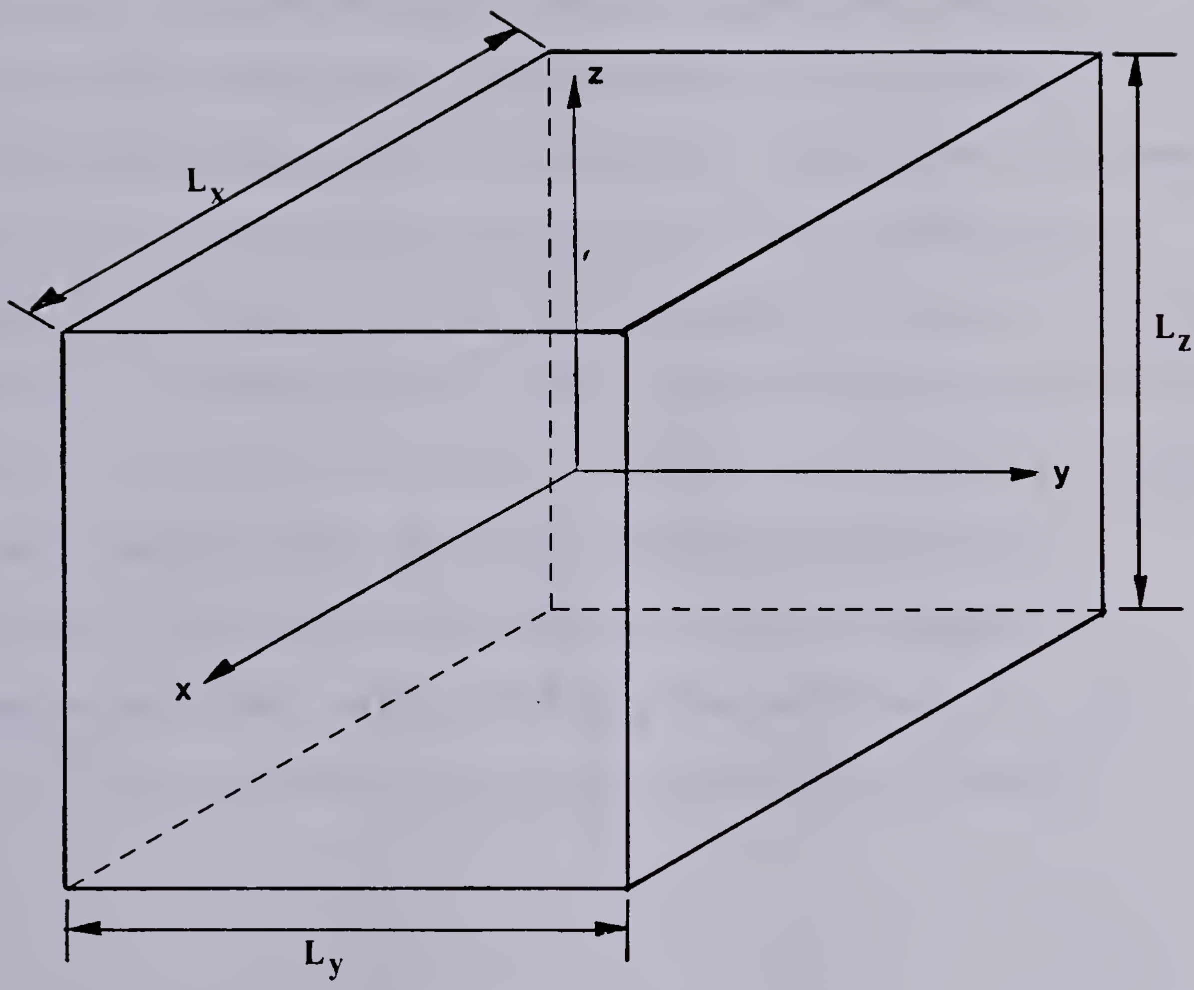

Figure 2.2 Dimensions and Co-ordinate System for a Rectangular Enclosure

The frequency of a given mode as given by Morse (5) is:

$$f = [\frac{c}{2} \left(\frac{n_x}{L_x}\right)^2 + \left(\frac{n_y}{L_y}\right)^2 + \left(\frac{n_z}{L_z}\right)^2]^{1/2} \tag{2.3.2}$$

The frequency f in Hertz can be calculated from the natural frequencies ω_x, ω_y, and ω_z according to equation (2.3.2) and knowing the velocity of sound in air at a given temperature. A characteristic value sometimes used to describe cavity resonances independent of c is $(\omega/c)^2$.

The mode shapes for a rectangular enclosure are given by Morse (5). A detailed description of the modes of a rectangular enclosure is not given here as they are not used explicitly in this analysis. The reader is referred to Morse (5) for a discussion of axial, oblique and tangential waves which are combinations of the aforementioned cavity resonances. The natural frequencies of rectangular enclosures are used later to study the accuracy of the acoustic finite element analysis compared to acoustic theory.

2.4 On Cylindrical Enclosures

Using equation (2.1.7) with the rigid wall boundary condition, the solution for the acoustic pressure variation in a cylindrical encosure as given by Morse (5) is given by equation (2.1.8). This leads to the following characteristic values of the frequency in Hertz:

$$f_z = n_z c/2L_z$$

$$f = \alpha_{mn} c/2a \qquad (2.4.1)$$

This solution gives the natural frequencies of a cylindrical enclosure with spatial orientation and dimensions as shown in Figure 2.3. The length L_z and radius 'a' given in the equations (2.4.1) to calculate the frequencies are as indicated. The values of α_{mn} are solutions to the equation

$$\frac{\partial J_m}{\partial \alpha}(\pi\alpha) = 0 \qquad (2.4.2)$$

which are related to the Bessel function described in equation (2.1.8). The procedure by which the values of α_{mn} are obtained is explained in detail by Morse (5). A table of various values of α_{mn} can be found in the same reference. For this analysis, α_{mn} for the lowest four modes is used. In Morse's derivation of α_{mn} the subscripts 'm' and 'n' denote the type of mode considered: 'm' represents the number of diametral nodal surfaces and 'n' represents the number of radial nodal surfaces. A similar description of modes is used in this analysis except three indices are used such that the axial modes are included.

Before proceeding further, a description of the various types of nodal surfaces is required. Figure 2.4 illustrates

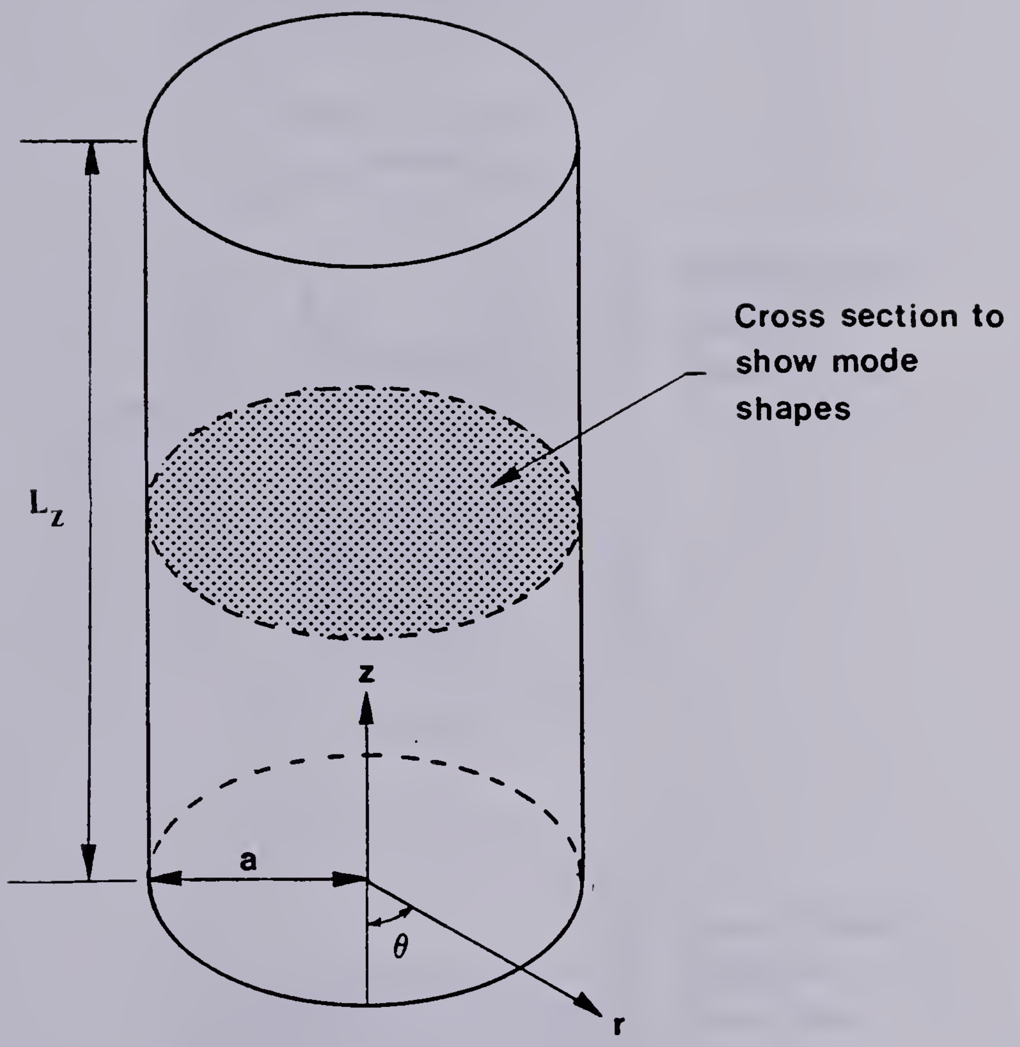

Figure 2.3 Dimensions and Co-ordinate System for a Cylindrical Enclosure

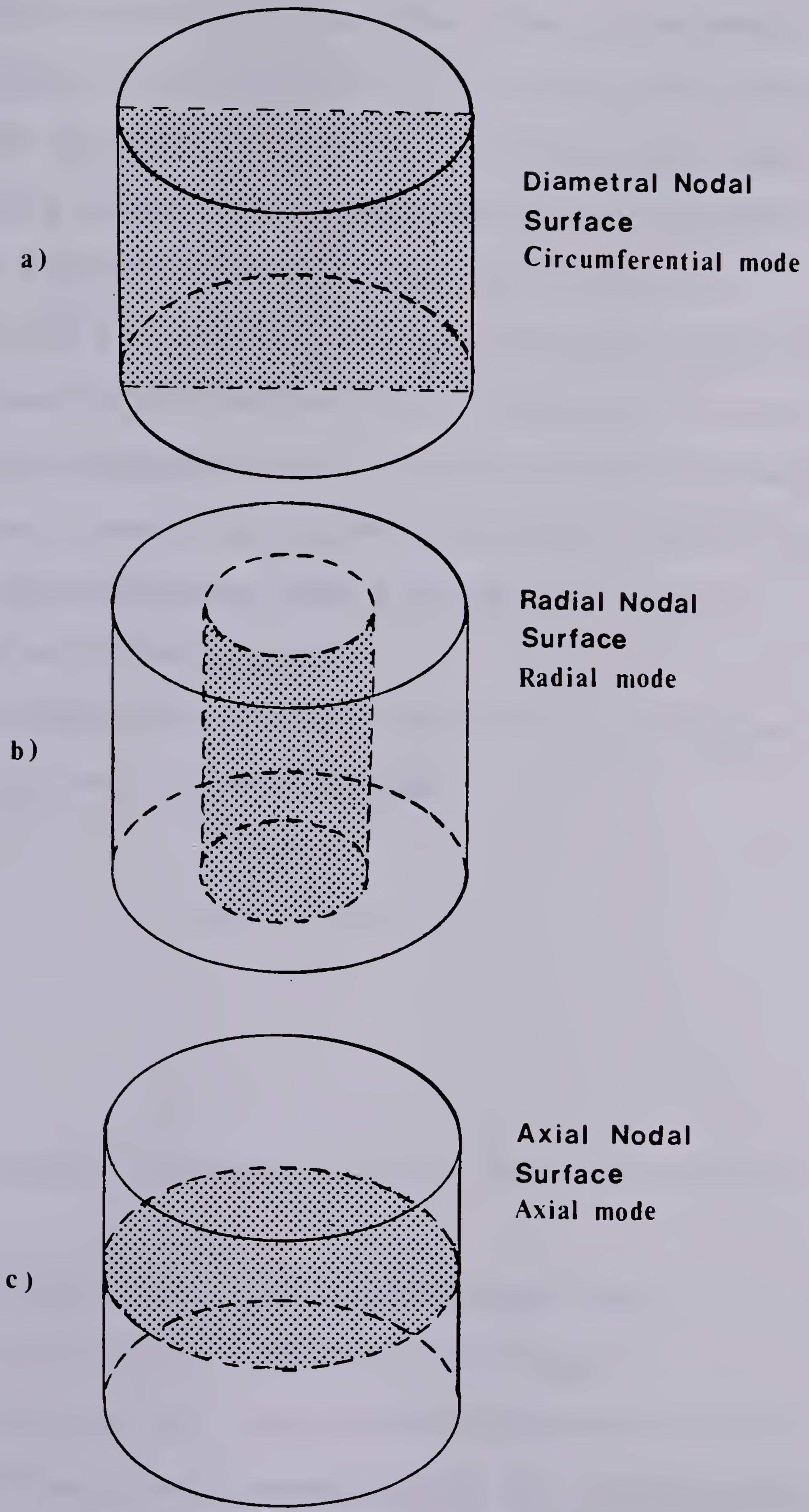

Figure 2.4 Three Basic Mode Types in a Cylindrical Enclosure

the three basic types of modes present in a cylindrical enclosure. Figure 2.4a has a diametral nodal plane which extends throughout the cylinder with no variation in the z direction. This is referred to as a circumferential mode. Figure 2.4b has a cylindrical nodal plane which extends throughout the cylinder with no variation in the z direction. This is referred to as a radial mode. Figure 2.4c has a nodal plane in the centre of the cylinder in the z direction. This is referred to as an axial mode. For each of these modes, the acoustic pressures on either side of the nodal surface have opposite phases similar to that of standing waves in a closed tube.

The three types of modes are referred to throughout this analysis in the following manner:

Mode (mnz)

where

m = number of diametral nodal surfaces (circumferential mode)

n = number of radial nodal surfaces (radial mode)

z = number of axial nodal surfaces (axial mode)[3]

As the values of 'm', 'n' and 'z' can each take on integer values from 0 to ∞, combinations of the different basic types of modes can exist. However, in this analysis,

---

[3] Nodal surfaces are surfaces of zero acoustic pressure.

which concentrates on the lowest modes, these combined modes are not considered. Mode (000) is the rigid enclosure mode which has a frequency of 0 Hz and is not considered to be the lowest mode of concern.

The circumferential and radial modes, as seen from equation (2.4.1) are dependent on the radius of the cylindrical enclosure. The axial modes are dependent on the axial length. For this analysis, the modes examined are the first three circumferential modes, the first radial mode and the first axial mode. Figure 2.5 shows cross sectional views of these modes in their relative order of magnitude. The nodal surface in three dimensions is projected as a dashed line in the plane cross section.

For the cylindrical enclosure, the lowest mode is the first circumferential mode (100) with one nodal diameter as shown in Figure 2.5a. Figure 2.5a shows a pair of modes for this frequency which are orthogonal to each other. From the analysis given by Morse (5) the circumferential modes occur in orthogonal pairs at the same frequency. Physically, this would mean that the location of the diametral nodal line is not fixed.

The next lowest mode is the second circumferential mode (200) which has two nodal diameters. Mode (200) and its orthogonal counterpart are illustrated in Figure 2.5b. The third mode is the first radial mode (010) which has one radial nodal surface as shown in Figure 2.5c. This mode exists without an orthogonal counterpart. Mode (300) is the

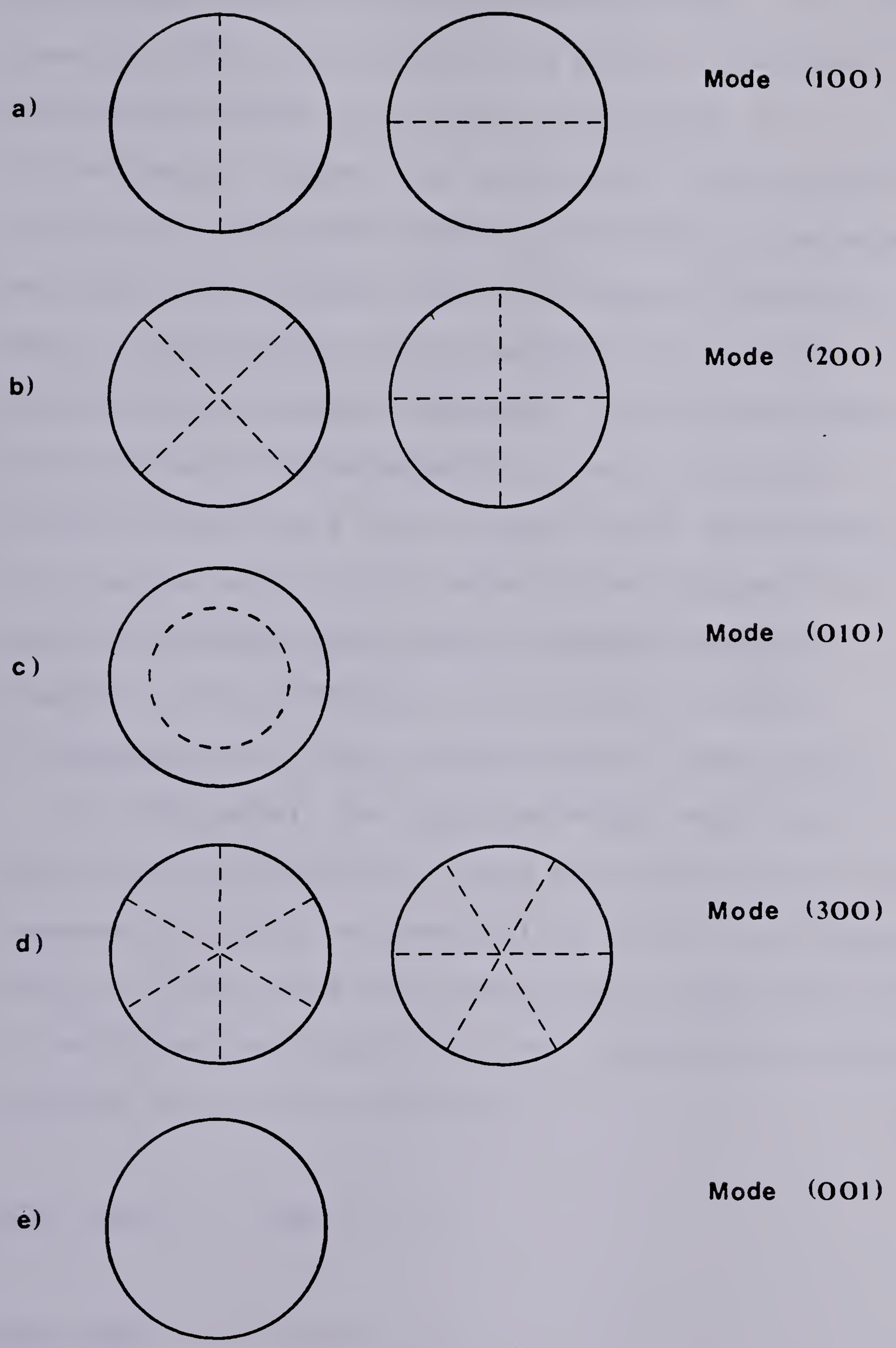

Figure 2.5 Cross Sectional Representation of the First Five Modes in a Cylindrical Enclosure

fourth mode which is a circumferential mode with three nodal diameters. This mode exists as a pair of orthogonal modes, of the same frequency similar to the other two circumferential modes. The axial mode (001) is placed fifth in order of magnitude. However, this mode is dependent on the axial length rather than the radius. Therefore, its order of magnitude varies depending on the length of the cylindrical enclosure considered. This becomes important in the analysis of the combustion chamber-cylinder configurations where the cylinder depth changes such that the relative order of the modes could change. Also, in more complicated geometries such as complex combustion chamber-cylinder configurations, purely radial, circumferential or axial modes may no longer exist.

At this point, the types of modes which exist in a cylindrical enclosure have been described. It is also necessary to obtain a numerical value for the frequencies which are associated with these modes. Using the values of α_{mn} obtained from Morse (5), the frequencies in Hertz are given as follows for each mode:

$$\begin{aligned} &\text{Mode (100)}\quad f = 0.5861\ c/2a \\ &\text{Mode (200)}\quad f = 0.9722\ c/2a \\ &\text{Mode (010)}\quad f = 1.2197\ c/2a \end{aligned} \tag{2.4.3}$$

Mode (300) $f = 1.3373\ c/2a$

Mode (001) $f = c/2L$

These values are provided for a cylindrical enclosure of length L and radius 'a'. A more detailed description of modes in cylindrical enclosures is given by Morse (5). For this analysis these modes or some combination thereof may be expected for the combustion chamber-cylinder configurations given.

3. FINITE ELEMENT THEORY

3.1 Basics

It is essential, in a study using acoustic finite elements, to have some knowledge of the finite element technique, in general. There are basic definitions which are used throughout the literature on finite elements which apply to this analysis. Three references have been used to obtain information on the finite element method, in general (12,13,14). Much of the work in these references is credited to various other authors.

It has been shown earlier that a continuum such as air in an enclosure can be represented by a governing equation and boundary condition (equations (2.1.3) and (2.1.4)) which often cannot be solved using analytical methods due to some irregular geometry. The idea behind finite element modelling of a continuum is to approximate the solution domain of the irregular geometry using a number of smaller regular shaped geometries (subdomains) such as cuboids, tetrahedrons or pyramids, and thereby approximate the solution to the governing equation and boundary condition using these subdomains. These smaller regular shaped entities are called elements.

In a continuum such as air in a rigid enclosure the unknown solution is the acoustic pressure variation throughout the enclosure. A continuum such as this is

composed of a infinite number of unknowns. Using finite elements, a continuum can be represented by an assemblage of elements which contain a finite number of unknowns (12).

The element is assigned a given number of nodes which represent the values of the unknown solution. For example, if a cuboid element is selected with nodes at each corner, eight values for the unknown variable can be found if one unknown per node is sought. In the analysis of combustion chamber-cylinder configurations, a knowledge of the acoustic pressure at various nodes provides an approximate solution to the problem. In finite element terminology, in this case, the acoustic pressure p, which is a scalar quantity, is the field variable.

There are numerous types of elements presented in the literature on finite elements. Pafec (15) and Zienkiewicz (12) give excellent references on the types of elements that can be used for different types of problems. The type of element which is selected is usually dependent on the desired accuracy of the solution, the geometry under consideration and even the availability of computer storage in solving the final matrix equations. Often, an element is used from the literature because its behaviour has been extensively studied. An element is said to be 'isoparametric' if it is capable of being distorted in a particular fashion. If the shape function used to distort an element is the same function used to approximate the field variable, the element is isoparametric.

Once the element type is chosen, an interpolation function is selected to satisfy certain continuity requirements. The interpolation function is the assumed approximation of the field variable over the element expressed in terms of the nodal values of the field variable. In this analysis, the interpolation function is a polynomial which is easy to integrate and differentiate. The degree of the interpolation polynomial depends on the number of nodes as well as the number of unknowns per node to satisfy continuity. Zienkiewicz (12) and Heubner (13) give detailed information from earlier work by other investigators on commonly used finite elements and their interpolation functions. The continuity requirements are described in these references on finite elements for the general case. Continuity requirements must be met so that the approximate solution converges to the exact solution as the number of elements increases.

Before discussing continuity requirements further, the relationship between the governing equation and the individual finite element must be found. Generally, throughout the literature on finite elements, there are four methods which are used to establish the finite element equations or matrix equations which represent the governing equation: 1) the direct approach, 2) Galerkin's method, 3) the variational approach and 4) the energy method (13). The method used for deriving the matrix equations depends on the nature of the problem. The variational procedure is

discussed here in some detail to give a brief overview of the mathematical nature of the finite element solution.

The variational procedure for deriving the finite element equations from the governing equation yields a volume integral which is called a functional. This functional represents the governing differential equation and boundary condition. In terms of the calculus of variations, if this functional is forced to have a stationary value, the unknown function which yields this stationary value is the approximate solution to the differential equation and boundary condition.

The functional is made stationary by taking the first variation and setting this equal to zero. This yields a set of matrix equations for the solution of the problem. The matrix equations contain volume integrations of the terms of the interpolation polynomial which are usually evaluated using numerical integration techniques.

The continuity requirements depend on the order of the derivatives appearing in the functional. The following continuity requirements for the interpolation function for functionals with (r+1)th derivatives must be met:

1) C^r continuity on element interfaces
2) $C^{(r+1)}$ continuity within an element

In addition to satisfying the continuity requirements, the numerical integration technique must be selected to evaluate the integrals in the finite element equations

within certain limits of accuracy. According to Cook (14), on the basis of previous work, if the numerical integration scheme evaluates the volume of the element exactly, this is an adequate integration scheme to assure convergence if the continuity requirements have been satisfied.

The matrix equations for a finite element represent the properties of an element according to the governing equation and boundary condition. To represent the entire continuum, the elements are assembled together knowing that the field variable is the same for common nodes of elements in the assemblage.

The assembly procedure yields a set of matrix equations which can be solved to obtain the unknown nodal values of the field variable. This is the basic procedure for obtaining a finite element solution to a given problem. An excellent reference giving detailed steps on finite element solutions is given in (13).

3.2 Acoustic Formulation of the Finite Element Equations

To determine the cavity resonances of combustion chamber-cylinder configurations, a solution to the Helmholtz equation (2.1.3) for the given boundary condition (2.1.4) must be obtained. The analytical solutions for rectangular and cylindrical enclosures have been discussed in some detail. A technique for establishing bounds for more complex geometrical configurations has been provided in Section 2.2. However, a more detailed description of the cavity

resonances as a function of cylinder depth for complex shaped combustion chamber-cylinder configurations has not been established.

The finite element method has been described as a method to approximate the solution to certain differential equations and boundary conditions. The procedure outlined in Section 3.1 is used to obtain the acoustic finite element equations.

By applying variational principles to equation (2.1.3) and satisfying the boundary condition equation (2.1.4), the following functional is obtained in terms of the acoustic pressure p:

$$I(p) = \frac{1}{2} \int_{\text{volume}} \left[(\nabla p)^2 - \left(\frac{\omega}{c}\right)^2 p^2 \right] dv \qquad (3.2.1)$$

This functional can be obtained using an energy approach as indicated by Gladwell (9).

The finite element equations are derived from the functional for one element. Often, the subscript (e) is used to denote that the equations represent one element; however, this notation will be suspended for this analysis. The reader should keep in mind that the resulting matrix equations represent an individual acoustic finite element.

In order to find a stationary value of the functional (3.2.1), an approximate solution must be assumed for the element (12). This approximate solution is given in terms of the interpolation polynomial described in Section 3.1, which

is chosen to satisfy the continuity requirements. For the acoustic problem, the interpolation function or the assumed approximation for the acoustic pressure variation should have

1) C^0 continuity on element interfaces, and
2) C^1 continuity throughout the element.

C^0 continuity exists if the field variable, acoustic pressure p, is continuous at element interfaces. C^1 continuity exists if the first derivatives of the field variable are continous, in addition to the field variable itself. This is the criterion which is used to select the interpolation polynomial for the acoustic finite element formulation. The interpolation polynomial is usually treated generally for the development of the matrix equations, and is referred to as a row vector $\lfloor N \rfloor$. The approximation for the acoustic pressure, then, takes the form:

$$p = \lfloor N \rfloor \{p\} \tag{3.2.2}$$

where {p} is a column vector representing the unknown acoustic pressure at each node of the element.

To minimize the functional I(p) in equation (3.2.1), the first variation of the functional is set to zero as described in Section 3.1.

$$\frac{\partial I(p)}{\partial p_i} = 0 \tag{3.2.3}$$

is used for i = 1,2, . . . m where 'm' is the number of nodes in the element.

Substituting equation (3.2.2) for the acoustic pressure in equation (3.2.1) and performing (3.2.3) the following matrix equations for an element are obtained:

$$([S] - (\frac{\omega}{c})^2 [P]) \{p\} = 0 \tag{3.2.4}$$

where

$$S_{ij} = \int\limits_{\text{volume}} \left(\frac{\partial N_i}{\partial x} \frac{\partial N_j}{\partial x} + \frac{\partial N_i}{\partial y} \frac{\partial N_j}{\partial y} + \frac{\partial N_i}{\partial z} \frac{\partial N_j}{\partial z} \right) dv$$

$$P_{ij} = \int\limits_{\text{volume}} (N_i N_j)\, dv \tag{3.2.5}$$

These are the finite element equations for an acoustic element in Cartesian co-ordinates (x,y,z). For this analysis, curved elements are needed to represent the curved boundaries of the combustion chamber-cylinder configurations. This transformation necessitates formulating the acoustic finite element equations in terms of a natural co-ordinate system (ξ,η,ζ). The transformation is a Jacobian transformation of a curved element in a global co-ordinate system (x,y,z) to a regular shaped element in a natural co-ordinate system (ξ,η,ζ) (see Figure 3.1) . This transformation is described by B.M. Irons in (12). To

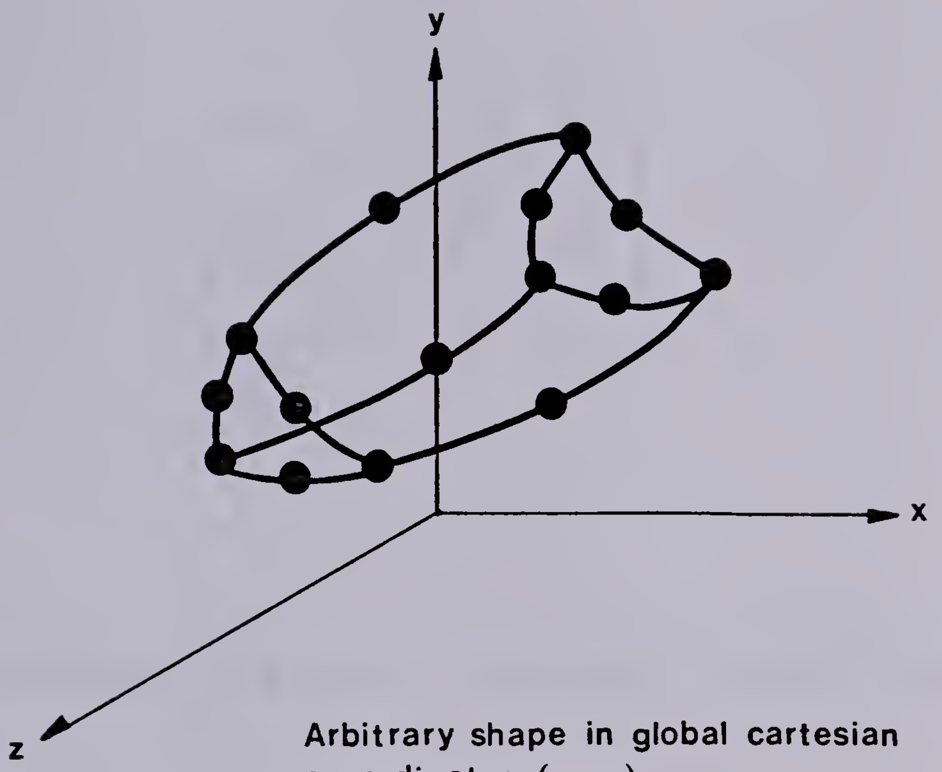

Arbitrary shape in global cartesian co-ordinates (x,y,z)

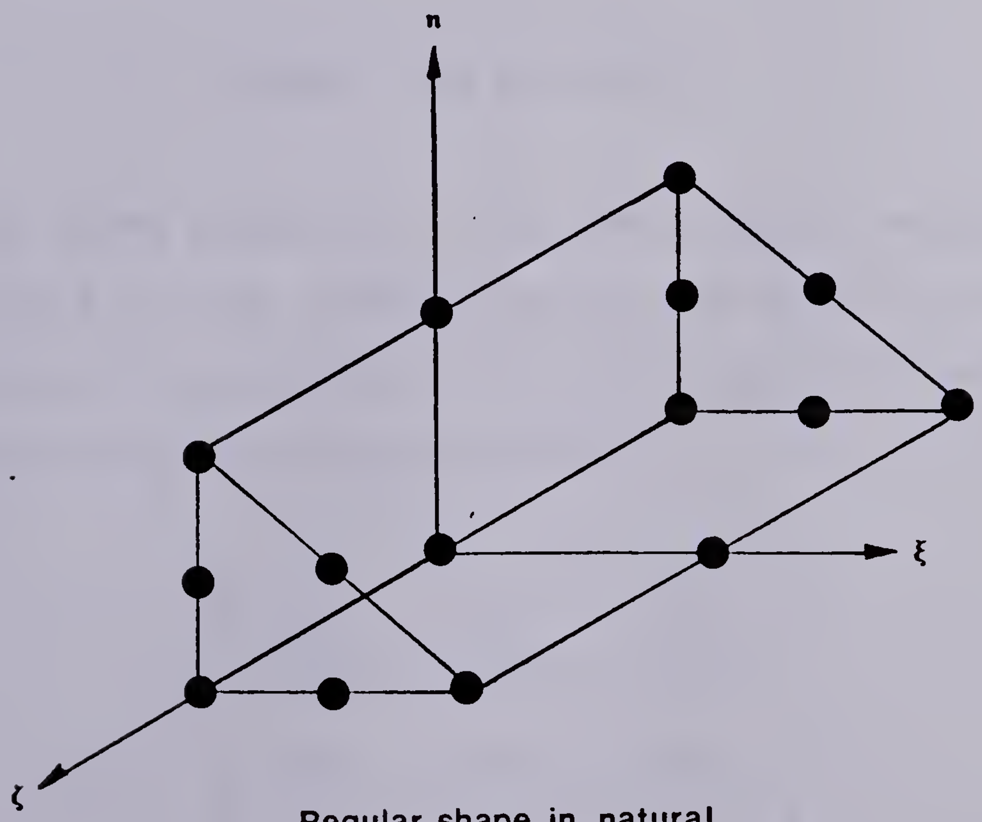

Regular shape in natural co-ordinates (ξ,n,ζ)

Figure 3.1 Jacobian Transformation

summarize, the global co-ordinate derivatives are found in terms of the natural co-ordinates in the following manner:

$$\begin{Bmatrix} \dfrac{\partial N_i}{\partial x} \\ \dfrac{\partial N_i}{\partial y} \\ \dfrac{\partial N_i}{\partial z} \end{Bmatrix} = [J]^{-1} \begin{Bmatrix} \dfrac{\partial N_i}{\partial \xi} \\ \dfrac{\partial N_i}{\partial \eta} \\ \dfrac{\partial N_i}{\partial \zeta} \end{Bmatrix} \qquad (3.2.6)$$

The volume integral is also transformed in the following manner:

$$dxdydz = \det [J] \, d\xi d\eta d\zeta \qquad (3.2.7)$$

In the above analysis $[J]$ is the Jacobian matrix, $[J]^{-1}$ is the inverse of the Jacobian matrix and $\det[J]$ is the determinant of the Jacobian matrix. The Jacobian matrix is formulated in the following manner:

$$[J] = \begin{bmatrix} \Sigma \dfrac{\partial N_i}{\partial \xi} x_i & \Sigma \dfrac{\partial N_i}{\partial \xi} y_i & \Sigma \dfrac{\partial N_i}{\partial \xi} z_i \\ \Sigma \dfrac{\partial N_i}{\partial \eta} x_i & \Sigma \dfrac{\partial N_i}{\partial \eta} y_i & \Sigma \dfrac{\partial N_i}{\partial \eta} z_i \\ \Sigma \dfrac{\partial N_i}{\partial \zeta} x_i & \Sigma \dfrac{\partial N_i}{\partial \zeta} y_i & \Sigma \dfrac{\partial N_i}{\partial \zeta} z_i \end{bmatrix} \qquad (3.2.8)$$

When the isoparametric formulation is used, as discussed in Section 3.1, $\lfloor N \rfloor$, which is the shape function in (3.2.6) and (3.2.8), is the same function used as the interpolation function for the acoustic pressure. The summations in (3.2.8) take place on i where i = 1, 2, . . . m and 'm' is the number of nodes.[4] Applying this transformation to the matrices in (3.2.5) gives the following matrix expressions in terms of the natural co-ordinate system (ξ,η,ζ) (see Figure 3.1):

$$
\begin{aligned}
[S] &= \int_{\text{volume}} \left(\left\lfloor \frac{\partial N}{\partial \xi}\ \frac{\partial N}{\partial \eta}\ \frac{\partial N}{\partial \zeta} \right\rfloor^T [J^{-1}]^T [J]^{-1} \left\lfloor \frac{\partial N}{\partial \xi}\ \frac{\partial N}{\partial \eta}\ \frac{\partial N}{\partial \zeta} \right\rfloor \det[J] \right) d\xi d\eta d\zeta \\
[P] &= \int_{\text{volume}} \left(\lfloor N \rfloor^T \lfloor N \rfloor \det\,[J] \right) d\xi d\eta d\zeta
\end{aligned}
\tag{3.2.9}
$$

In this case, the interpolation function of the acoustic pressure and the shape function are expressed in terms of the natural co-ordinate system (ξ,η,ζ). Equations (3.2.9) represent the matrices which describe an acoustic finite element in terms of the interpolation function $\lfloor N \rfloor$. The interpolation function can be broken down in the following form:

---

[4] x, y, and z represent the global co-ordinate values of the nodes.

$$\lfloor N \rfloor = \lfloor F \rfloor \, [G]^{-1} \qquad (3.2.10)$$

The interpolation function $\lfloor N \rfloor$ is expressed as the product of a row vector $\lfloor F \rfloor$ and an inverse matrix [G] of the natural co-ordinates (ξ, η, ζ) of each of the nodes expressed in terms of the polynomial $\lfloor F \rfloor$. This derivation of the interpolation function is explained in more detail in (13). In the derivation of the equations for a particular element, (see Section 4.1), the transformations are more easily understood. Substituting the expression for $\lfloor N \rfloor$ given in equation (3.2.10) into the matrix equations (3.2.9) gives the following result:

$$[S] = \int_{\text{volume}} \left([G^{-1}]^T \left\lfloor \frac{\partial F}{\partial \xi} \, \frac{\partial F}{\partial \eta} \, \frac{\partial F}{\partial \zeta} \right\rfloor^T [J^{-1}]^T [J]^{-1} \left\lfloor \frac{\partial F}{\partial \xi} \, \frac{\partial F}{\partial \eta} \, \frac{\partial F}{\partial \zeta} \right\rfloor [G]^{-1} \right.$$

$$\left. \det[J] \right) d\xi d\eta d\zeta \qquad (3.2.11)$$

$$[P] = \int_{\text{volume}} (\lfloor G^{-1} \rfloor^T \lfloor F \rfloor^T \lfloor F \rfloor \, [G]^{-1} \det\,[J] \; d\xi d\eta d\zeta$$

These matrices represent the acoustic finite element properties for an individual acoustic element. Matrix [S] represents a volume integral of the square of the gradient of the acoustic pressure. Matrix [P] represents a volume integral of the square of the acoustic pressure. Going back to the energy considerations of a sound wave in Section 2.1,

the [S] matrix represents the kinetic energy of an elemental enclosure and the [P] matrix represents the potential energy of an elemental enclosure. This result was obtained directly by Gladwell (9) using energy considerations only.

Once the element matrices are obtained, the elements can be assembled together summing up the contributions of kinetic energy and potential energy of common nodes. In this analysis, a computer subroutine is used to assemble elements together. Once the elements are assembled together a kinetic energy matrix and potential energy matrix are obtained which represent the entire enclosure with rigid boundaries. The matrix equation which is solved to obtain the acoustic cavity resonances (eigenvalues) of the enclosure and their associated mode shapes (eigenvectors) is:

$$([S] - (\frac{\omega}{c})^2 [P]) \{p\} = 0 \qquad (3.2.12)$$

This is an eigenvalue problem which is solved using a standard eigenvalue subroutine. The eigenvalues are obtained in terms of the non-dimensionalized natural frequency $(\omega/c)^2$. The order of the square matrices [S] and [P] is dependent on the number of nodes describing the total enclosure. This is the number of degrees of freedom of the solution which determines the number of eigenvalues and eigenvectors.

4. DEVELOPMENT OF ACOUSTIC ELEMENT PR15

4.1 Finite Element Equations for PR15

For the analysis of the combustion chamber-cylinder configurations, a three-dimensional isoparametric prism element was chosen to model the enclosures. The element is shown in Figure 4.1 , being referred to as element PR15. This element has fifteen nodes, or in other words, fifteen degrees of freedom. The element was chosen because its isoparametric form can easily model a pie shape.[5]

The interpolation function for element PR15 was derived similar to the procedure given by equation (3.2.10). The interpolation function was not used directly in computing the finite element equations, but rather the technique described in Section 3.2 was used where

$$\lfloor N \rfloor = \lfloor F \rfloor \, [G]^{-1} \qquad (4.1.1)$$

The polynomial $\lfloor F \rfloor$ was one used by Pafec (15). $\lfloor F \rfloor$ is a row vector expressed in terms of the natural co-ordinates (ξ, η, ζ) as follows:

$$\lfloor F \rfloor = \lfloor 1 \;\; \xi \;\; \eta \;\; \xi^2 \;\; \xi\eta \;\; \eta^2 \;\; \zeta \;\; \eta\zeta \;\; \xi\zeta \;\; \xi\eta\zeta \;\; \zeta^2 \;\; \xi^2\zeta \;\; \eta^2\zeta \;\; \xi\zeta^2 \;\; \eta\zeta^2 \rfloor \qquad (4.1.2)$$

---

[5] This is a desirable characteristic for modelling three-dimensional axisymmetric cylinders.

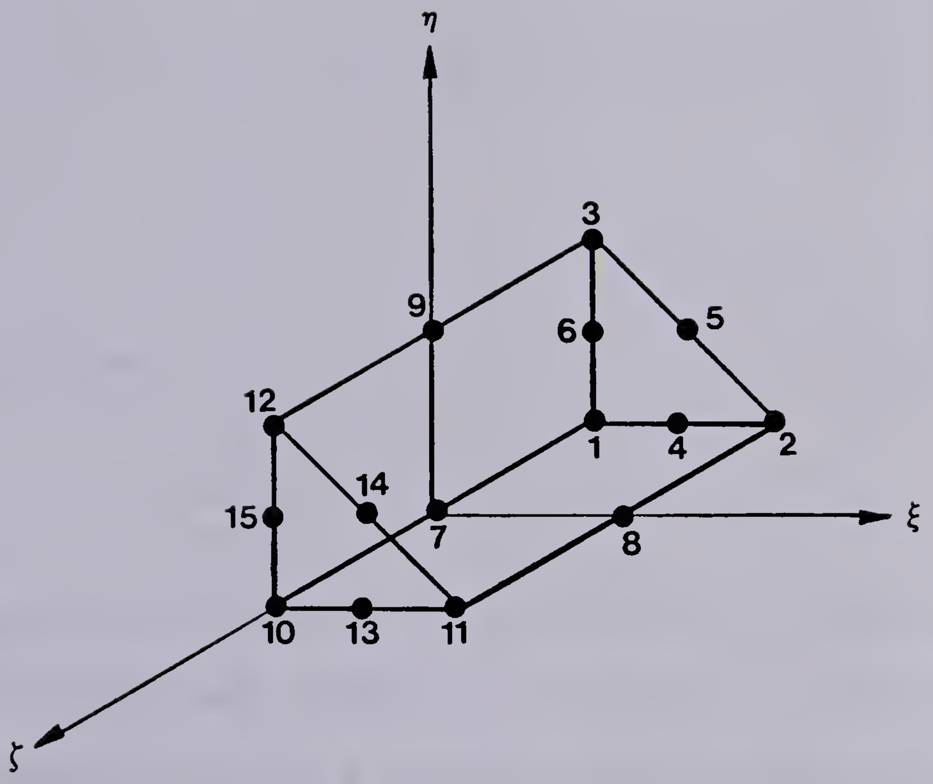

Limits of ξ; $0 \leq \xi \leq 1$
Limits of η; $0 \leq \eta \leq 1$
Limits of ζ; $^{-}1 \leq \zeta \leq 1$

Figure 4.1 Element PR15 in Natural Co-ordinates

Figure 4.1 shows element PR15 in the (ξ,η,ζ) co-ordinate system. The nodes are numbered in a specific order such that the the [G] matrix given in equation (4.1.2) was evaluated in the following manner:

$$[G] = \begin{bmatrix} 1 & \xi_1 & \eta_1 & \xi_1^2 & \xi_1\eta_1 & \eta_1^2 & \zeta_1 & \eta_1\zeta_1 & \xi_1\zeta_1 & \xi_1\eta_1\zeta_1 & \zeta_1^2 & \xi_1^2\zeta_1 & \eta_1^2\zeta_1 & \xi_1\zeta_1^2 & \eta_1\zeta_1^2 \\ 1 & \xi_2 & \cdots & & & & & & & & & & & & \eta_2\zeta_2^2 \\ 1 & & & & & & & & & & & & & & \\ \cdot & & & & & & & & & & & & & & \\ \cdot & & & & & & & & & & & & & & \\ \cdot & & & & & & & & & & & & & & \\ \cdot & & & & & & & & & & & & & & \\ 1 & \xi_{15} & \eta_{15} & \xi_{15}^2 & \xi_{15}\eta_{15} & \cdots & & & & & & & & & \eta_{15}\zeta_{15}^2 \end{bmatrix} \tag{4.1.3}$$

The subscripts of the natural co-ordinates in the [G] matrix correspond to the node numbers in Figure 4.1. This system of numbers was used so that a computer subroutine could be written to evaluate the element properties for numerous elements by repeatedly using this scheme. The matrix [G] is a 15 x 15 matrix containing the natural co-ordinates. The inverse of this matrix was obtained using a standard computer subroutine.

To evaluate the element matrices given in equations (3.2.11), which consist of volume integrals, a numerical integration scheme was used. Instead of the traditional numerical integration schemes for a triangle presented in references on finite elements (13), a modified approach was implemented.

The integration scheme is shown in Figure 4.2. The element triangular face was subdivided in the $\xi\eta$ plane, see Figure 4.2a, into 16 triangles of equal area. The value of the polynomial $\lfloor F \rfloor$ was evaluated at the centroid of each of the triangles and multiplied by a weighting factor. The weighting factor was equal to 1/16 of the area of the triangular face. In the ζ direction, see Figure 4.2b, a 3-point Gaussian quadrature (16) was used to evaluate the polynomial. The integration scheme allowed the volume integrals for the finite element equations to be evaluated numerically with computer subroutines.

The values of the polynomial $\lfloor F \rfloor$ were calculated at each of the integration points on three $\xi\eta$ faces as shown in Figure 4.2b. The Jacobian matrix [J], the inverse Jacobian and the determinant of the Jacobian were also evaluated at each of the integration points. Standard computer subroutines are used to evaluate the inverse matrix and determinant. The values of the parameters in the volume integral of the matrices given in equation (3.2.11) were evaluated at each integration point and the results summed together. The volume integrals can then be interpreted as a summation in the following form:

$$[S] = \sum_{k=1}^{3} \sum_{i=1}^{16} [G^{-1}]^T \lfloor \frac{\partial F}{\partial \xi} (\xi_i \; \eta_i \; \zeta_k) \; \frac{\partial F}{\partial \eta} (\xi_i \; \eta_i \; \zeta_k) \; \frac{\partial F}{\partial \zeta} (\xi_i \; \eta_i \; \zeta_k) \rfloor^T$$

$$[J(\xi_i \; \eta_i \; \zeta_k)^{-1}]^T [J(\xi_i \; \eta_i \; \zeta_k)]^{-1} \lfloor \frac{\partial F}{\partial \zeta} (\xi_i \; \eta_i \; \zeta_k) \frac{\partial F}{\partial \eta} (\xi_i \; \eta_i \; \zeta_k)$$

$$\frac{\partial F}{\partial \zeta} (\xi_i \; \eta_i \; \zeta_k) \rfloor \; [G]^{-1} \det [J(\xi_i \; \eta_i \; \zeta_k)] \; W_i W_k$$

$$[P] = \sum_{k=1}^{3} \sum_{i=1}^{16} [G^{-1}]^T \lfloor F(\xi_i \; \eta_i \; \zeta_k) \rfloor^T \lfloor F(\xi_i \; \eta_i \; \zeta_k) \rfloor \; [G]^{-1} \det[J(\xi_i \; \eta_i \; \zeta_k)] W_i W_k \qquad (4.1.4)$$

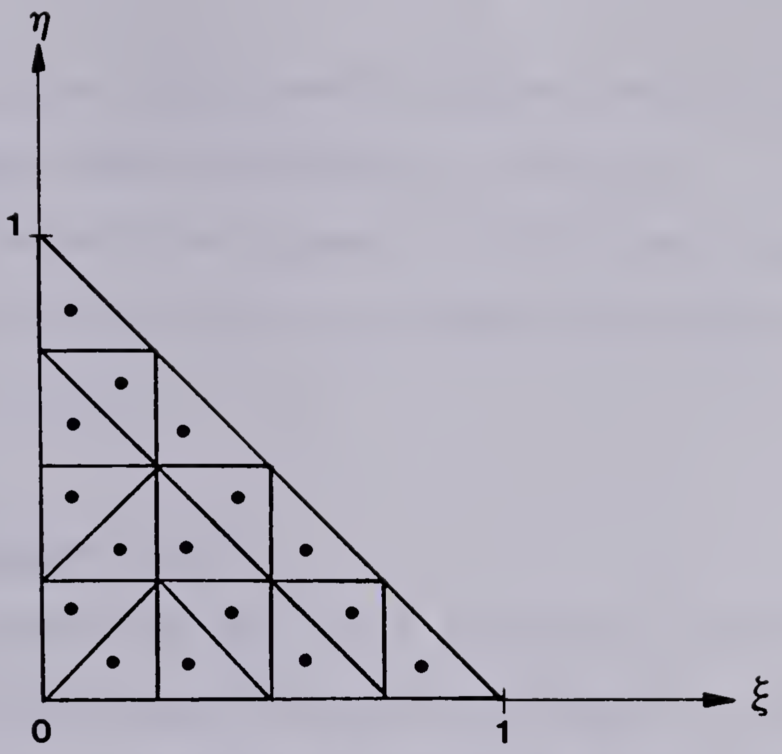

a)Integration on $\xi\eta$ face – 16 points

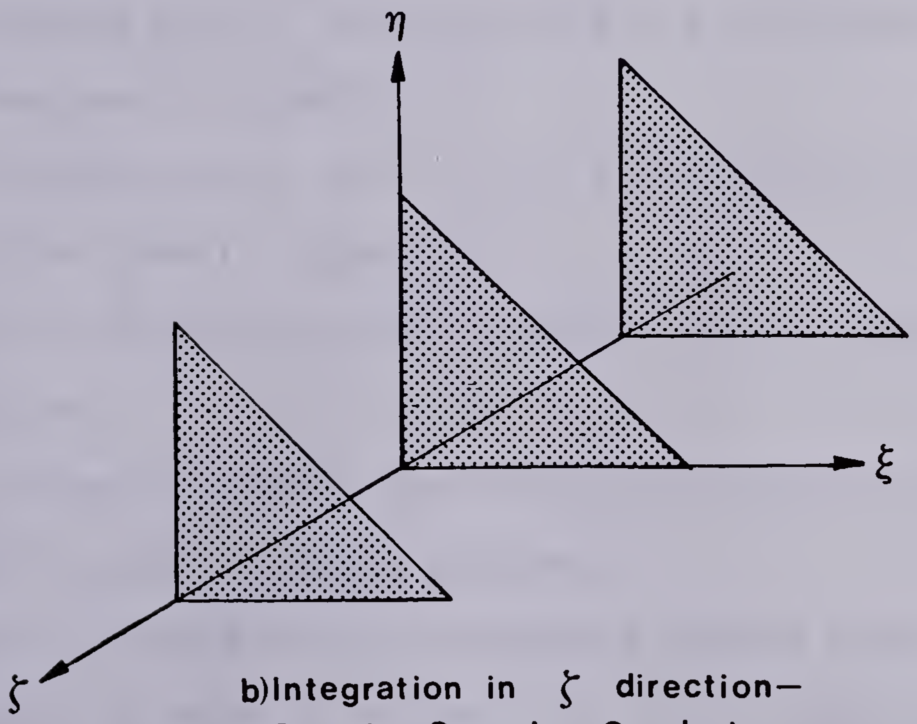

b)Integration in ζ direction– 3 point Gaussian Quadrature

Figure 4.2 Numerical Integration Scheme for PR15

These matrices give the acoustic properties of element PR15. By using element PR15 evaluated in natural co-ordinates transformed from global co-ordinates (x,y,z), computer subroutines were written to obtain the matrices given in equations (4.1.4).

4.2 Behaviour of Element PR15

An acoustic problem is set up in a global co-ordinate system (x,y,z). To illustrate the use of element PR15, a rectangular enclosure is presented composed of two PR15 elements. Figure 4.3 shows a cuboid with sides of length 1 mm.

The following information is required to calculate the cavity resonances and mode shapes by formulating the [S] and [P] matrices according to equations (4.1.4) through the use of the subroutines in Appendix 1.

1.(x,y,z) co-ordinates of each node, according to the number assigned to the node in Figure 4.1.

This is used in formulating the Jacobian matrix according to equation (3.2.8).

2. A global assembly matrix specifying the location of each of the nodes for the assembly process.

This is done according to the numbering system prescribed in the development of PR15 in Figure 4.1. This numbering system is used because the computer subroutines evaluate the element in the natural co-ordinate (ξ,η,ζ) system according to this scheme.

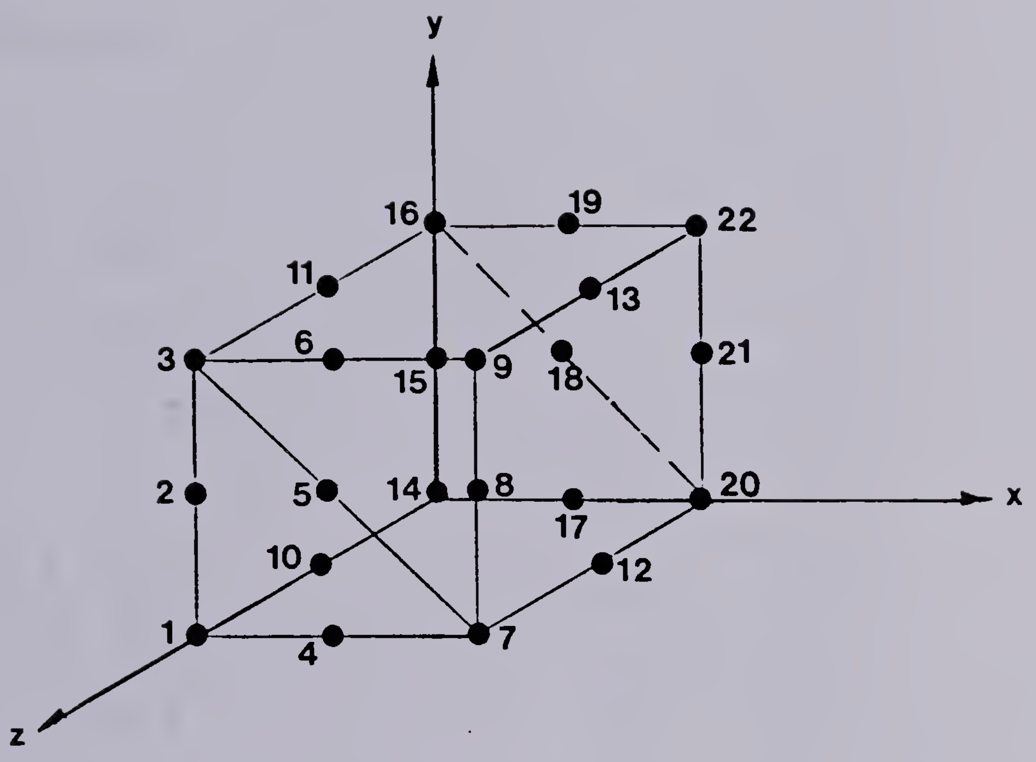

Figure 4.3 Sample Problem of a Rectangular Enclosure

The computer subroutines were written to numerically evaluate the [S] and [P] matrices for an element through two callable subroutines. The [S] and [P] matrices for the entire enclosure are assembled from the element matrices using the global assembly matrix in an assembly subroutine. For the problem of the rectangular enclosure the following data is used:

	X	Y	Z
1	0.0	0.0	0.0
2	1.0	0.0	0.0
3	0.0	1.0	0.0
4	0.5	0.0	0.0
5	0.5	0.5	0.0
6	0.0	0.5	0.0
7	0.0	0.0	0.5
8	1.0	0.0	0.5
9	0.0	1.0	0.5
10	0.0	0.0	1.0
11	1.0	0.0	1.0
12	0.0	1.0	1.0
13	0.5	0.0	1.0
14	0.5	0.5	1.0
15	0.0	0.5	1.0

Global Assembly Matrix (2,15)

14 20 16 17 18 15 10 12 11 1 7 3 4 5 2

22 16 20 19 18 21 13 11 12 9 3 7 6 5 8

The [S] and [P] matrices for each element are generated by calling the subroutines ES and EP. The subroutines are included in Appendix 1.

For the problem under consideration, there are 22 degrees of freedom. After the two elements have been assembled, the problem is solved by finding the eigenvalue solution to equation (3.2.12) for the given assembled matrices [S] and [P]. The are 22 eigenvalues in terms of $(\omega/c)^2$ and their associated eigenvectors. The results can be compared to acoustic theory by examining the frequencies for a rectangular enclosure using equations (2.3.1). A rigid enclosure mode $(\omega/c)^2 = 0.0000$ Hz should appear in the solution. The results for the rectangular enclosure are given below for the first 3 modes compared to the exact solution.

Numerical $(\omega/c)^2$	Exact $(\omega/c)^2$
00.0000	0.00
11.51343	9.86960
11.83771	9.86960

11.99967	9.86960

This method of evaluating the natural frequencies of an enclosure can be used to examine the convergence of element PR15. By increasing the number of elements, one would expect the solution to converge to the exact acoustic theory. From earlier considerations, the convergence of an element is dependent on the integration scheme, in addition to the continuity requirements of the interpolation polynomial (see Section 3.1). The volume of one PR15 element is evaluated numerically at a value of 0.499997973. This is slightly less than the exact value of 0.500000000. This indicates that the integration scheme is of a slightly lower order and the convergence may not be quite as expected, ie. the solutions may not converge monotonically from above (14).

The convergence of element PR15 was evaluated by modelling a rectangular enclosure (similar to the example) using an increasing number of elements. The behaviour of element PR15 was examined by increasing the number of elements first in the z direction and second in the y direction. Figures 4.4 & 4.5 show the configurations used to evaluate the convergence.

For the z direction, Figure 4.4, from 1 to 7 elements were specified. The convergence results are presented in Figure 4.4 for the first mode. The percentage error is given in terms of the exact solution for a rectangular enclosure of the given dimensions. The solution converges from above, but actually becomes slightly lower than the exact value for

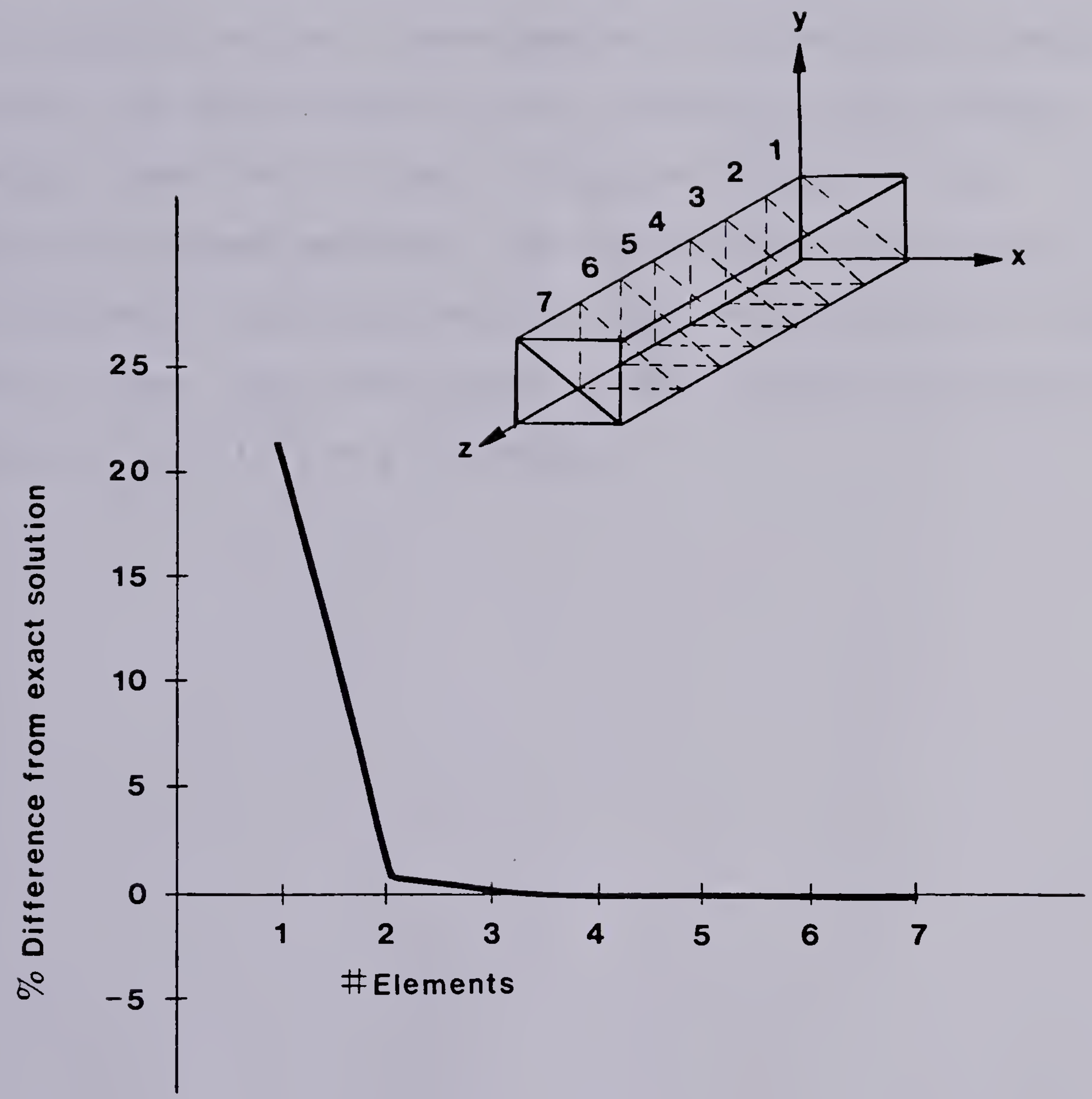

Figure 4.4 Z Convergence of PR15 for lowest mode

more than 5 elements.

For the y direction, Figure 4.5, from 1 to 5 elements were specified. The convergence results are presented in Figure 4.5 for the first mode. The percentage error is given, similar to the z convergence, in terms of the exact solution. The convergence in the y direction is slightly different from that in the z direction because of the integration scheme employed. The x direction convergence is not evaluated. From considerations of the integration scheme on the $\xi\eta$ face, the convergence in the x direction should be similar to that in the y direction.

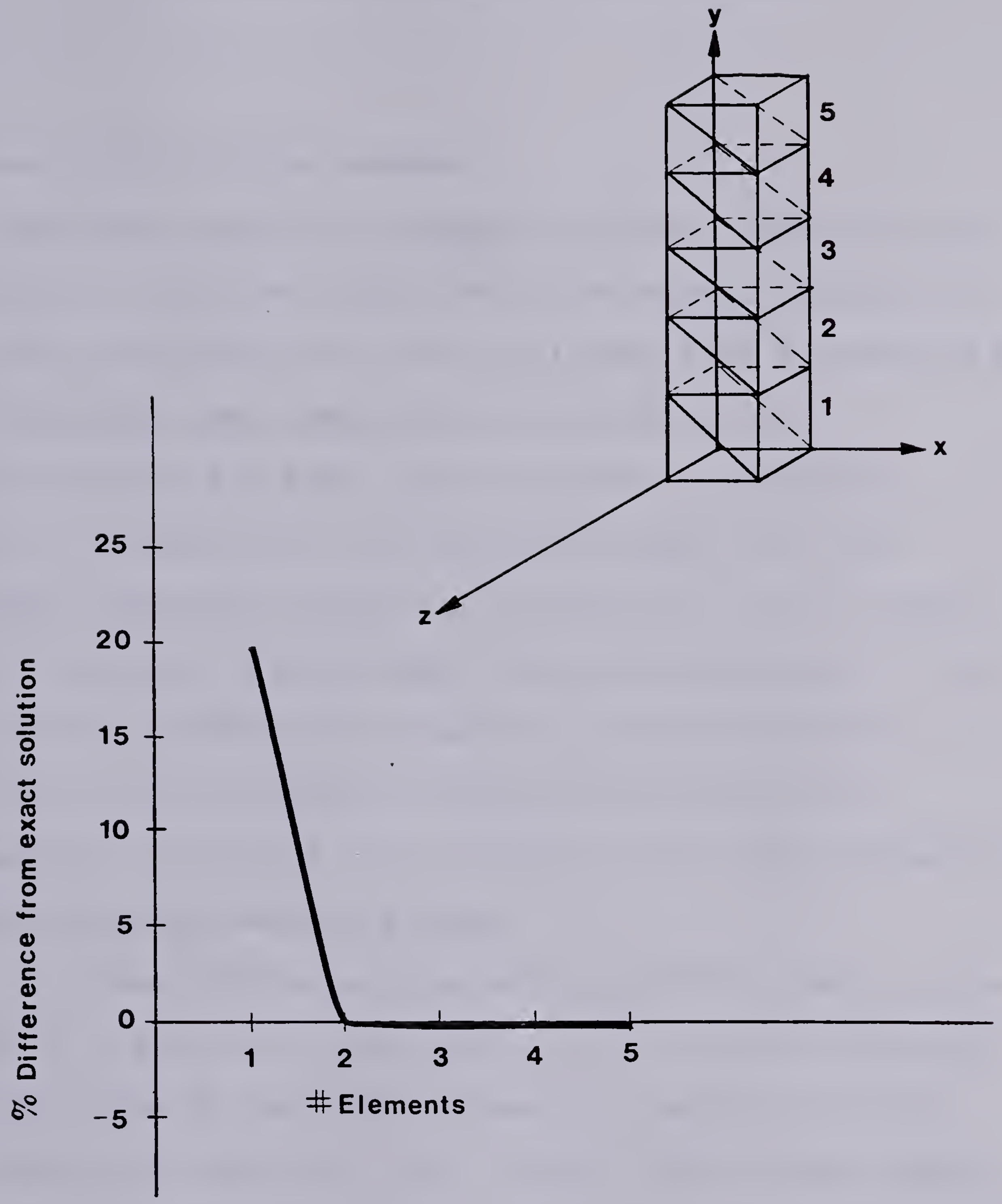

Figure 4.5 Y Convergence of PR15 for lowest mode

5. COMBUSTION CHAMBER-CYLINDER ANALYSIS

5.1 Description of the Problem

The three combustion chamber-cylinder configurations considered in this analysis are illustrated in Figure 5.1. All three configurations have a cylinder with a radius of 50 mm. This radius was arbitrarily selected to be characteristic of a spark ignition engine. Combustion chamber 1, Figure 5.1a, has a radius larger than the cylinder. Combustion chamber 2, Figure 5.1b, has a radius equal to that of the cylinder. Combustion chamber 3, Figure 5.1c, has a radius smaller than that of the cylinder. In each case, both combustion chamber and cylinder are axisymmetric cylinders. The volumes of the three combustion chambers are approximately equal.

The three configurations were selected to demonstrate trends in the cavity resonances as a function of cylinder depth and type of combustion chamber. The depth of the cylinder was varied from 1 mm - 50 mm. The smallest depth represents a top dead center configuration similar to that which occurs as the piston approaches the top of its stroke in an engine.

Combustion chamber 2 is of particular interest because the radius of the cylinder is equal to that of the combustion chamber. Therefore, this configuration is simply a cylindrical enclosure. The analysis given in Section 2.4

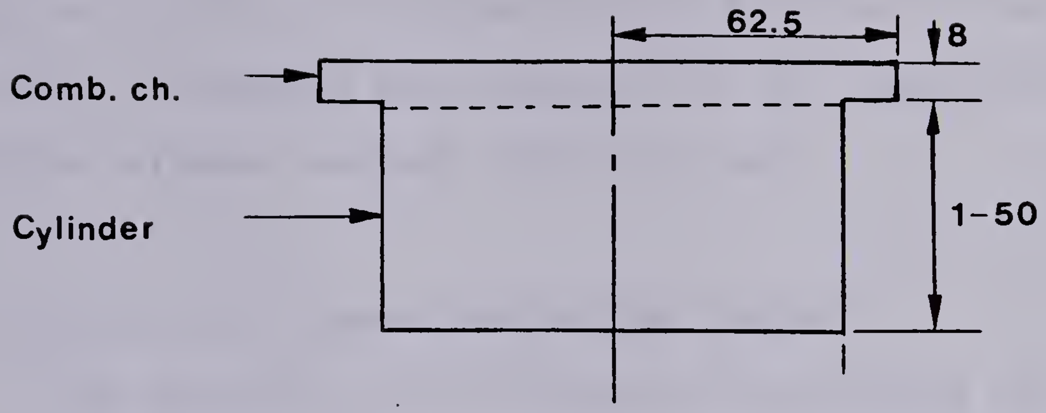

a) Combustion chamber-cylinder 1

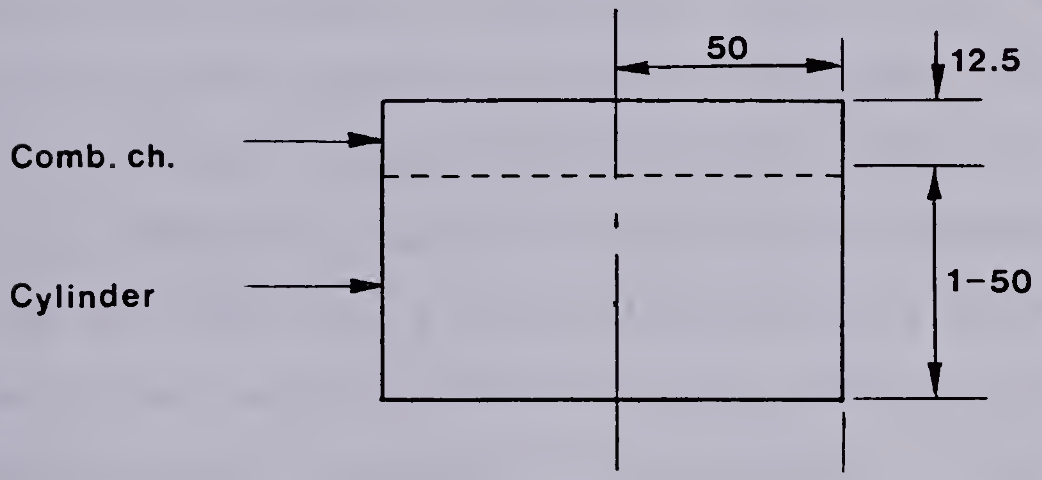

b) Combustion chamber-cylinder 2

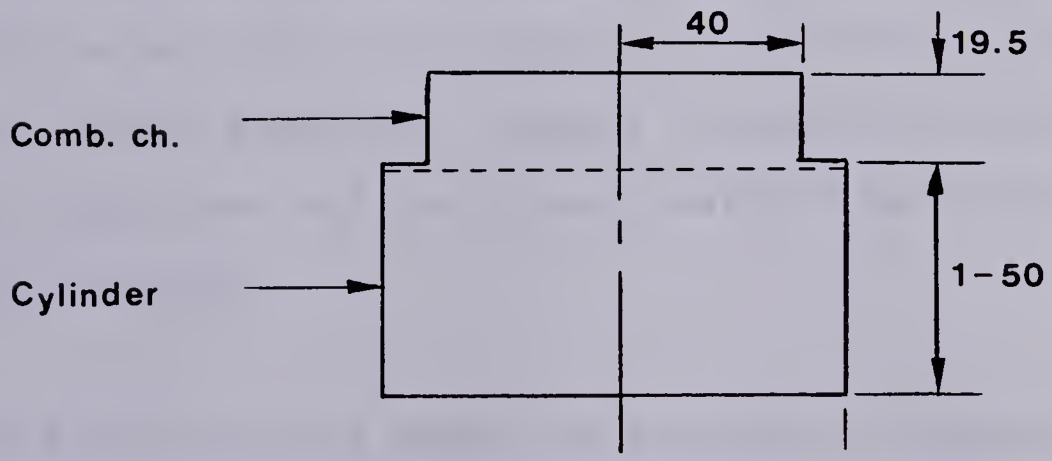

c) Combustion chamber-cylinder 3
All dimensions in mm

Figure 5.1 Combustion Chamber-Cylinder Dimensions

applies to this configuration and the analytical results can be used to examine the validity of the numerical technique (finite element method) which is used.

5.2 Analytical Approximation for Bounds

The analysis for cylindrical enclosures can also be used to establish bounds for the numerical results. Based on the dimensions presented in Figure 5.1, the bounds were determined in terms of frequency. These values were calculated from equations (2.4.3) for modes (100), (200), (010), and (300) substituting for the radius 'a', the radius of the combustion chamber or cylinder as indicated earlier.[6] The two bounds were joined together by a curve to give an idea of the behaviour of the cavity resonances using the approximation to compare to the numerical results.

The rigid enclosure mode was not considered and the axial modes were not examined, at this point, because the axial modes are a function of cylinder depth. This technique establishes bounds for complex combustion chamber-cylinder configurations and could even possibly be used as an approximation.

5.3 Finite Element Models of Axisymmetric Combustion Chamber-Cylinder Configurations

The three finite element models for the axisymmetric combustion chamber-cylinder configurations are presented in

---

[6] The radius of the combustion chamber gives one bound and radius of the cylinder gives another.

Figure 5.2. PR15 acoustic finite elements were used to model one half of the combustion chamber-cylinder configurations as indicated in Figure 5.2. The details of the actual models are not presented, that is, the global co-ordinates and assembly matrices. The standard procedures described in Section 4.2 were used to solve the problem.

The finite element models are slightly different for each configuration. Figure 5.2a shows a three-dimensional half chamber model composed of 24 elements. The bottom 6 elements have a variable depth to model different cylinder depths. This model represents combustion chamber 1. Figure 5.2b shows a three-dimensional half chamber model composed of 12 elements. The bottom 6 elements have a variable depth to represent the different cylinder depths. The second model represents combustion chamber 2. Figure 5.2c shows a three-dimensional half chamber model composed of 24 elements, where the bottom 18 elements have a variable depth. This configuration represents combustion chamber 3.

A computer program was used to evaluate the [S] and [P] matrices for each combustion chamber-cylinder configuration by assembling the individual elements shown in Figure 5.2. The eigenvalue problem given by equation (3.2.12) was solved for each system, for a given cylinder depth. The program was rerun to obtain several different cylinder depths giving the cavity resonances of each configuration as a function of cylinder depth.

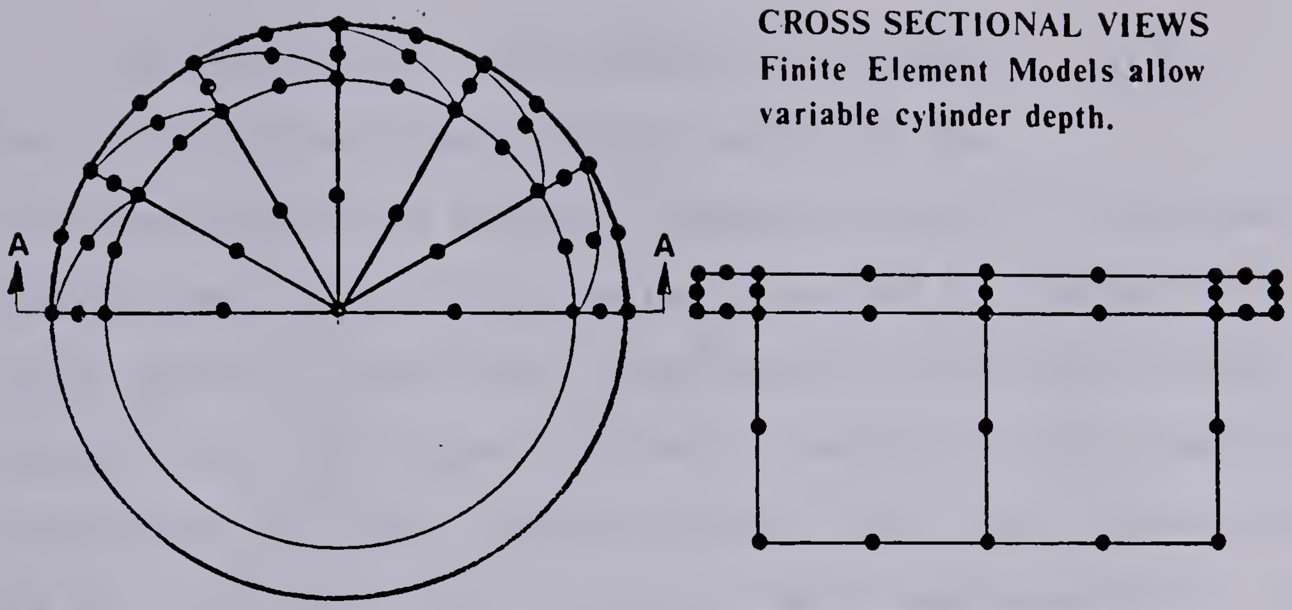

CROSS SECTIONAL VIEWS
Finite Element Models allow
variable cylinder depth.

a) Half-chamber model

Combustion chamber 1
Section A–A

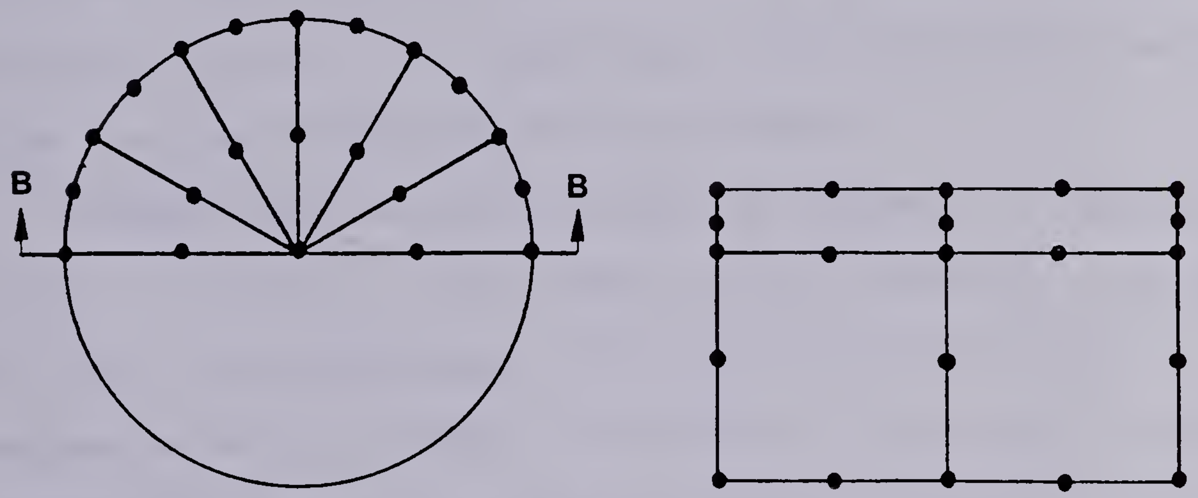

b) Half-chamber model

Combustion chamber 2
Section B–B

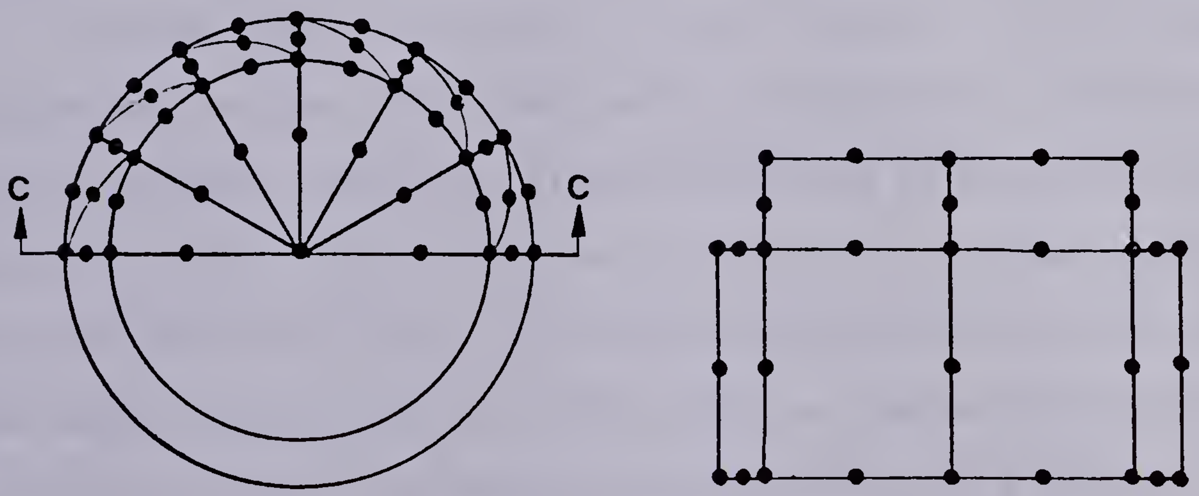

c) Half-chamber model

Combustion chamber 3
Section C–C

Figure 5.2 Finite Element Models of Combustion Chamber-Cylinders

The results for each combustion chamber-cylinder configuration were obtained in terms of the non-dimensionalized natural frequencies $(\omega/c)^2$, which are eigenvalues. These values were converted to frequency in Hertz using c = 346 m/sec. The computer subroutine used sorted the eigenvalues in order of magnitude from smallest to largest. For each configuration, the lowest value which was obtained was $(\omega/c)^2 = 0.0000$ which represents the rigid enclosure mode. These values were not used as a cavity resonance. Hence, the lowest mode considered was the lowest value next to the rigid enclosure mode.

Because the theory proposed by Draper (1) suggests that knock is related to the lowest cavity resonance, excluding the rigid enclosure mode, only the first few cavity resonances were examined. In terms of frequency, a range of 1,000-5,000 Hz was selected to examine the cavity resonances for cylinder depths ranging from 1 mm - 50 mm.

Another major concern in this analysis is the mode shapes associated with the cavity resonances. From the finite element results, eigenvalues and eigenvectors were obtained. The eigenvalues were the cavity resonances as already discussed and the eigenvectors were the mode shapes. The mode shapes give an indication of the acoustic pressure variation within the modelled enclosure for a given frequency. Values of the acoustic pressure were obtained for each node in the finite element model from the eigenvectors.

The mode shapes from the finite element results for the three different combustion chamber-cylinder configurations were examined at one specific depth of 4.5 mm at the cross section at the end of the cylinder. This depth represents a small cylinder depth such as that which might occur near top dead center. The finite element results show the acoustic pressure variation along the diameter of the configuration for a cross section taken at the bottom of the cylinder. The depth selected for the cylinder and the cross section examined were based upon foreknowledge of the experimental setup to allow for comparisons between the finite element method and measured values.

5.4 Experimental Models of Axisymmetric Combustion Chamber-Cylinder Configurations

A question of considerable importance in any mathematical analysis, be it numerical or analytical, is the validity of the analysis in comparison to experimental values. It is for this reason that experimental models were constructed to simulate the combustion chamber-cylinder geometries at various cylinder depths.

The experimental models are schematically shown in Figure 5.3. Photographs of the models follow the schematics in Plates 1- 3. The experimental models consisted of 200 mm x 200 mm panels of plexiglass with holes bored through the centers of inner dimensions comparable to the radii of the combustion chambers (see Figure 5.1) and cylinders. The

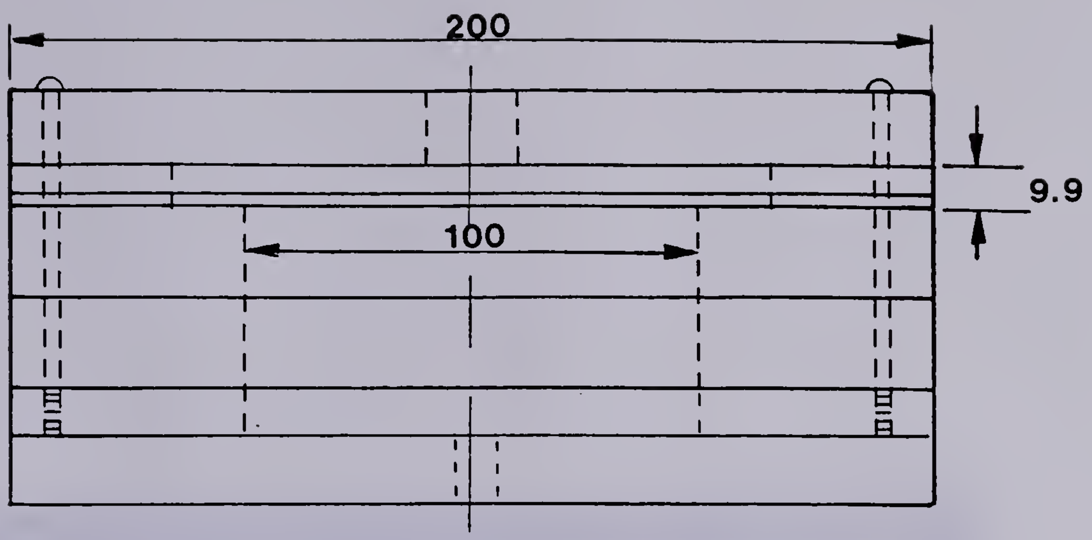

a) Combustion chamber 1

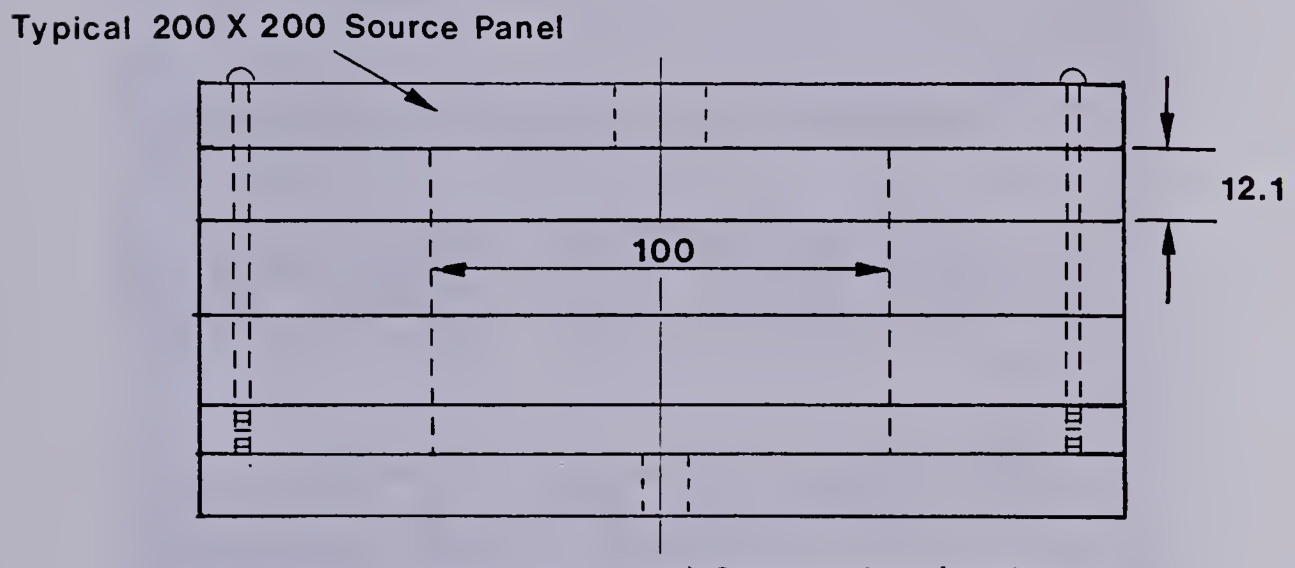

b) Combustion chamber 2

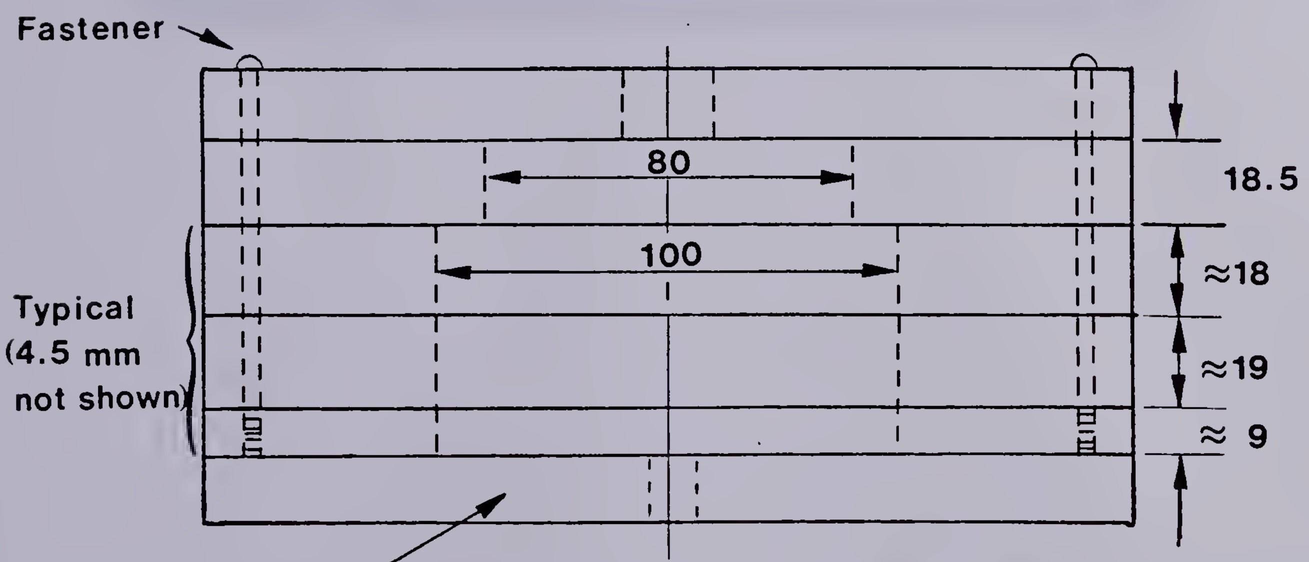

c) Combustion chamber 3

Figure 5.3 Schematic of the Experimental Models

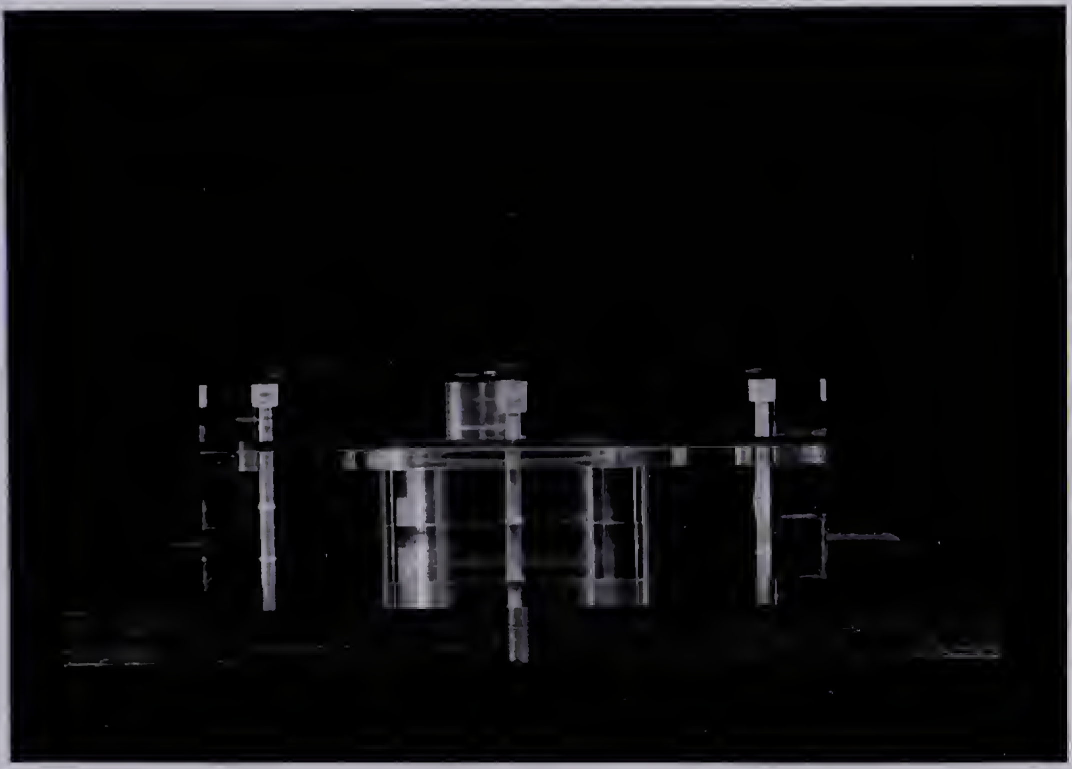

Plate 5.1 Experimental Model for Combustion Chamber 1

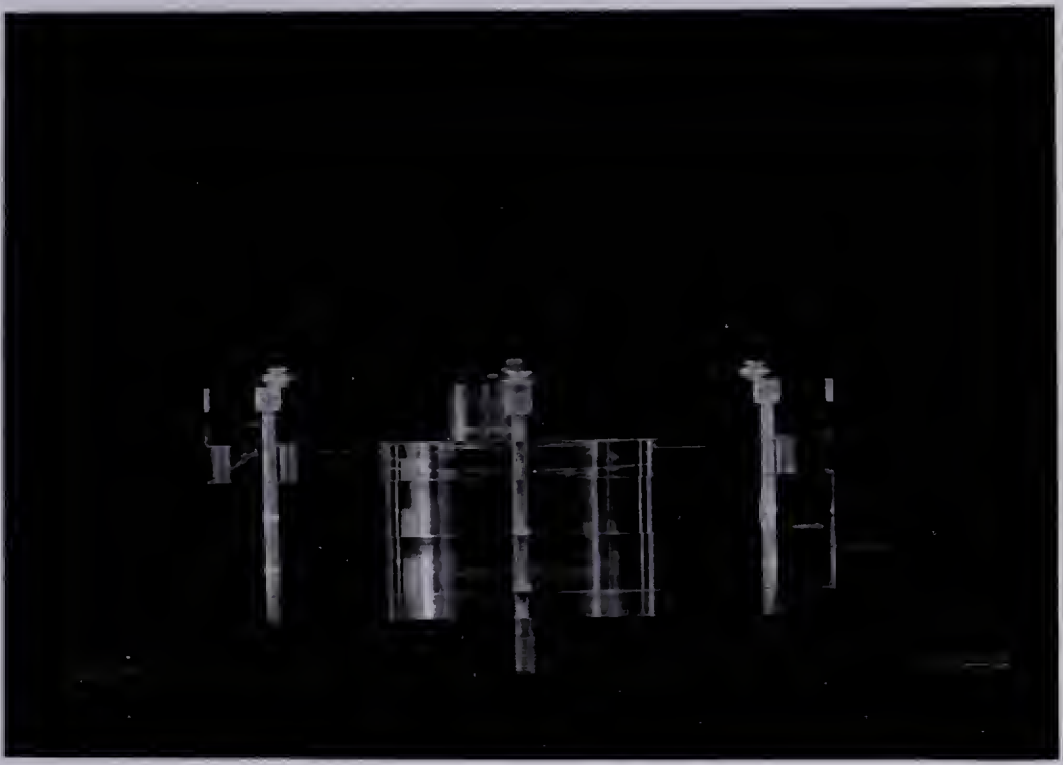

Plate 5.2 Experimental Model for Combustion Chamber 2

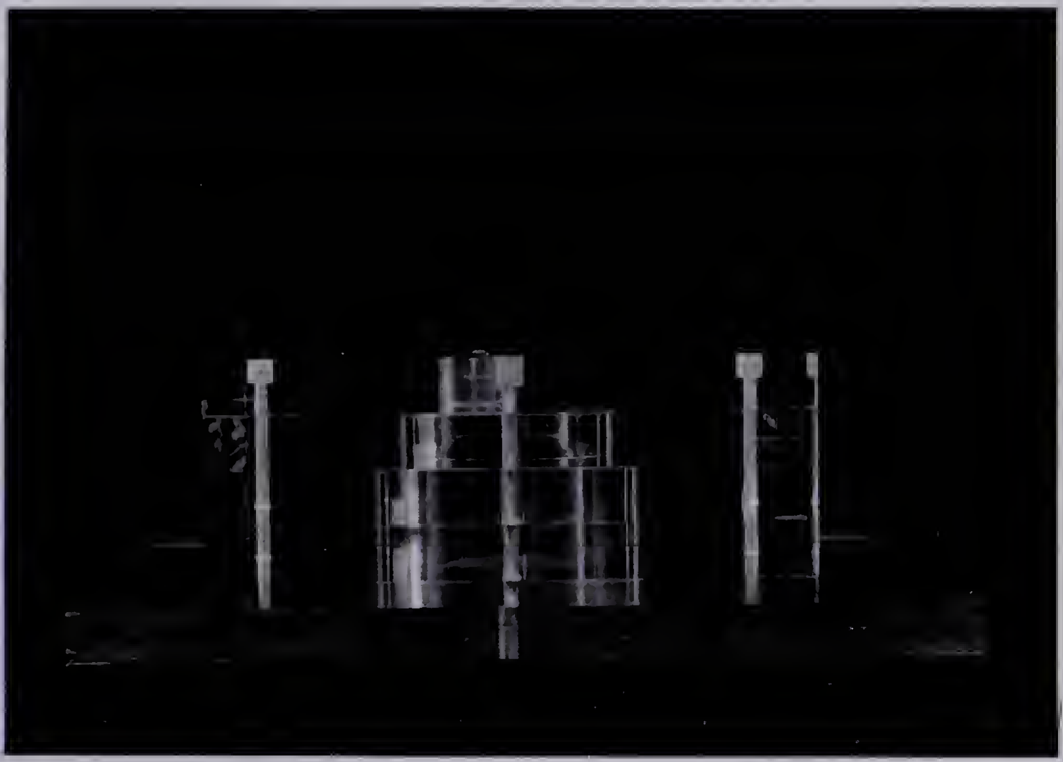

Plate 5.3 Experimental Model for Combustion Chamber 3

small holes located mid-side on each panel represent holes for fastening screws. In each of the three cases, the panels were placed together in different combinations to obtain the three different combustion chambers at different cylinder depths. The cylinder portion of the model consisted of several plexiglass panels with holes of radius 50 mm. The panels had depths of ≃4.5 mm, ≃9.0 mm and ≃18.0 mm which were placed together to obtain cylinder depths ranging from ≃(4.5 mm to 46.0 mm). The combustion chamber portion of the model consisted of three different panels of radii 40 mm, 50 mm and 62.5 mm with depths of ≃ 9.9 mm, ≃ 12.1 mm, and ≃ 18.5 mm respectively. The depth of the combustion chambers were not exactly the same as those in the finite element model because standard thicknesses of plexiglass material were used. Plexiglass was used to simulate the rigid boundary condition. The panels were fastened together with screws to obtain the seven cylinder depths for the three cases considered.

From the schematics in Figure 5.3, it can be seen that the inner dimensions of the plexiglass models represented the combustion chamber-cylinder configurations used in the finite element analysis (see Figure 5.1).

An 200 mm x 200 mm plexiglass panel[7] with a 25 mm hole drilled off center was mounted on each combustion chamber as shown in Figure 5.3. This allowed a 25 mm microphone to be placed such that the microphone was flush mounted in the

---

[7] Source Panel.

combustion chamber slightly off center. This panel was screwed together (fastening holes as indicated in Figure 5.4) with the combustion chamber and cylinder plexiglass panels (see Figure 5.3) to obtain various cylinder depths. A 300 mm x 200 mm plexiglass[8] panel as shown in Figure 5.4 with a 6 mm hole drilled in the center was placed over the end of the cylinder. This panel was not fastened to the combustion chamber-cylinder configuration so that movement of the panel was possible. A 6 mm microphone was placed in the hole such that the microphone was flush mounted in the cylinder. The source and receiver panels were marked TOP and BOTTOM to indicate the orientation used during the experiments. The models were turned upside down to conduct the experiments such that the cylinder was above the combustion chamber. This was done purely to accomodate movement of the receiving panel.

A general schematic is given in Figure 5.5 for the experimental models of the combustion chamber-cylinder configurations. Each of the three configurations can be described in this general manner showing an enclosure of air. The experimental models were set up such that there was an axisymmetric cylindrical plexiglass enclosure representing the combustion chamber with a 25 mm microphone mounted flush in the chamber. There was another axisymmetric cylindrical plexiglass enclosure joined and open to the combustion chamber to represent the cylinder, with a 6 mm

---

[8] Receiving Panel.

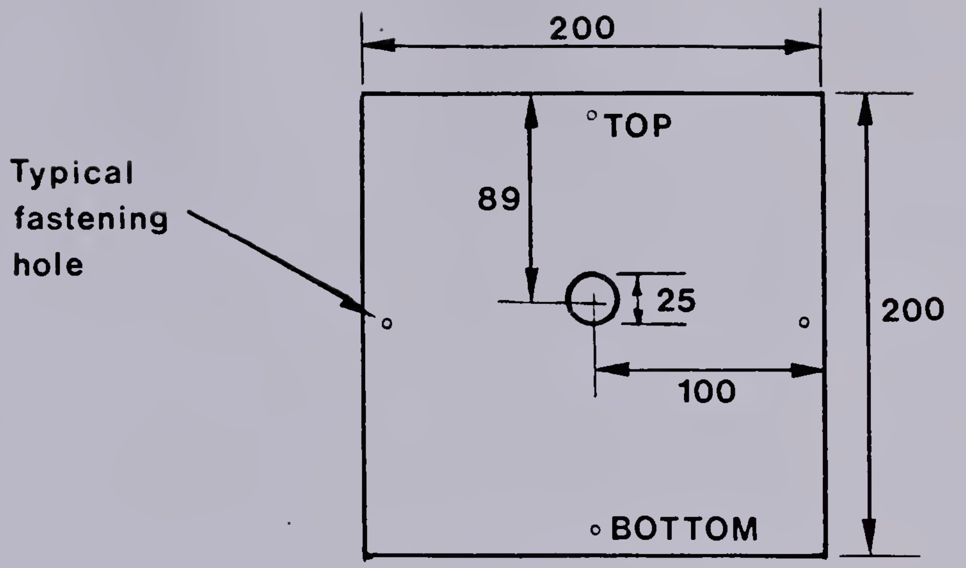

a) Source Panel

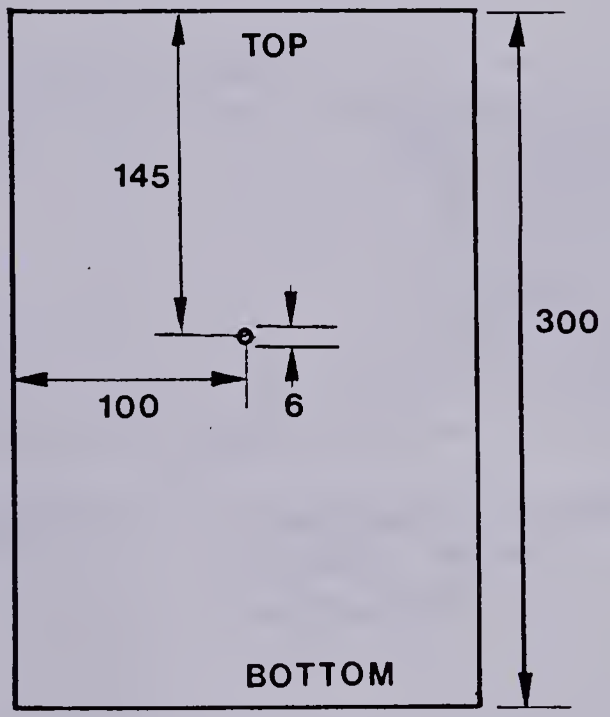

b) Receiving Panel

Figure 5.4 Source and Receiving Panels

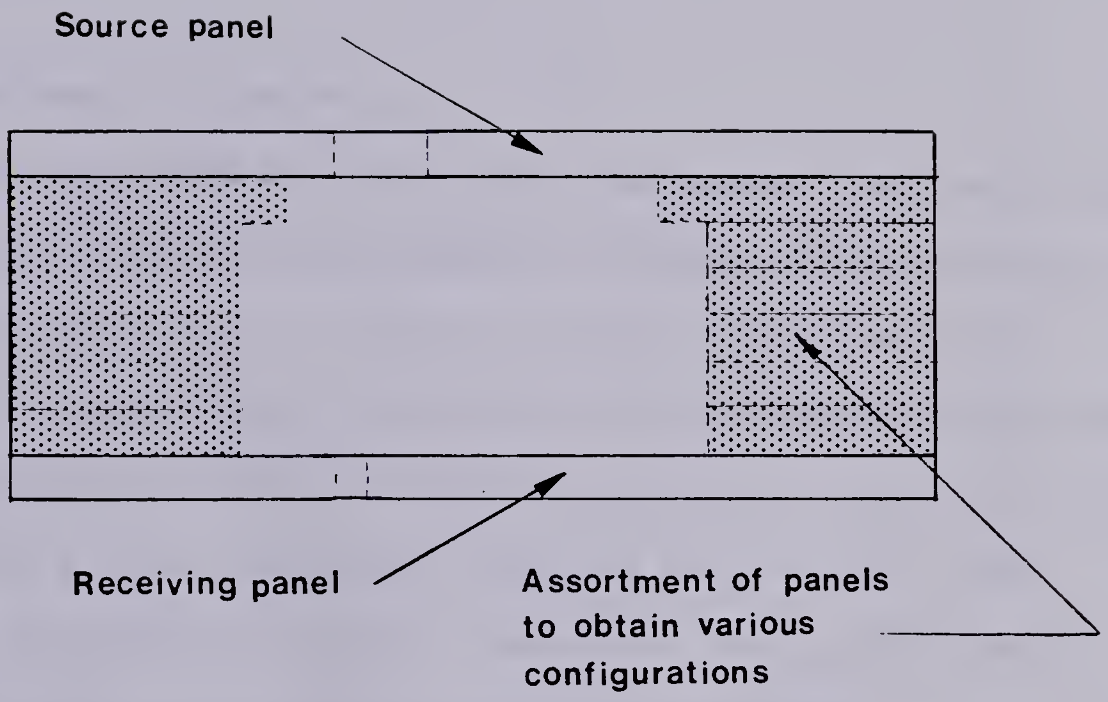

Figure 5.5 General Experimental Set Up

microphone mounted flush with the cylinder. The 6 mm microphone acted as a receiver. The 25 mm microphone acted as a transmitting source. By exciting the air inside the combined combustion chamber-cylinder configuration with the 25 mm source and measuring the response with the 6 mm receiver, the cavity resonances were experimentally determined. In addition, by moving the location of the 6 mm receiver on the surface of the cylinder, the mode shape at that cross section for a given depth of 4.5 mm was determined.

5.5 Experimental Procedure

The evaluation of the cavity resonances and mode shapes for the three combustion chamber-cylinder configurations using the experimental models followed the same basic procedure for each configuration. The problem was examined in terms of the general schematic given in Figure 5.5. There was air in a rigid enclosure excited by a source. The response was measured with a receiver. The panels were screwed together to obtain a given combustion chamber-cylinder configuration at a specific depth.

The equipment used in the experimental analysis is shown in Figure 5.6. The source was a 25 mm condenser microphone excited by a sinusoidal sweep of frequencies using a function generator. The 25 mm microphone was offset so that it was not located on a potential nodal surface. The sweep was used to examine the response of the enclosure in

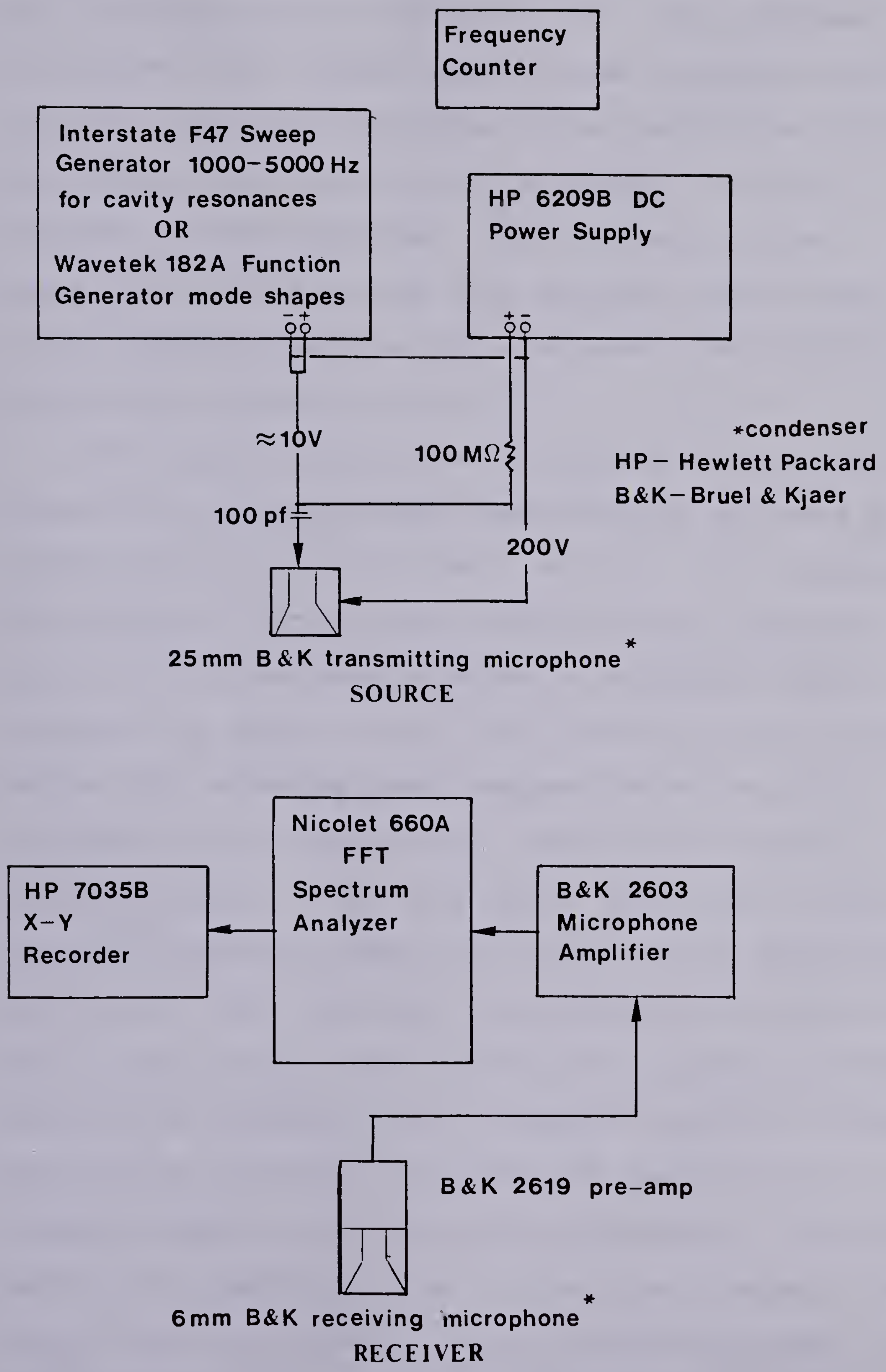

Figure 5.6 Experimental Equipment

the range of frequencies from 1,000 - 5,000 Hz (see Section 5.2). The response was measured with a 6 mm condenser microphone. The response from the 6 mm microphone was passed through a microphone amplifier via a preamplifier into a dual channel spectrum analyzer to obtain a trace of frequency versus amplitude in the frequency range. Approximately 1000 samples were analyzed. These traces are called frequency spectra. All experiments were conducted in an anechoic chamber at $T \simeq 25\ ^{o}C$.

The frequency spectra were obtained for each of three combustion chamber-cylinder configurations at seven cylinder depths, ranging from $\simeq$(4.5 mm - 46.0 mm). Four locations (see Figure 5.7) were used to determine the frequency spectra of a given configuration at a specific depth. The locations are shown in plan view relative to the cylinder, because the receiving panel was mounted on the end of the cylinder to take measurements. These four locations (Configurations I - IV) were chosen such that no modes in the given frequency range were missed on the frequency spectra, ie. when the receiving microphone was placed on a nodal line. A nodal line exhibits zero acoustic pressure and therefore no reading from a microphone would be obtained. By measuring at different locations and examining four frequency spectra, all the cavity resonances, indicated by peaks on the spectrum trace, in the given frequency range, should have been present. In the second measurement location (Configuration II), where the microphone was placed in the

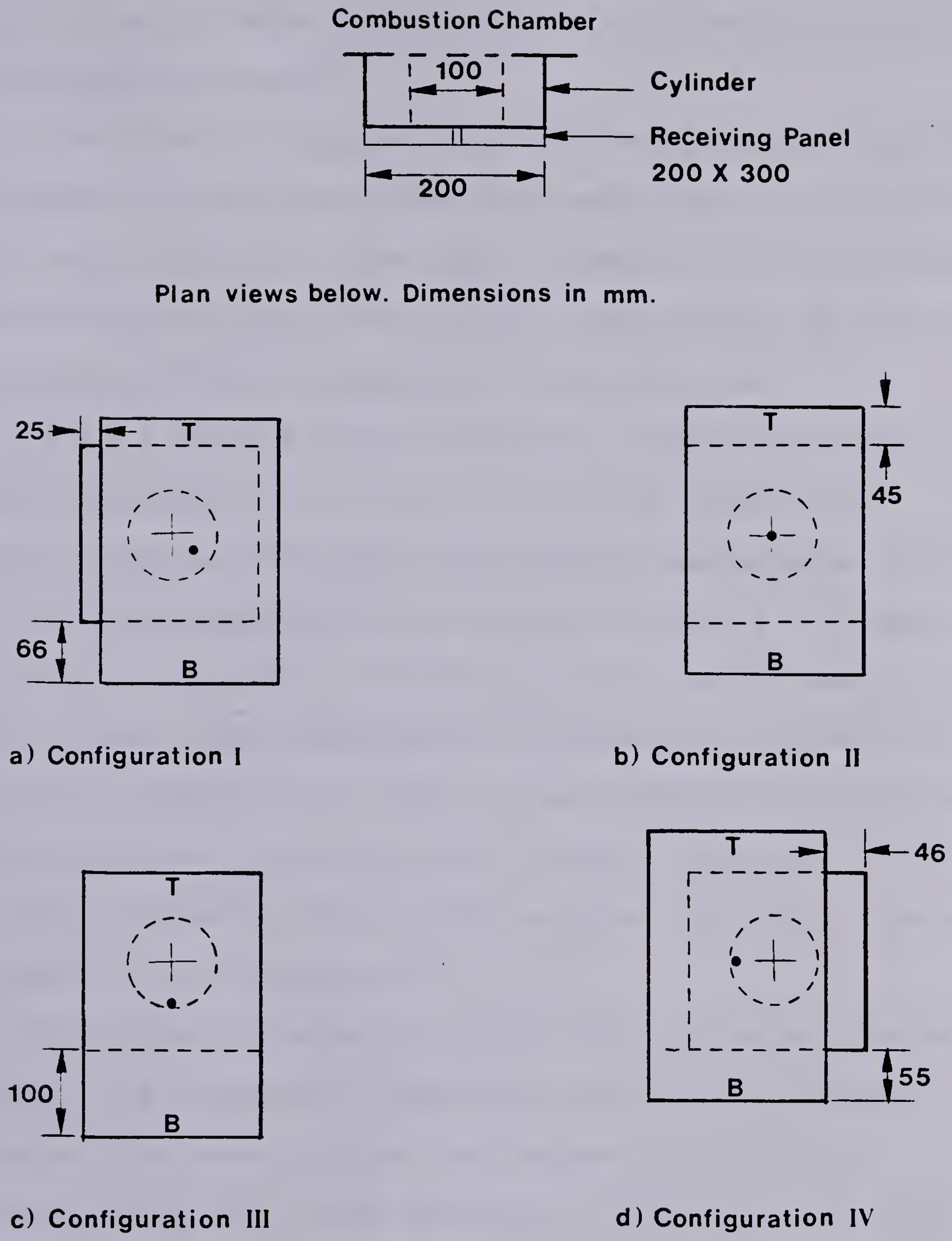

a) Configuration I

b) Configuration II

c) Configuration III

d) Configuration IV

Figure 5.7 Measurement Locations of the Receiving Microphone

center of the cylinder cross section, only radial or axial modes should be present.[1]

In addition to assuring that all cavity resonances were experimentally determined, the four measurement locations gave a rough idea as to the types of modes on the cylinder cross section the given frequencies represented, by relating the position of the microphone to the mode type.

Figure 5.8 gives sample frequency spectra or traces for combustion chamber 2 at a depth of 4.5 mm. These four frequency spectra represent measurements conducted at the four different measurement configurations shown in Figure 5.7. Cavity resonances are shown as peaks on the spectrum traces. Figure 5.8b indicates the presence of one mode at a frequency of 4150.00 Hz, where the microphone is located at the center of the cylinder cross section. The other modes are likely circumferential modes because the frequencies do not appear in configuration II.

The frequency traces are shown for combustion chamber 2 in Figure 5.8 because it represents a simple cylindrical enclosure. The behaviour of the frequency spectra at different locations can be examined in regard to the mode shapes discussed earlier (see Figure 2.5).

At a depth of 4.5 mm based on the analytical solution, four cavity resonances, or peaks on the spectrum traces, should be apparent in the traces. The following modes should be experimentally determined: mode (100) f_1 = 2028 Hz, mode

---

[1] These modes are the only type without a nodal line passing through the center of the cross section.

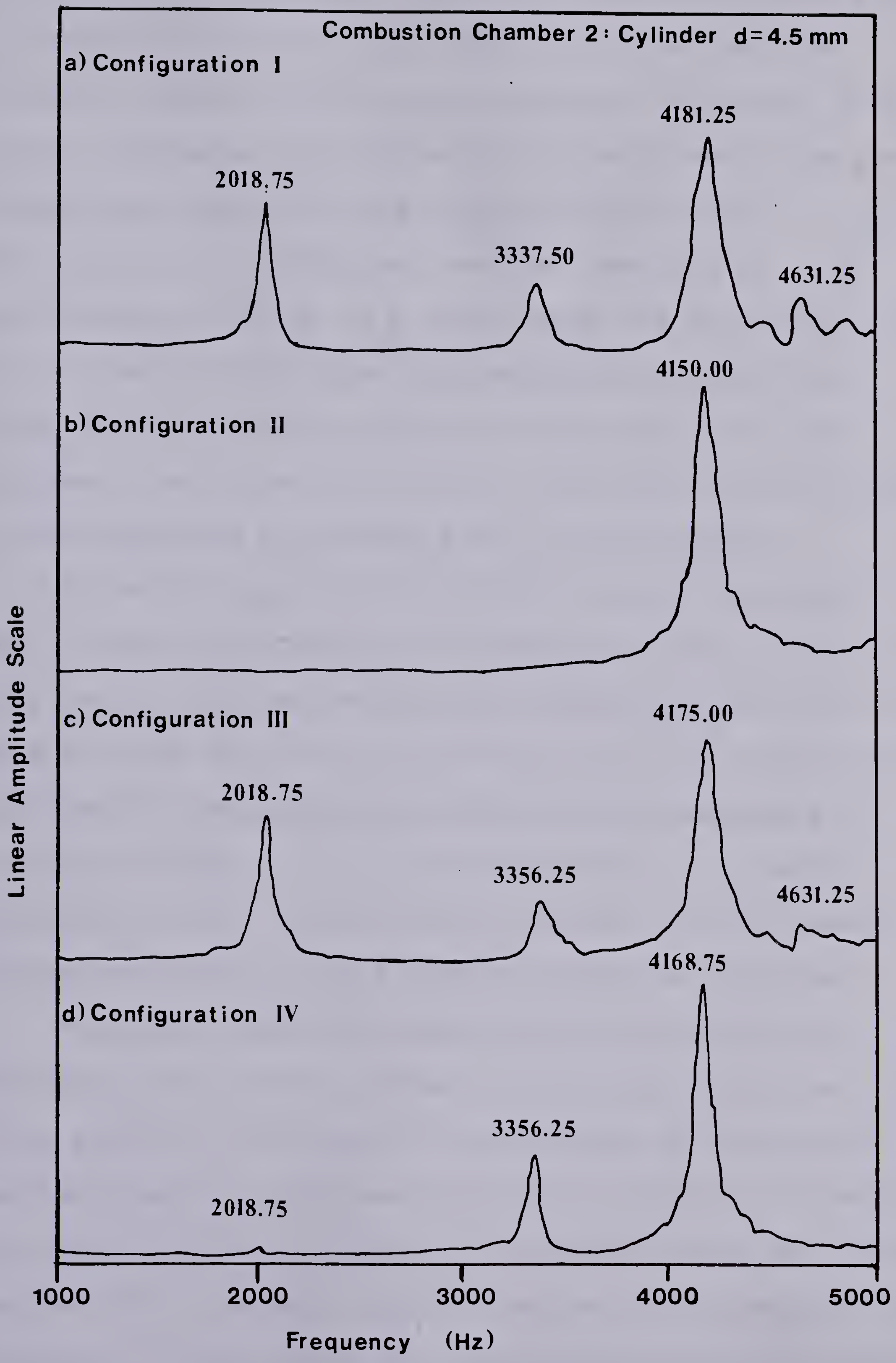

Figure 5.8 Sample Spectrum Traces

[illegible]

(200) f_2 = 3364 Hz, mode (010) f_3 = 4220 Hz and mode (300) f_4 = 4626 Hz, in that order. Upon examining the four frequency spectra taken at the different locations, four cavity resonances are indicated at approximately the same frequencies given from the analytical analysis. Configuration II indicates that the resonance at approximately 4150 Hz is a radial mode and the other three are circumferential modes. Circumferential modes have a point of zero acoustic pressure at the center of the cylinder (see Figure 2.5), hence, the receiving microphone at configuration II did not pick up these modes.[10]

The mode shapes for the lowest cavity resonances for each of the three combustion chamber-cylinder configurations at a depth of 4.5 mm on the cross section at the end of the cylinder were obtained. In addition, the mode shapes were obtained for the second and third cavity resonances of combustion chamber 2, in a similar manner, to compare to analytical theory and the finite element results because combustion chamber 2 is a simple cylindrical enclosure.

The mode shapes were obtained experimentally by measuring the acoustic pressure at various locations on the cross section at the end of the cylinder by moving the receiving panel to various locations. A grid of 21 points was used as shown in Figure 5.9. The microphone was moved to each of the 21 points, where a reading of the pressure was measured in volts using the instantaneous value of amplitude

---

[10] Note: There is some variation in the frequencies for different measurement locations.

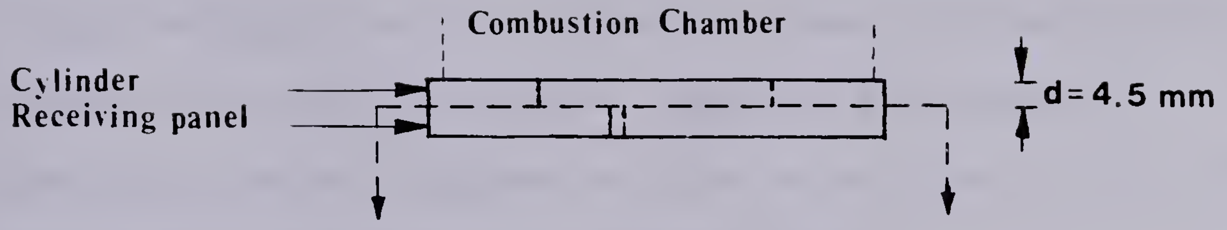

Mode shapes taken on the cross section at end of cylinder

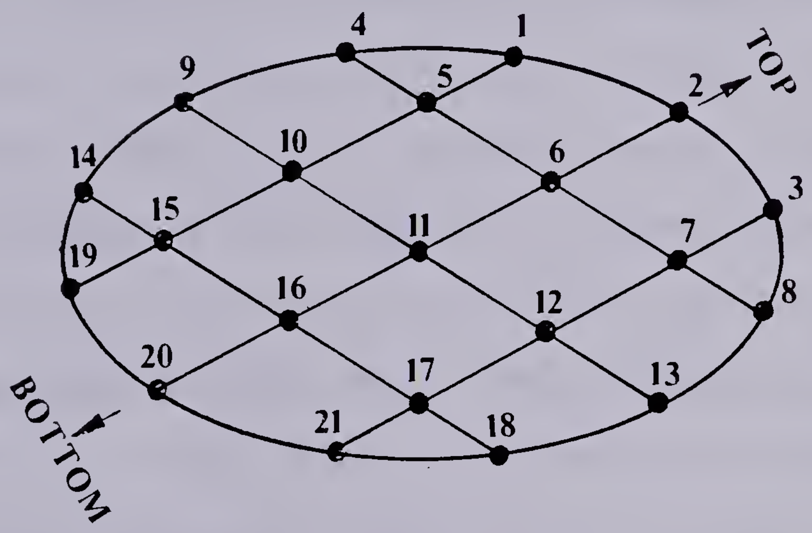

Isometric view of mode shape X-section

Figure 5.9 Experimental Mode Shape Grid

on the spectrum analyzer for each point. By plotting these voltages at various locations, the mode shape was obtained. Not all of the 21 points were used in the mode shapes given in this analysis as the picture became too complicated. The pressure variation along one diameter was plotted to determine the mode shapes and the nodal line of the cross section was indicated as a dashed line.

A given mode was excited by setting the function generator to a sine wave of a given frequency which was obtained from the experimental cavity resonance analysis. The acoustic pressure distribution was measured for a given frquency at the locations indicated in Figure 5.9. For, example, there was a cavity resonance at f = 2018.75 Hz for combustion chamber 2 at a depth of 4.5 mm. To examine the mode shape on the end of the cylinder, the function generator was set to 2031 Hz.[11] The acoustic pressure was measured at 21 points. The results were plotted on the cylinder cross section to demonstrate the mode shape. The nodal line of the cross section was drawn, using linear interpolation where necessary.

By repeating this procedure, experimental mode shapes for the other two combustion chamber-cylinder configurations at a depth of 4.5 mm were obtained. Likewise, the mode shapes for the second and third cavity resonances of combustion chamber 2 were obtained for comparison with analytical theory. Combustion chamber 2 has been repeatedly

---

[11] This value was slightly higher than the frequency given in the cavity resonance analysis.

studied in more detail because it is a simple cylindrical enclosure and analysis of these results gives an indication of the validity of the mathematical models both approximate (finite element results) and exact (analytical solution).[12]

---

[12] Note: This method does not guarantee that the mode shape is the maximum amplitude associated with the cavity resonance.

6. COMBUSTION CHAMBER-CYLINDER RESULTS

6.1 Cavity Resonances

The bounds for the numerical results were calculated on the basis of section 5.2 as an approximation. Figures 6.1 - 6.3 show the approximate curves for the three configurations for the first four modes.

The acoustic finite element results for combustion chamber 1 are presented in Figure 6.4, indicated by solid lines. The curves are presented in order of magnitude such that the lowest curve is the lowest cavity resonance, the second curve the second lowest cavity resonance and so on. The unusual shape of the curves for the higher resonances (2nd, 3rd . . .) for large cylinder depths suggests that some unusual behaviour is occurring. [13] These changes in the curves are due to the presence of axial modes as the length of the cylinder increases. Therefore, the curves presented in order of magnitude do not necessarily represent one specific mode except for the lowest cavity resonance which does not exhibit this unusual behaviour. The results presented for the higher modes are not as accurate as the lowest mode partly because the finite element results lose accuracy for higher modes due to the approximate assumed

---

[13] It should be noted here, that the curves do not occur in pairs as did the modes for a cylindrical enclosure. This is due to the use of a half chamber finite element model which gives only one of any orthogonal pair. This does not affect this analysis as the pairs of frequencies are identical for axisymmetric cylinders such as these.

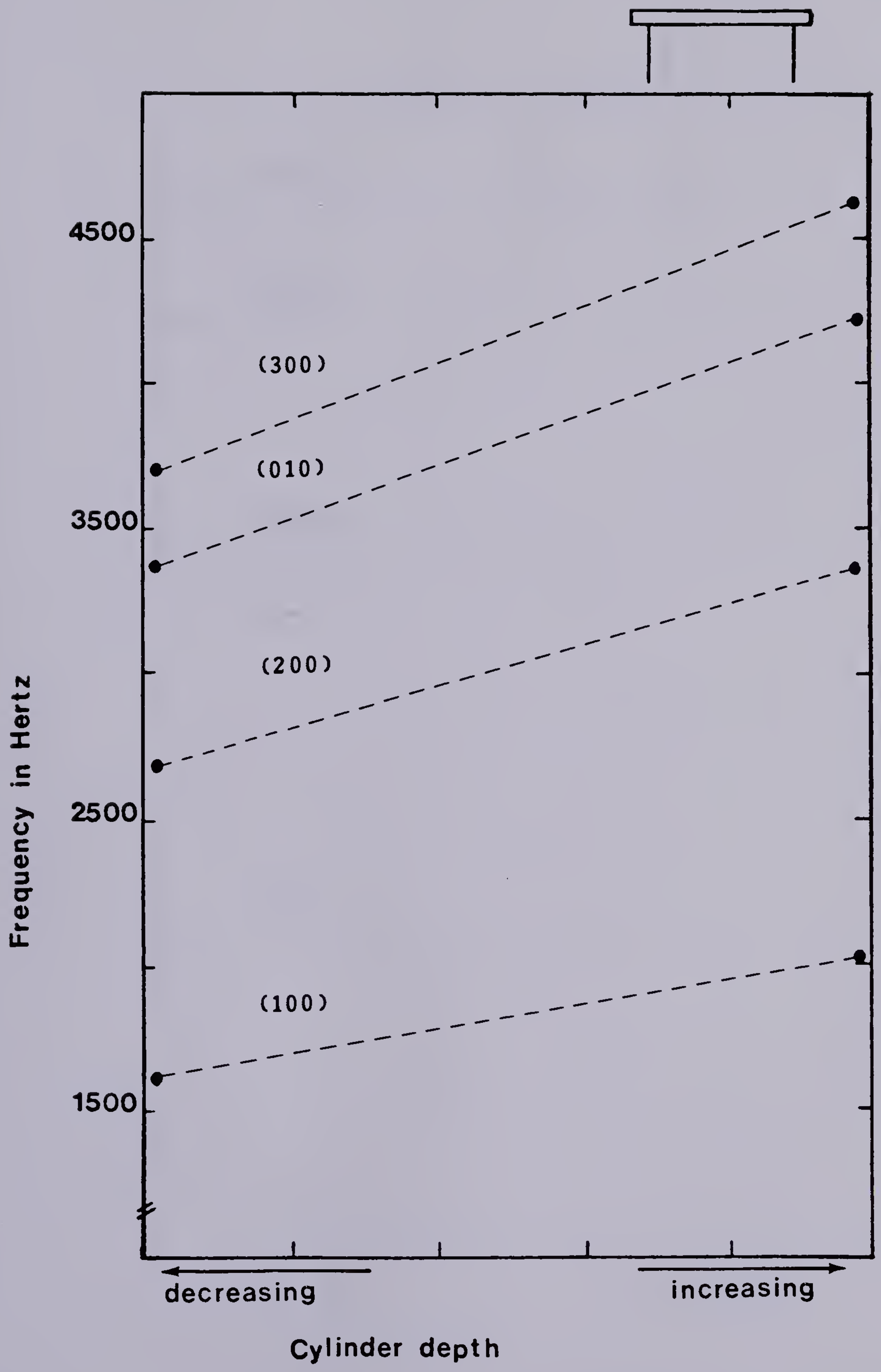

Figure 6.1 Bounds for Numerical Results-Combustion Chamber

1

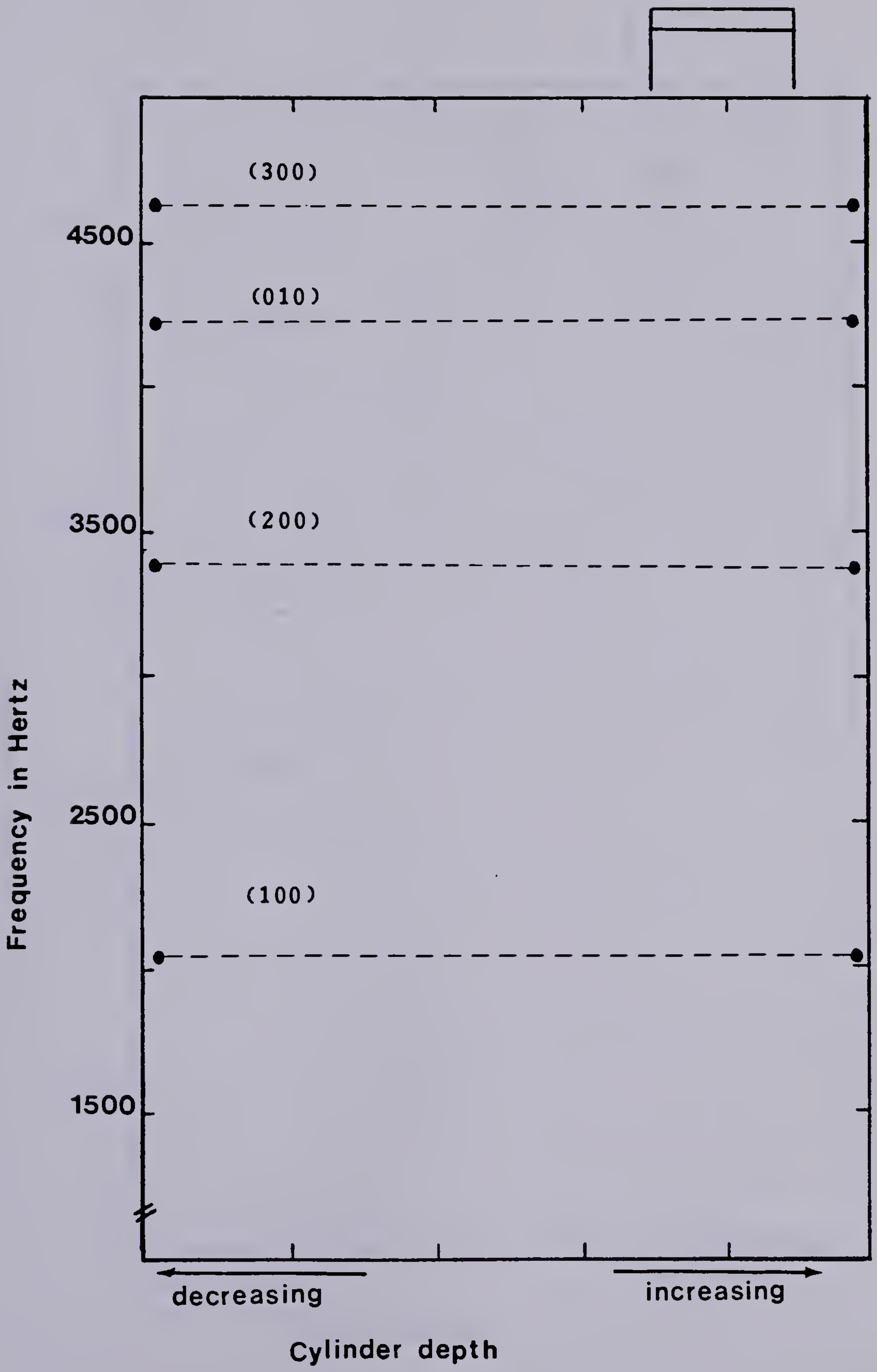

Figure 6.2 Bounds for Numerical Results-Combustion Chamber 2

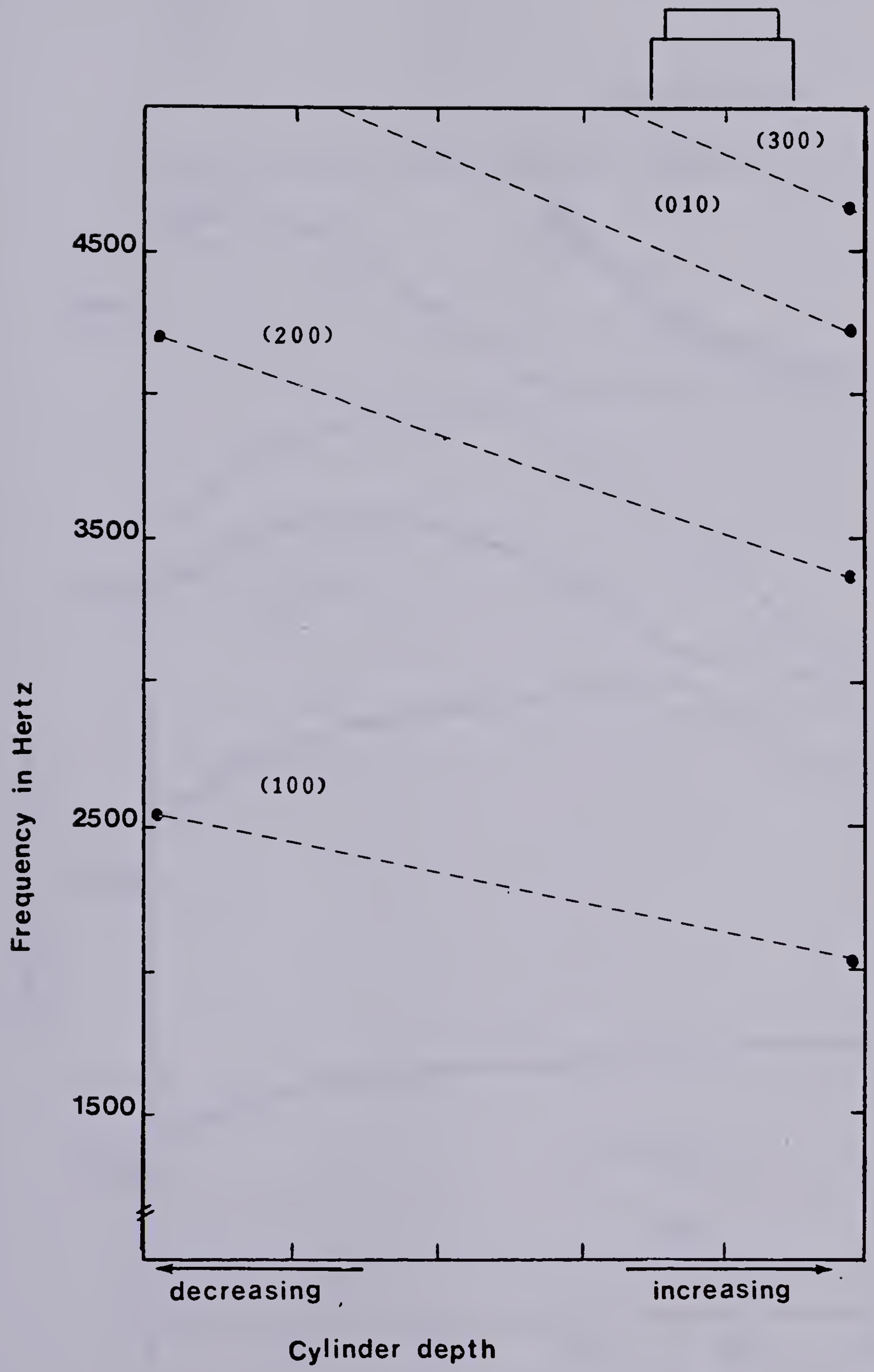

Figure 6.3 Bounds for Numerical Results-Combustion Chamber 3

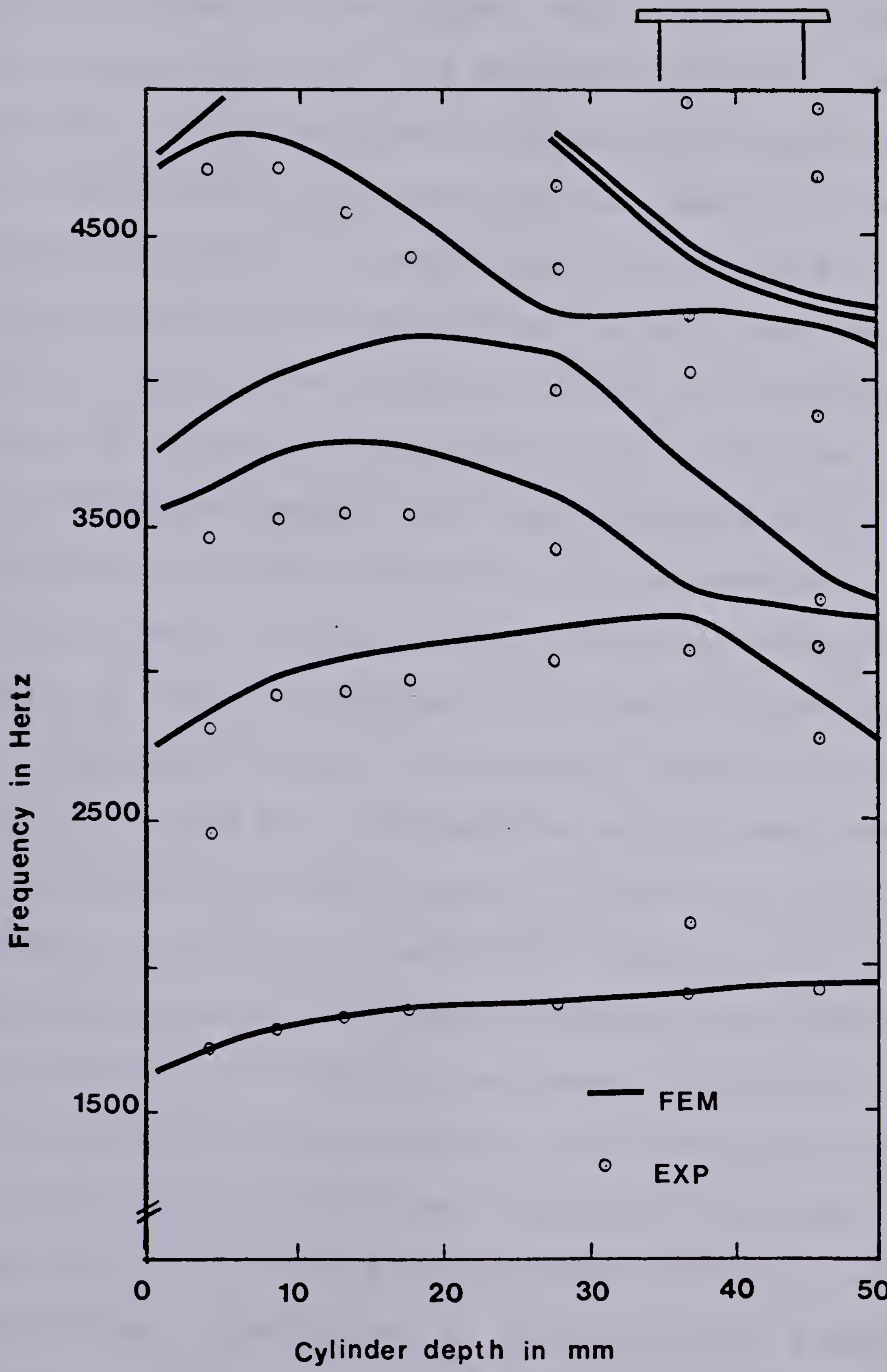

Figure 6.4 Cavity Resonances for Combustion Chamber 1

solution for the acoustic pressure. The results are presented merely to give an indication of the behaviour of the different cavity resonances as a function of cylinder depth. Accuracy of the higher modes can be obtained by using more elements to model the enclosure. However, the computer solution of large eigenvalue problems is expensive. Figure 6.1, which shows the bounds for the numerical results for combustion chamber 1 agrees well with Figure 6.4. The frequencies for the lowest mode increase with increasing depth in both cases. Figure 6.1 does not illustrate the effect of the axial modes as only the radial and circumferential modes, which are indicated by arrows, were examined to determine bounds. From the standpoint of engine knock at small cylinder depths, the axial modes do not appear to play a significant role for this configuration.

The finite element results for combustion chamber 2 are shown in Figure 6.5, indicated by solid lines. The curves are plotted in the same manner as those for combustion chamber 1, in order of magnitude. These results are of particular interest because the combustion chamber-cylinder configuration is simply an axisymmetric cylinder. Therefore, the analytical solution given in section 2.4 can be used. The cavity resonances (exact solution) calculated from equations (2.3.3) are also presented in Figure 6.5, shown by dashed lines. The analytical solution gives a good indication of the accuracy of the finite element model. Excellent agreement was obtained between the finite element

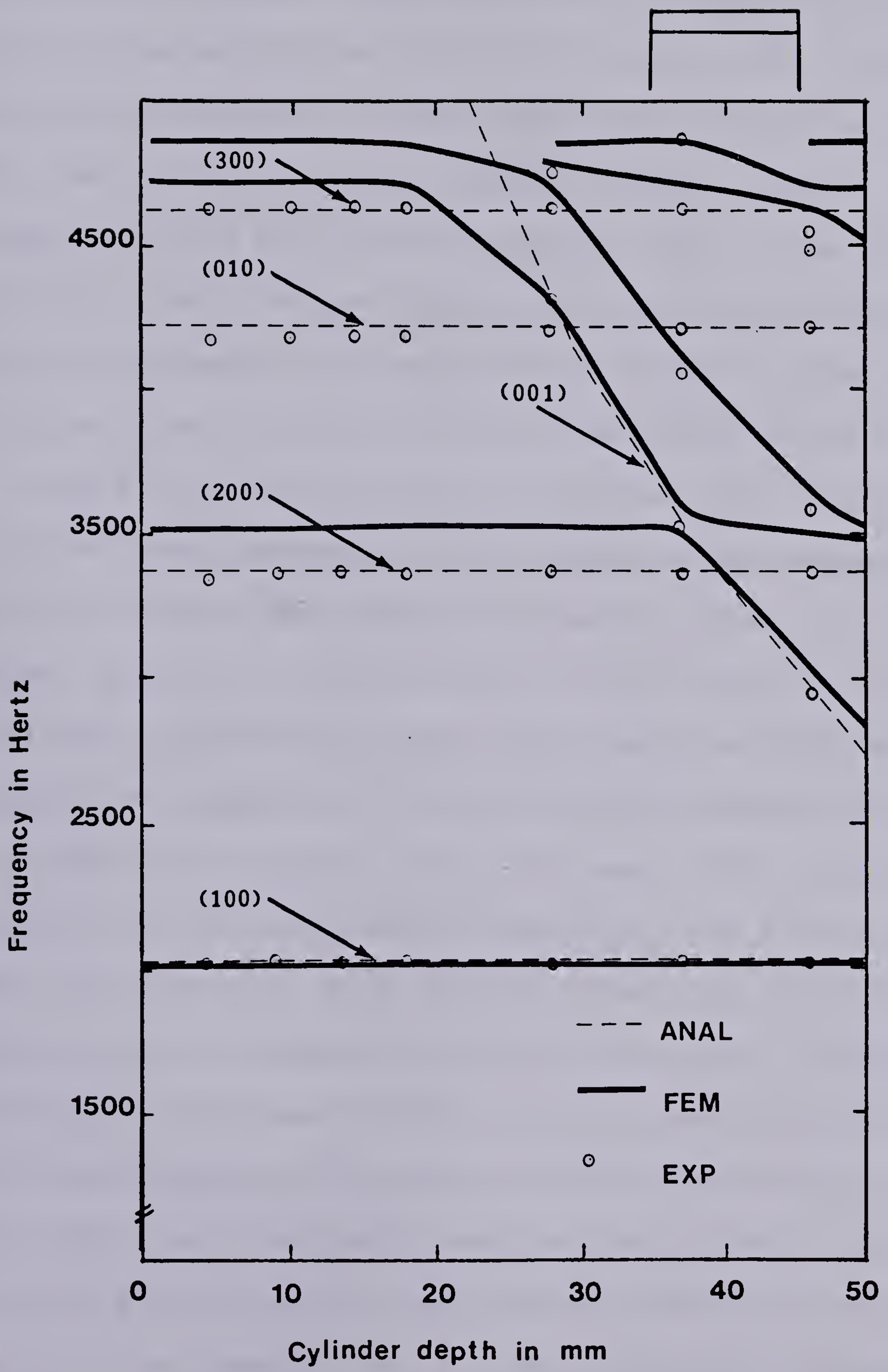

Figure 6.5 Cavity Resonances for Combustion Chamber 2

approximation and acoustic theory for the lowest mode.

The analytical curves are labeled with arrows indicating the mode types which the frequencies represent based on the analytical solution. Modes (100), (200), (010), and (300) are shown in that order. The first axial mode is also shown which occurs at large cylinder depths. The presence of the axial mode indicates why the second resonance curve changes shape such that mode (200) exists as the second lowest resonance until a depth of approximately 37 mm and then the second lowest resonance is an axial mode.

The analytical solution shows that the finite element solution loses accuracy at the higher modes compared to acoustic theory. The second resonance curve from the finite element analysis is approximately 4.5% higher than the analytical solution for mode (200) until a depth of 37 mm is reached. At a depth of 37 mm the finite element solution is very close to acoustic theory for mode (001). This change in accuracy can be explained by examining the finite element model, Figure 5.2b, more closely. There are six elements used in the circumferential direction. Hence, based on the convergence of element PR15, finite element predictions in the circumferential direction should be extremely good for mode (100), and reaonably good for mode (200) with decreasing accuracy for the higher circumferential modes. There is one element in the radial direction. Hence, the finite element predictions for first radial mode (010) will not be very accurate. There are two elements used in the

axial direction. Therefore, finite element predictions for the first axial mde (001) are quite good. Going back to Figure 6.5, the differences between analytical theory and the finite element results can be justified by the finite element model. The extensive study of combustion chamber 2 is very useful in understanding the behaviour of the finite element models.

Figure 6.5 can also be compared to Figure 6.2 which shows the bounds for the numerical results. However, in this case the bounds are merely the analytical solution to the problem.

The finite element results for combustion chamber 3 are shown in Figure 6.6, indicated by solid lines. The curves are plotted, similar to those for the other two configurations. The lowest cavity resonance is a smooth curve. The higher cavity resonances are unusually shaped, a similar behaviour to that exhibited by the higher modes for combustion chambers 1 and 2. This phenomena is attributed to the axial modes which have a dependence on cylinder depth rather than the radius.

A comparison of Figures 6.3 and 6.6, shows a good agreement between the bounds for the numerical results and the numerical results themselves for combustion chamber 3. The frequencies for the different modes tend to be decreasing with increasing cylinder depth. Figure 6.3 does not illustrate the axial modes. Only bounds for modes (100), (200), (010) and (300) are given.

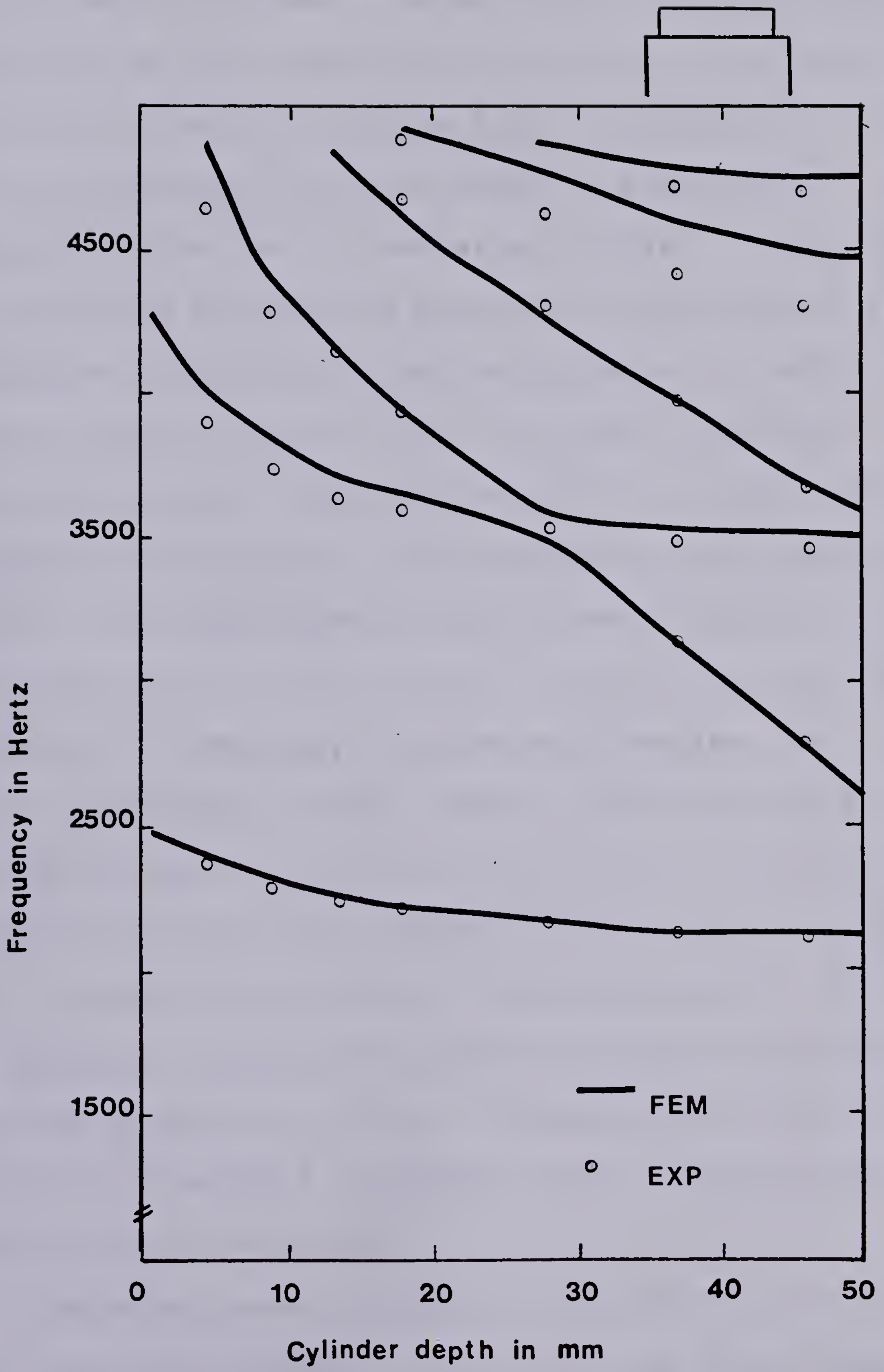

Figure 6.6 Cavity Resonances for Combustion Chamber 3

The lowest cavity resonance in each of three cases is a continuous smooth curve. This seems to indicate that one type of mode is present. As has been previously shown, the main focus of this analysis is to examine the lowest cavity resonance in detail. Figures 6.4 - 6.6 show the lowest cavity resonances for three types of axisymmetric combustion chambers of the same volume as a function of cylinder depth.

Spectrum traces were experimentally obtained for each combustion chamber-cylinder configuration at seven cylinder depths ranging from ≃(4.5 mm - 46.0 mm) to compare to the numerical results. The experimental cavity resonances are plotted in Figures 6.4 - 6.6 along with the finite element results. The experimental results are indicated by circles, such that the radius of the circle shows the experimental variation in frequency for the measurements. The frequency spectrum analyzer, a dual channel FFT device, had a resolution of 6.25 Hz on the range used. In addition, the temperature inside the anechoic chamber varied from 24.2 - 26.2 °C during the course of the measurements. Therefore, the peaks on the spectral traces varied from configuration I to IV by as much as 30 Hz. [14] Repeatability tests were conducted on several configurations to substantiate that the spectral peaks were valid.

The experimental results in all three cases agree well with the finite element results for the lowest cavity resonance. The agreement with combustion chamber 2 is

---

[14] This variation is not justified by the resolution alone.

exceptionally good especially compared to the analytical solution.

6.2 Mode Shapes

The mode shapes are presented in Figures 6.7 - 6.11 in pairs to compare the finite element mode shapes to the experimental mode shapes. [15] Each figure shows the comparison for a given combustion chamber for a given mode at a depth of 4.5 mm on the cylinder cross section. Figures 6.7a - 6.9a show the lowest modes predicted from the finite element analysis for combustion chambers 1, 2 and 3 respectively. The finite element predictions indicate that these modes are first circumferential modes (100) at the depth indicated. An acoustic pressure variation across the diameter is plotted for the finite element results and the nodal line is shown as a dashed line. Only the pressure variation along one diameter was plotted because the grid points for the models did not coincide with the experimental grid points. However, a distinct comparison can be made between the experimental mode shapes and the finite element mode shapes by considering the dashed line in each case.

The validity of the mode shapes can be determined in a similar manner to that done for the cavity resonances. Combustion chamber 2 can be examined in comparison to the analytical theory. Again, for simplicity, the modes were

---

[15] The experiments were conducted such that the combustion chamber-cylinder models were turned upside down with the receiving panel on top.

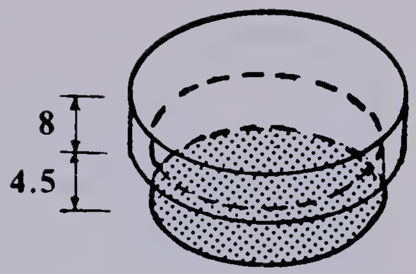

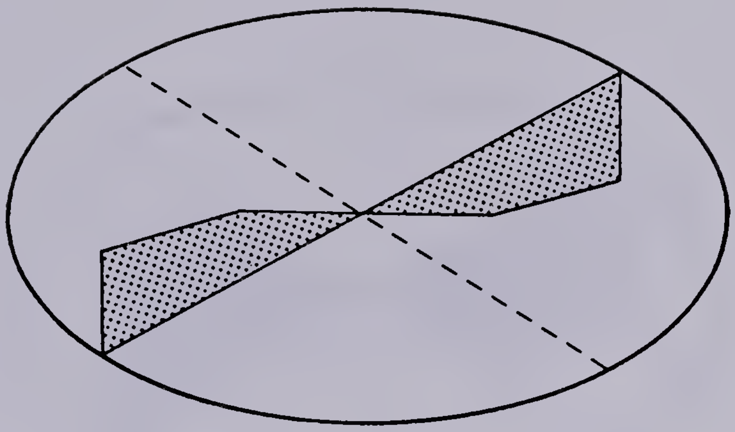

a)Finite Element f= 1724 Hz

---- Nodal Surface

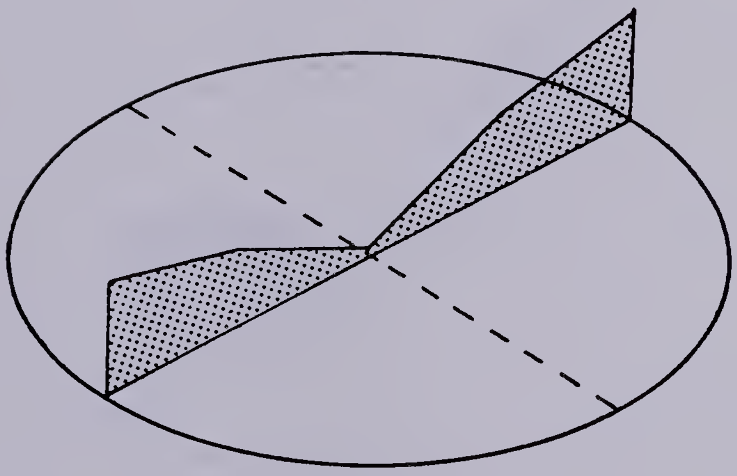

b)Experimental f=1725 Hz

Figure 6.7 Mode Shapes for Lowest Cavity Resonance-Combustion Chamber 1

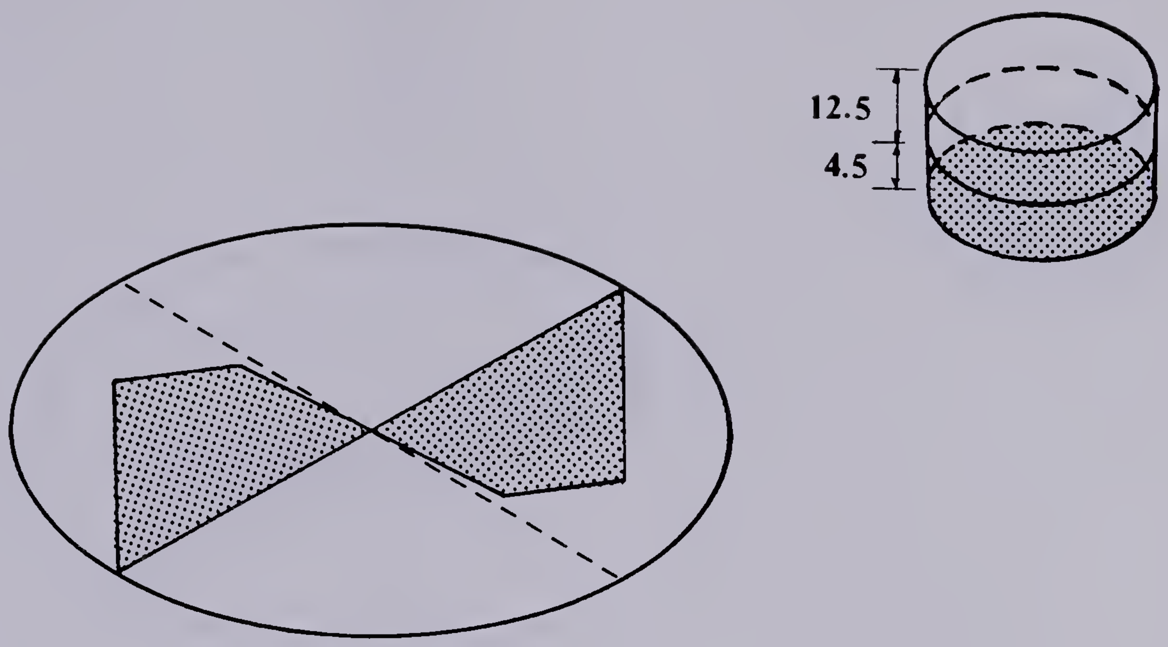

a)Finite Element f = 2023 Hz

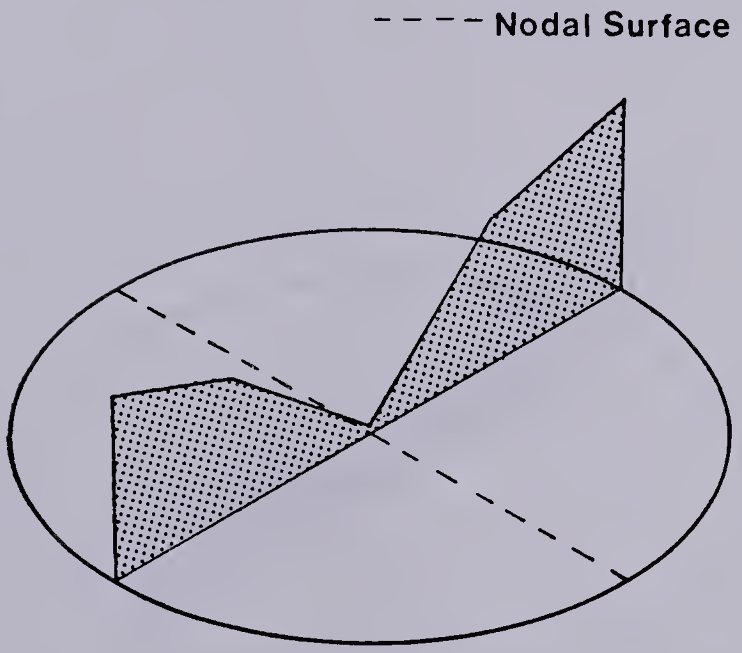

b)Experimental f = 2031 Hz

Figure 6.8 Mode Shapes for Lowest Cavity Resonance-Combustion Chamber 2

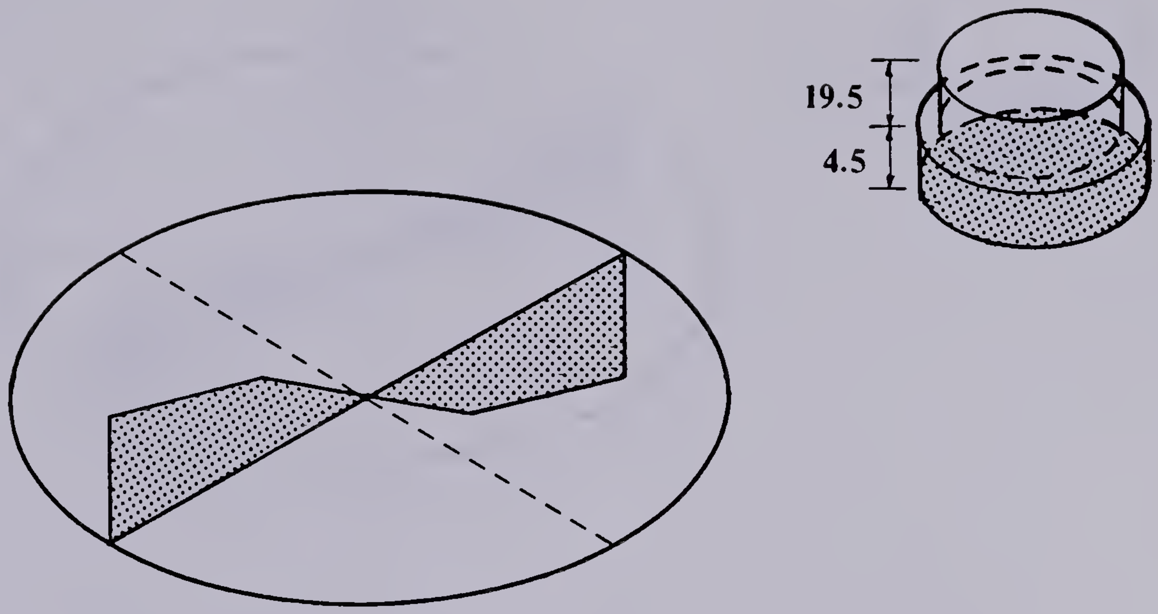

a)Finite Element f = 2388 Hz

- - - - Nodal Surface

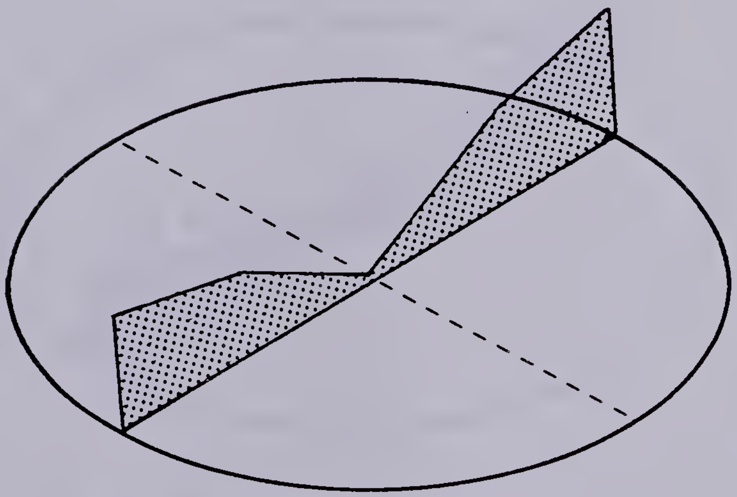

b) Experimental f = 2375 Hz

Figure 6.9 Mode Shapes for Lowest Cavity
Resonance-Combustion Chamber 3

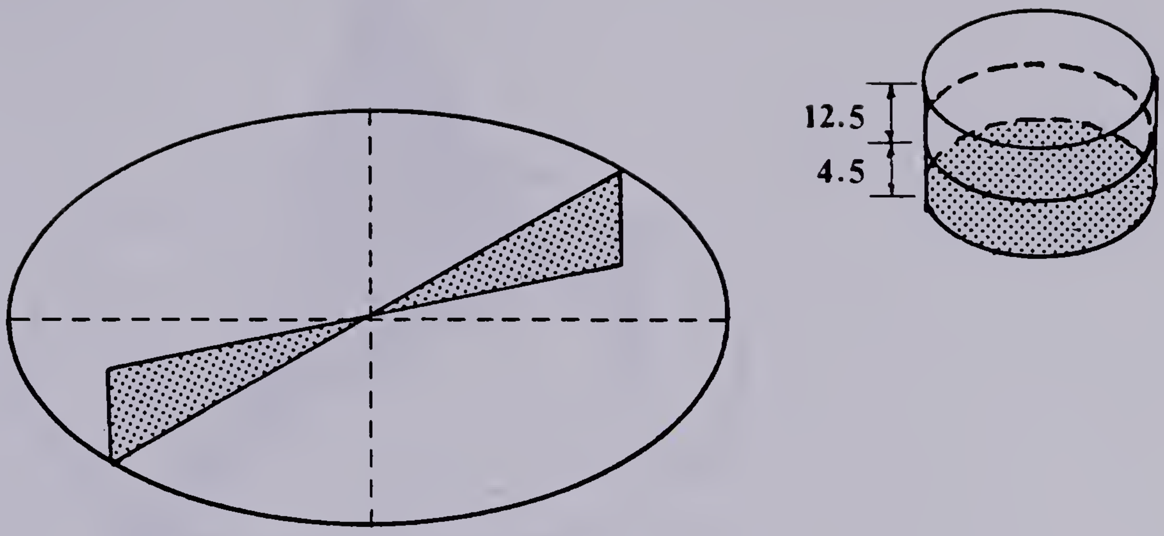

a)Finite Element f= 3513 Hz

----- Nodal Surface

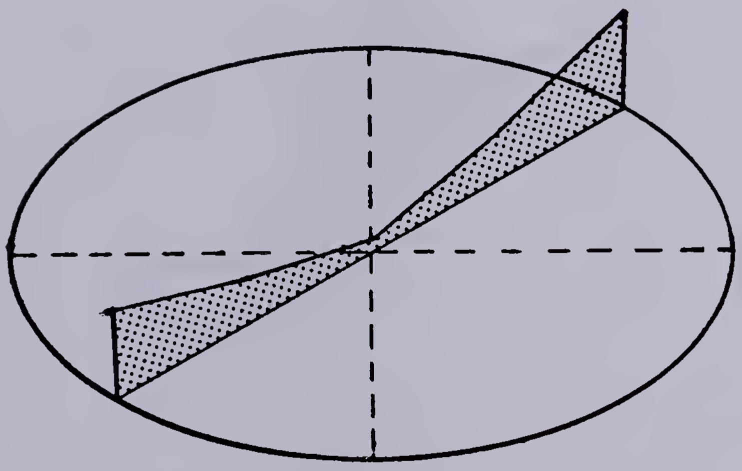

b)Experimental f = 3369 Hz

Figure 6.10 Mode Shapes for Second Cavity Resonance-Combustion Chamber 2

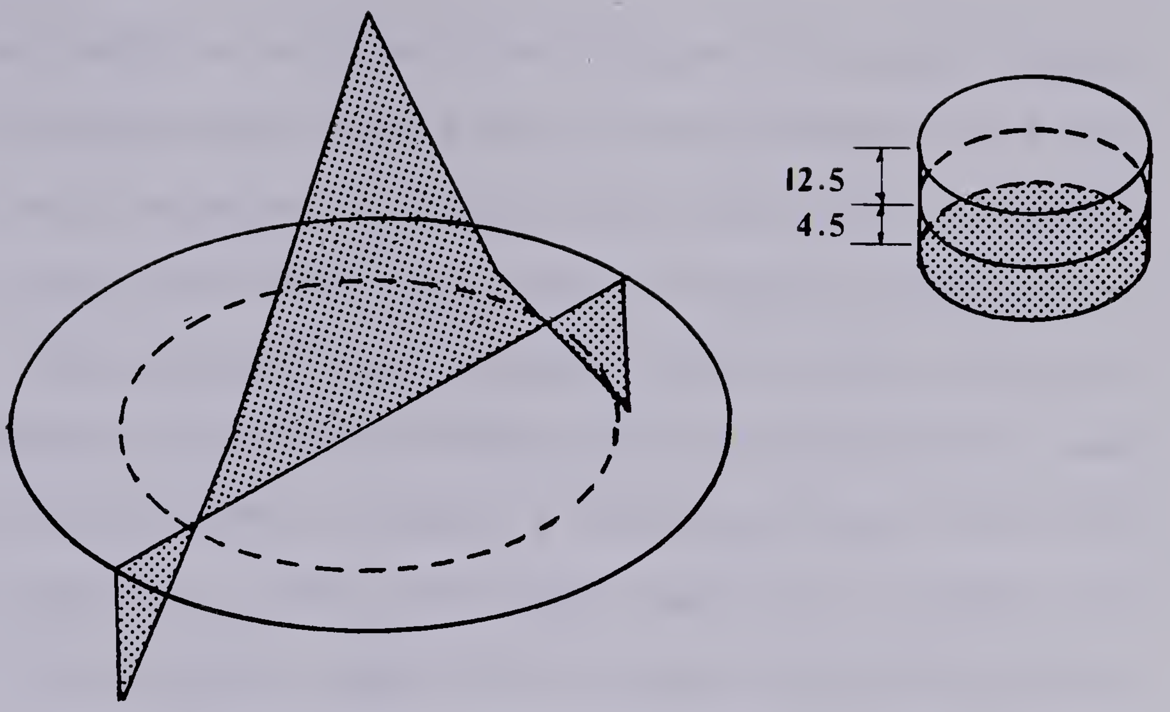

a)Finite Element f = 4724 Hz

- - - - Nodal Surface

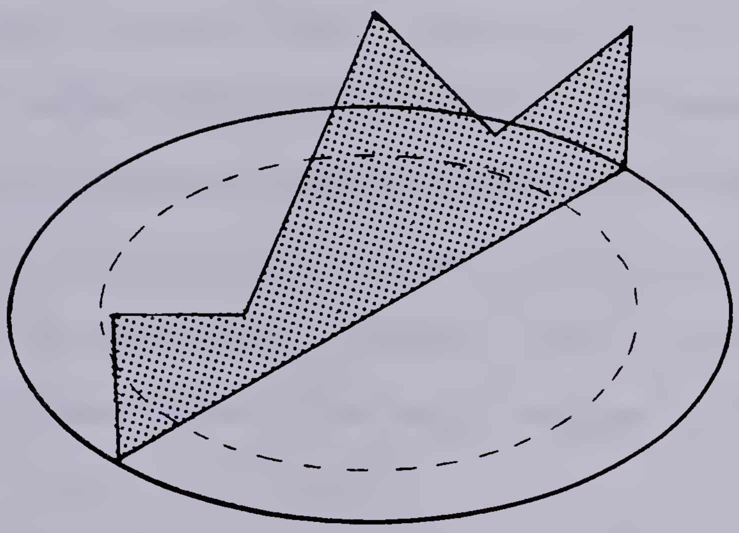

b)Experimental f = 4200 Hz

Figure 6.11 Mode Shapes for Third Cavity Resonance-Combustion Chamber 2

examined at depth of 4.5 mm. From Figure 2.5, there should be one circumferential mode with one nodal diameter. Figure 6.8 shows both experimentally and from the finite element results a cross sectional view with one nodal diameter. Secondly, there should be a circumferential mode with two nodal diameters. Figure 6.10 shows both experimentally and from the finite element results a cross sectional view with two nodal diameters. The third mode should be a radial mode. Figure 6.11 shows both experimentally and from the finite element results a cross sectional view with a radial nodal line. In the case of the radial mode, linear interpolations were performed to locate the zero acoustic pressure location. Both experimentally and with the finite element analysis, the mode shapes were symmetric with respect to the nodal lines. In the higher modes from the finite element analysis, mode (010) for example, the mode shapes began to lose their expected shapes compared to analytical theory. This is not surprising as the cavity resonances were not as accurate for the higher modes. Again, because of the concern with the lowest mode, the mode shapes seem to be extremely good.

An interesting note to mention regarding the measurement of the mode shapes is in regard to the actual value of the frequency required to excite a given mode. As discussed earlier, the frequency of excitation was established from values obtained from the frequency spectrums for a given cavity resonance. During the course of

the experiments, it was found that the excitation frequency could be varied with certain limits while still maintainiing one specific mode shape. Considering combustion chamber 2, for example, a mode shape was obtained at an excitation of f = 2019 Hz which was very similar to that obtained at 2031 Hz. The mode shape at 2019 Hz was not included because there were some difficulties with the function generator maintaining an excitation of 2019 Hz. However, it is interesting to note that the actual frequency associated with a given mode shape experimentally is not very precise. In other words, the mode shape is not necessarily the maximum amplitude mode shape associated with resonance. This is of considerable importance in some of the modes where there was considerable variation in frequency from run to run.

From the analytical analysis of standing waves in enclosures, a positive amplitude on one side of a nodal surface is expected and a negative amplitude on the other. The negative amplitude indicates a phase difference which was not obtained experimentally. However, the phase difference was obtained from the finite element analysis as indicated in the figures .

7. FURTHER CONSIDERATIONS

Axisymmetric combustion chambers represent only a portion of the complex combustion chambers as discussed earlier. However, the finite element analysis provided in this research would be equally valid for asymmetric combustion chambers.

As an extension to the experimental work which was done on the axisymmetric combustion chambers, one asymmetric combustion chamber was examined at a depth of 4.5 mm. This combustion chamber was similar to combustion chamber 3 (radius = 40 mm) except that the combustion chamber was offset as shown in Figure 7.1.

The cavity resonances were experimentally obtained in a similar manner to those for the axisymmetric combustion chambers. The spectrum trace for configuration I is shown in Figure 7.2.

The results for the lowest cavity resonance indicate that two frequencies exist at very near to the same value. This indicates that the asymmetry of the combustion chamber separates the orthogonal pairs of circumferential modes (100) into two separate modes, of slightly different frequencies.

The experimental mode shapes which were obtained for the two lowest cavity resonances are presented in Figure 7.3. Figure 7.3b at 2400 Hz shows a circumferential mode (100). Figure 7.3a at 2300 Hz shows a combined mode.[16]

---

[16] The excitation frequencies were chosen slightly higher than and slightly lower than each mode to uncouple the

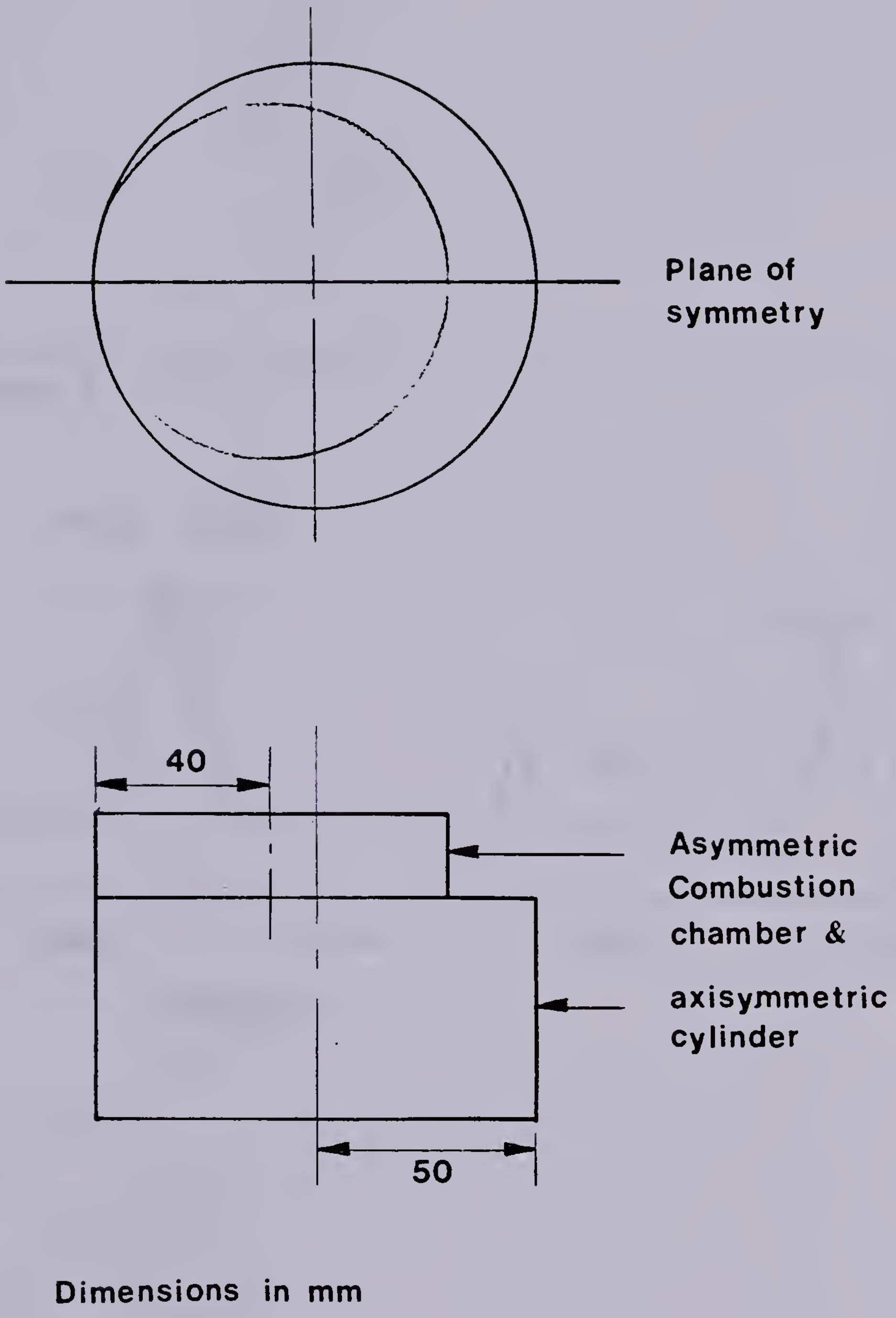

''(cont'd)
Figure 7.1 Asymmetric Combustion Chamber

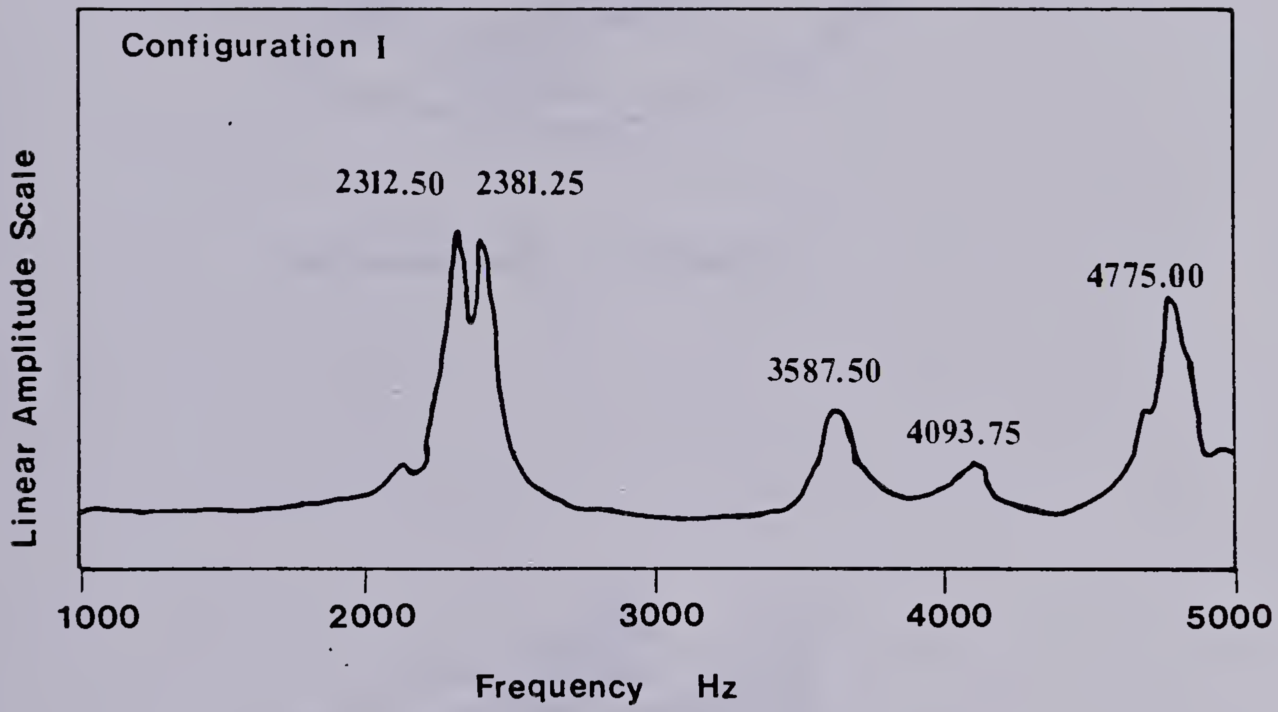

''(cont'd)
Figure 7.2 Spectrum Trace for Asymmetric Combustion Chamber

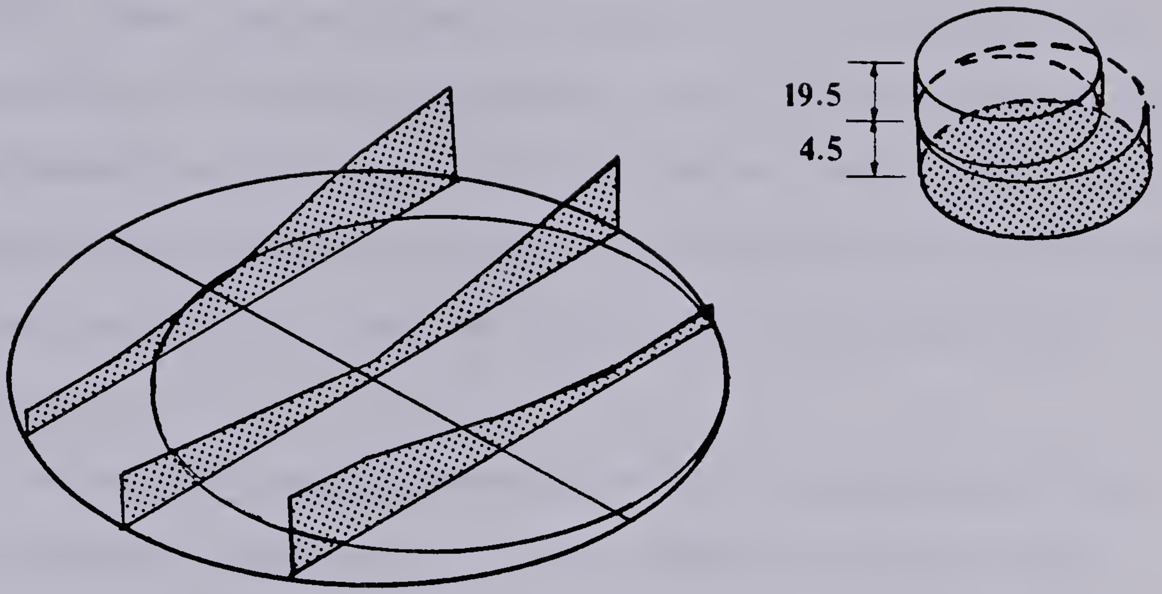

a)Experimental f = 2300 Hz

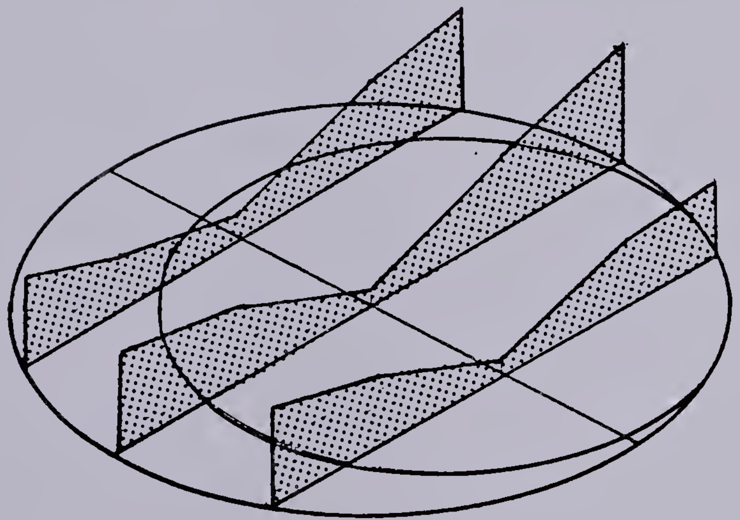

b)Experimental f = 2400 Hz

''(cont'd)
Figure 7.3 Mode Shapes for Asymmetric Combustion Chamber

If one superimposes two (100) modes orthogonal to one another, the mode shape given in Figure 7.3a is similar to the combination of these two modes, with some distortion due to the asymmetry of the combustion chamber. Evidently, the experimental mode shape in Figure 7.3a (representing 2312.50 Hz) was not uncoupled from the other mode (representing 2381.25 Hz).

This experiment was conducted as a recommendation for areas of further research. For more complex asymmetrical combustion chambers, finite element analyses could be performed and compared to experimental results similar to that done in this work. The mode shapes as a function of cylinder depth could be studied to shed more light on cavity resonances of complex shaped enclosures.

''(cont'd)modes.

8. CONCLUSIONS

8.1 Cavity Resonances

The cavity resonance results for the three combustion chamber-cylinder configurations as a function of cylinder depths are summarized in Figures 6.4 - 6.6. For each combustion chamber, there was good agreement between the finite element predictions and the experimental results for the lowest cavity resonance. The difference between the finite element results and the experimental results increases for the higher modes. This is confirmed particularily for combustion chamber 2 where the comparison is made to acoustic theory. Acoustic theory agrees very well with experimental values for all the modes considered for combustion chamber 2, within the frequency range. The approximation for the complex geometries using the analytical equations for the first four modes is quite good for the geometries considered. It gives a reliable indication of the behaviour of the modes as the cylinder depth changes.

8.2 Mode Shapes

The experimental mode shapes and finite element mode shapes are summarized in Figures 6.7 - 6.11. For each combustion chamber, there was good agreement between the finite element predictions and the experimental results for

the lowest cavity resonance at the given depth. For all three combustion chambers at the cylinder depth considered, the lowest cavity resonance was a circumferential mode (100) with one nodal diameter. The agreement with analytical theory for combustion chamber 2 mode shapes validates the usefulness of the finite element method for predicting cavity resonances of rigid enclosures.

8.3 For Engine Knock

Although this analysis considered air in combustion chamber-cylinder geometries, the results could be quite useful in considering engine knock if one knows the properties of the gas in the actual engine cycle. The observed trends in the cavity resonances as a function of cylinder depth would be the same for a different velocity of sound as would the location of the nodal surfaces. However, the actual values of the frequencies would be much higher in a running engine. This analysis does give some insight into the acoustic nature of complex shaped enclosures in regard to engine knock as well as insight into the natural frequencies of complex shaped rigid enclosures, in general.

REFERENCES

1. Draper, C.S., Pressure Waves Accompanying Detonation in the Internal Combustion Engine. Journal of Aeronautical Sciences, Vol.5 No.6, 1938, p219-226.

2. Obert, E., Internal Combustion Engines. International Textbook Company, 1950.

3. By, A., Kempinski, B., Rife, J.M., Knock in Spark Ignition Engines. SAE Technical Paper 810147, 1981.

4. Hickling, R., Feldmaier, D.A., Sung, S.H., Knock-Induced Cavity Resonances in Open Chamber Diesel Engines. J. Acoust. Soc. Am., Vol.65 No.6, 1979, p1474-1479.

5. Morse, P.M., Vibration and Sound. Acoustical Society of America, 1976.

6. Taylor, C.F., Taylor, E.S., The Internal Combustion Engine. International Textbook Company, 1961.

7. Draper, C.S., Li, Y.T., A New High Performance Engine Indicator of the Strain Gage Type. Journal of Aeronautical Sciences, Vol.16 No.10, 1949, p593-610.

8. Craggs, A., The Use of Simple Three-Dimensional Acoustic Finite Elements for Determining the Natural Modes and Frequencies of Complex Shaped Enclosures. J. Sound & Vib., Vol.23 No.3, 1972, p331-339.

9. Gladwell, G.M., A Finite Element Method for Acoustics. 5e Congres International d'Acoustique, Liege 7-14 Septembre, 1965.

10. Sung, S.H., Acoustic Finite Element Analysis of the Asymmetric Combustion Chamber of the DDAD 8.21 Engine. GMREPORT 248C, 1977.

11. Craggs, A., Lorimer, S., Finite Element Analysis for G.M. Chevette Engine Combustion Chamber and Cylinder. GM Contract Report #CR-81-09-EM, 1981.

12. Zienkiewicz, O.C., The Finite Element Method in Engineering Science. 2nd Edition, McGraw Hill Publishing Company Ltd., 1971.

13. Heubner, K.E., The Finite Element Method for Engineers.

John Wiley & Sons, Inc., 1975.

14. Cook, R.D., Concepts and Applications of Finite Element Analysis. John Wiley & Sons, Inc., 1969.

15. PAFEC Report 70+ With Extensions to August 1974. Edited by R.D. Henshell, 1972.

16. Carnahan, B., Luther, H.A., Wilkes, J.O., Applied Numerical Methods. John Wiley & Sons, Inc., 1969.

BIBLIOGRAPHY

Frederiksen, E., Microphones Used as Sound Sources. Bruel & Kjaer Technical Review, No.3, 1977.

Gladwell, G.M., Zimmermann, G., On Energy and Complementary Energy Formulations of Acoustic and Structural Vibration Problems. ISAV Memorandum No.130, 1965.

Kinsler, L.E., Frey, A.R., Fundamentals of Acoustics. John Wiley & Sons, Inc., 1950.

Mason, V., On the Use of Rectangular Finite Elements. ISVR Report No.161, 1967.

Petyt, M., Lea, J., Koopman, G.H., A Finite Element Method for Determining the Acoustic Modes of Irregular Shaped Cavities. J. Sound & Vib., Vol.54 No.4, 1976, p495-502.

Rayleigh, J.W.S., The Theory of Sound. Vol.1 & 2, Dover Publications, 1945.

Redheffer, R.M., Sokolnikoff, I.S., Mathematics of Physics and Modern Engineering. McGraw Hill Book Company, 1966.

Roberson, J.A., Crowe, C.T., Engineering Fluid Mechanics. Houghton Miflin Company, 1975.

Tse, F.S., Morse, I.E., Hinkle, R.T., Mechanical Vibrations: Theory and Applications. Allyn and Bacon, Inc., 1978.

APPENDIX 1

```
C THIS SUBROUTINE CALCULATES THE P MATRIX FOR
C A 15 NODE TRIANGULAR ISOPARAMETRIC ELEMENT
C
 SUBROUTINE PR15EP(EP,X,Y,Z,M,N)
 DIMENSION
 G(15,15),GAXI(16),GAET(16),GAZE(3),EP(M,M),WK(15,15)
 DIMENSION FTF(15,15),GT(15,15),X(15),Y(15),Z(15),W1(3)
 CALL GINV15(G,M)
 CALL NUMIN(GAXI,GAET,GAZE,N,W,W1)
 CALL FTXF(FTF,N,M,W,W1,GAXI,GAET,GAZE,G,X,Y,Z)
 DO 1 I=1,M
 DO 1 J=1,M
 WK(I,J)=0.0
 DO 1 K=1,M
 1 WK(I,J)=WK(I,J)+FTF(I,K)*G(K,J)
 DO 2 I=1,M
 DO 2 J=1,M
 2 GT(I,J)=G(J,I)
 DO 3 I=1,M
 DO 3 J=1,M
 EP(I,J)=0.0
 DO 3 K=1,M
 3 EP(I,J)=EP(I,J)+GT(I,K)*WK(K,J)
 RETURN
 END
C
C THIS SUBROUTINE CALCULATES THE KERNEL OF THE
C P MATRIX FOR A 15 NODE TRIANGULAR ISOPARAMETRIC
C ELEMENT
C
 SUBROUTINE FTXF(FTF,N,M,W,W1,GAXI,GAET,GAZE,G,X,Y,Z)
 REAL FT(15),FTF(M,M),GAXI(N),GAET(N),JAC(3,3),JACT(3,3)
 DIMENSION X(M),Y(M),Z(M),G(M,M),W1(3),GAZE(3)
 DO 3 I=1,M
 DO 3 J=1,M
 3 FTF(I,J)=0.0
 DO 5 L=1,3
 DO 4 K=1,N
 FT(1)=1.0
 FT(2)=GAXI(K)
 FT(3)=GAET(K)
 FT(4)=GAXI(K)**2
 FT(5)=GAXI(K)*GAET(K)
 FT(6)=GAET(K)**2
 FT(7)=GAZE(L)
 FT(8)=GAET(K)*GAZE(L)
 FT(9)=GAXI(K)*GAZE(L)
 FT(10)=GAXI(K)*GAET(K)*GAZE(L)
 FT(11)=GAZE(L)**2
 FT(12)=GAXI(K)**2*GAZE(L)
 FT(13)=GAET(K)**2*GAZE(L)
 FT(14)=GAXI(K)*GAZE(L)**2
```

```
 FT(15)=GAET(K)*GAZE(L)**2
 CALL JACOB3(JAC,JACT,DETJ,K,L,M,GAXI,GAET,GAZE,N,X,Y,Z,G)
 DO 1 I=1,M
 DO 1 J=1,M
 1 FTF(I,J)=FTF(I,J)+FT(I)*FT(J)*DETJ*W*W1(L)
 4 CONTINUE
 DO 2 I=1,M
 DO 2 J=1,M
 2 FTF(I,J)=FTF(I,J)
 5 CONTINUE
 RETURN
 END
C
C THIS SUBROUTINE SETS THE NATURAL CO-ORDINATES
C FOR THE 15 NODE TRIANGULAR ELEMENT
C
 SUBROUTINE PR15(XI,ET,ZE,M)
 DIMENSION XI(M),ET(M),ZE(M)
 XI(1)=0.0
 XI(2)=1.0
 XI(3)=0.0
 XI(4)=0.5
 XI(5)=0.5
 XI(6)=0.0
 XI(7)=0.0
 XI(8)=1.0
 XI(9)=0.0
 XI(10)=0.0
 XI(11)=1.0
 XI(12)=0.0
 XI(13)=0.5
 XI(14)=0.5
 XI(15)=0.0
 ET(1)=0.0
 ET(2)=0.0
 ET(3)=1.0
 ET(4)=0.0
 ET(5)=0.5
 ET(6)=0.5
 ET(7)=0.0
 ET(8)=0.0
 ET(9)=1.0
 ET(10)=0.0
 ET(11)=0.0
 ET(12)=1.0
 ET(13)=0.0
 ET(14)=0.5
 ET(15)=0.5
 ZE(1)=-1.0
 ZE(2)=-1.0
 ZE(3)=-1.0
 ZE(4)=-1.0
 ZE(5)=-1.0
 ZE(6)=-1.0
```

```
 ZE(7)=0.0
 ZE(8)=0.0
 ZE(9)=0.0
 ZE(10)=1.0
 ZE(11)=1.0
 ZE(12)=1.0
 ZE(13)=1.0
 ZE(14)=1.0
 ZE(15)=1.0
 RETURN
 END
C
C THIS SUBROUTINE FORMS THE GINV MATRIX FOR THE
C NATURAL CO-ORDINATES OF THE 15 NODE TRIANGULAR
C ELEMENT
C
 SUBROUTINE GINV15(G,M)
 DIMENSION G(M,M),LK(15),MK(15),XI(15),ET(15),ZE(15)
 CALL PR15(XI,ET,ZE,M)
 DO 1 I=1,M
 G(I,1)=1.0
 G(I,2)=XI(I)
 G(I,3)=ET(I)
 G(I,4)=XI(I)**2
 G(I,5)=ET(I)*XI(I)
 G(I,6)=ET(I)**2
 G(I,7)=ZE(I)
 G(I,8)=ET(I)*ZE(I)
 G(I,9)=XI(I)*ZE(I)
 G(I,10)=XI(I)*ET(I)*ZE(I)
 G(I,11)=ZE(I)**2
 G(I,12)=XI(I)**2*ZE(I)
 G(I,13)=ET(I)**2*ZE(I)
 G(I,14)=XI(I)*ZE(I)**2
 1 G(I,15)=ET(I)*ZE(I)**2
 CALL MINV(G,M,D,LK,MK)
 RETURN
 END
C
C THIS SUBROUTINE CALCULATES THE S MATRIX FOR
C A 15 NODE TRIANGULAR ISOPARAMETRIC ELEMENT
C
 SUBROUTINE PR15ES(ES,X,Y,Z,M,N)
 DIMENSION
 G(15,15),GT(15,15),GAXI(16),GAET(16),GAZE(3),ES(M,M)
 DIMENSION DFTXDF(15,15),WK(15,15),W1(3)
 DIMENSION X(M),Y(M),Z(M)
 CALL GINV15(G,M)
 CALL NUMIN(GAXI,GAET,GAZE,N,W,W1)
 CALL DFTF(DFTXDF,N,M,W,W1,GAXI,GAET,GAZE,G,X,Y,Z)
 DO 1 I=1,M
 DO 1 J=1,M
 WK(I,J)=0.0
 DO 1 K=1,M
```

```
 1 WK(I,J)=WK(I,J)+DFTXDF(I,K)*G(K,J)
 DO 2 I=1,M
 DO 2 J=1,M
 2 GT(I,J)=G(J,I)
 DO 3 I=1,M
 DO 3 J=1,M
 ES(I,J)=0.0
 DO 3 K=1,M
 3 ES(I,J)=ES(I,J)+GT(I,K)*WK(K,J)
 RETURN
 END
C
C THIS SUBROUTINE CALCULATES THE KERNEL OF THE
C S MATRIX FOR A 15 NODE ISOPARAMETRIC ELEMENT
C
 SUBROUTINE DFTF(DFTXDF,N,M,W,W1,GAXI,GAET,GAZE,G,X,Y,Z)
 DIMENSION DF(3,15),WK(3,15),WK1(3,15),DFTXDF(M,M)
 REAL GAXI(N),GAET(N),G(M,M),JAC(3,3),JACT(3,3)
 DIMENSION X(15),Y(15),Z(15),GAZE(3),W1(3)
 DO 1 I=1,M
 DO 1 J=1,M
 1 DFTXDF(I,J)=0.0
 DO 5 L=1,3
 DO 2 K=1,N
 DF(1,1)=0.0
 DF(1,2)=1.0
 DF(1,3)=0.0
 DF(1,4)=2.0*GAXI(K)
 DF(1,5)=GAET(K)
 DF(1,6)=0.0
 DF(1,7)=0.0
 DF(1,8)=0.0
 DF(1,9)=GAZE(L)
 DF(1,10)=GAET(K)*GAZE(L)
 DF(1,11)=0.0
 DF(1,12)=2.0*GAXI(K)*GAZE(L)
 DF(1,13)=0.0
 DF(1,14)=GAZE(L)**2
 DF(1,15)=0.0
 DF(2,1)=0.0
 DF(2,2)=0.0
 DF(2,3)=1.0
 DF(2,4)=0.0
 DF(2,5)=GAXI(K)
 DF(2,6)=2.0*GAET(K)
 DF(2,7)=0.0
 DF(2,8)=GAZE(L)
 DF(2,9)=0.0
 DF(2,10)=GAXI(K)*GAZE(L)
 DF(2,11)=0.0
 DF(2,12)=0.0
 DF(2,13)=2.0*GAET(K)*GAZE(L)
 DF(2,14)=0.0
 DF(2,15)=GAZE(L)**2
```

```
 DF(3,1)=0.0
 DF(3,2)=0.0
 DF(3,3)=0.0
 DF(3,4)=0.0
 DF(3,5)=0.0
 DF(3,6)=0.0
 DF(3,7)=1.0
 DF(3,8)=GAET(K)
 DF(3,9)=GAXI(K)
 DF(3,10)=GAXI(K)*GAET(K)
 DF(3,11)=2.0*GAZE(L)
 DF(3,12)=GAXI(K)**2
 DF(3,13)=GAET(K)**2
 DF(3,14)=2.0*GAXI(K)*GAZE(L)
 DF(3,15)=2.0*GAET(K)*GAZE(L)
 CALL JACOB3(JAC,JACT,DETJ,K,L,M,GAXI,GAET,GAZE,N,X,Y,Z,G)
 DO 3 I=1,3
 DO 3 J=1,M
 WK(I,J)=0.0
 DO 3 LL=1,3
 3 WK(I,J)=WK(I,J)+JAC(I,LL)*DF(LL,J)
 DO 6 I=1,3
 DO 6 J=1,M
 WK1(I,J)=0.0
 DO 6 LL=1,3
 6 WK1(I,J)=WK1(I,J)+JACT(I,LL)*WK(LL,J)
 DO 4 I=1,M
 DO 4 J=1,M
 DO 4 LL=1,3
 4 DFTXDF(I,J)=DFTXDF(I,J)+DF(LL,I)*WK1(LL,J)*DETJ*W*W1(L)
 2 CONTINUE
 DO 7 I=1,M
 DO 7 J=1,M
 7 DFTXDF(I,J)=DFTXDF(I,J)
 5 CONTINUE
 RETURN
 END
C
C THIS SUBROUTINE FORMS THE JACOBIAN FOR A 3 DIMENSIONAL
C 15 NODE TRIANGULAR ISOPARAMETRIC ELEMENT
C
 SUBROUTINE
 JACOB3(JAC,JACT,DETJ,K,L,M,GAXI,GAET,GAZE,N,X,Y,Z,G)
 REAL
 JAC(3,3),JACT(3,3),GAXI(N),GAET(N),GAZE(3),X(M),Y(M),Z(M)
 DIMENSION WK1(15),WK2(15),WK3(15),G(M,M),DFXI(15),DFET(15)
 DIMENSION DFZE(15)
 DIMENSION LK(3),MK(3)
 DO 4 I=1,3
 DO 4 J=1,3
 4 JAC(I,J)=0.0
 DO 5 I=1,M
 WK1(I)=0.0
 WK2(I)=0.0
```

```
5 WK3(I)=0.0
DFXI(1)=0.0
DFXI(2)=1.0
DFXI(3)=0.0
DFXI(4)=2.0*GAXI(K)
DFXI(5)=GAET(K)
DFXI(6)=0.0
DFXI(7)=0.0
DFXI(8)=0.0
DFXI(9)=GAZE(L)
DFXI(10)=GAET(K)*GAZE(L)
DFXI(11)=0.0
DFXI(12)=2.0*GAXI(K)*GAZE(L)
DFXI(13)=0.0
DFXI(14)=GAZE(L)**2
DFXI(15)=0.0
DFET(1)=0.0
DFET(2)=0.0
DFET(3)=1.0
DFET(4)=0.0
DFET(5)=GAXI(K)
DFET(6)=2.0*GAET(K)
DFET(7)=0.0
DFET(8)=GAZE(L)
DFET(9)=0.0
DFET(10)=GAXI(K)*GAZE(L)
DFET(11)=0.0
DFET(12)=0.0
DFET(13)=2.0*GAET(K)*GAZE(L)
DFET(14)=0.0
DFET(15)=GAZE(L)**2
DFZE(1)=0.0
DFZE(2)=0.0
DFZE(3)=0.0
DFZE(4)=0.0
DFZE(5)=0.0
DFZE(6)=0.0
DFZE(7)=1.0
DFZE(8)=GAET(K)
DFZE(9)=GAXI(K)
DFZE(10)=GAXI(K)*GAET(K)
DFZE(11)=2.0*GAZE(L)
DFZE(12)=GAXI(K)**2
DFZE(13)=GAET(K)**2
DFZE(14)=2.0*GAZE(L)*GAXI(K)
DFZE(15)=2.0*GAZE(L)*GAET(K)
DO 1 J=1,M
DO 1 I=1,M
WK1(J)=WK1(J)+DFXI(I)*G(I,J)
WK2(J)=WK2(J)+DFET(I)*G(I,J)
1 WK3(J)=WK3(J)+DFZE(I)*G(I,J)
DO 2 I=1,M
JAC(1,1)=JAC(1,1)+WK1(I)*X(I)
JAC(2,1)=JAC(2,1)+WK2(I)*X(I)
```

```
JAC(3,1)=JAC(3,1)+WK3(I)*X(I)
JAC(1,2)=JAC(1,2)+WK1(I)*Y(I)
JAC(2,2)=JAC(2,2)+WK2(I)*Y(I)
JAC(3,2)=JAC(3,2)+WK3(I)*Y(I)
JAC(1,3)=JAC(1,3)+WK1(I)*Z(I)
JAC(2,3)=JAC(2,3)+WK2(I)*Z(I)
2 JAC(3,3)=JAC(3,3)+WK3(I)*Z(I)
CALL MINV(JAC,3,DETJ,LK,MK)
DO 3 I=1,3
DO 3 J=1,3
3 JACT(I,J)=JAC(J,I)
RETURN
END
SUBROUTINE NUMIN(GAXI,GAET,GAZE,N,W,W1)
DIMENSION GAXI(N),GAET(N),GAZE(3),W1(3)
GAXI(1)=1.0/12.0
GAXI(2)=1.0/6.0
GAXI(3)=1.0/12.0
GAXI(4)=1.0/3.0
GAXI(5)=1.0/12.0
GAXI(6)=1.0/6.0
GAXI(7)=1.0/3.0
GAXI(8)=5.0/12.0
GAXI(9)=1.0/12.0
GAXI(10)=1.0/6.0
GAXI(11)=1.0/3.0
GAXI(12)=5.0/12.0
GAXI(13)=7.0/12.0
GAXI(14)=8.0/12.0
GAXI(15)=7.0/12.0
GAXI(16)=10.0/12.0
GAET(1)=10.0/12.0
GAET(2)=8.0/12.0
GAET(3)=7.0/12.0
GAET(4)=7.0/12.0
GAET(5)=5.0/12.0
GAET(6)=1.0/3.0
GAET(7)=1.0/3.0
GAET(8)=5.0/12.0
GAET(9)=1.0/6.0
GAET(10)=1.0/12.0
GAET(11)=1.0/12.0
GAET(12)=1.0/6.0
GAET(13)=1.0/3.0
GAET(14)=1.0/6.0
GAET(15)=1.0/12.0
GAET(16)=1.0/12.0
W=1.0/32.0
GAZE(1)=0.0
GAZE(2)=0.7745966692
GAZE(3)=-GAZE(2)
W1(1)=8.0/9.0
W1(2)=5.0/9.0
W1(3)=W1(2)
```

```
RETURN
END
```